



**RETURNING MATERIALS:**

Place in book drop to  
remove this checkout from  
your record. FINES will  
be charged if book is  
returned after the date  
stamped below.

--	--	--

MICELLE STABILIZED ROOM TEMPERATURE PHOSPHORESCENCE  
BY FLOW INJECTION ANALYSIS  
AND  
A DUAL BEAM FIBER OPTIC-BASED PHOTOMETRIC COMPARATOR

by

Paul Robert Kraus

A DISSERTATION

Submitted to  
Michigan State University  
in partial fulfillment of the requirements  
for the degree of

DOCTOR OF PHILOSOPHY

Department of Chemistry

1988

## ABSTRACT

### MICELLE STABILIZED ROOM TEMPERATURE PHOSPHORESCENCE BY FLOW INJECTION ANALYSIS AND A DUAL BEAM FIBER OPTIC-BASED PHOTOMETRIC COMPARATOR

by

Paul Robert Kraus

A system is presented for routinely performing room temperature phosphorescence (RTP) measurements of analytes in fluid solution. RTP spectrometry has been used as a detection system for flow injection analysis (FIA). This combination utilizes the speed and automation of FIA, and the inherent selectivity and sensitivity of RTP. Results are presented to demonstrate the utility for the RTP/FIA configuration.

System components include a commercially available peristaltic pump, a rotary sample injection valve, a flow-through fluorescence cell, and a spectrofluorometer as the detector. Two spectrofluorometers were used: a commercially available instrument, and a microprocessor controlled home-built instrument. All instrumentation used is described in detail. Results are presented for the characterization of the dominant source of noise under the conditions normally encountered in the RTP experiments.

The removal of ubiquitous molecular oxygen, an efficient triplet state quencher, from the analytical solutions was the major problem encountered in this research. Several methods for deoxygenating a flowing stream are evaluated for their applicability to the RTP/FIA configuration. These methods include diffusion of oxygen across a gas permeable membrane into an oxygen scavenging solution of Cr(II), vacuum deoxygenation through a gas permeable membrane, and deoxygenation through the

reduction of oxygen to water by sulfite ion; the latter was the most effective. The rise in RTP to a steady-state intensity is observed to be rapid after an initial lag time.

Calibration curves obtained for naphthalene, 2-bromonaphthalene, and biphenyl are observed to be linear up to two orders of magnitude in concentration. The rise in RTP for pyrene and for higher concentrations of biphenyl was observed to follow an exponential rise. Although a steady-state intensity was not obtained for pyrene, the steady-state intensity was predicted from an exponential model. Results are presented demonstrating the usefulness of this technique.

An inexpensive and portable dual-beam photometric comparator has been developed. It has an advantage over existing single beam systems in that direct comparisons about a critical decision point can be made, and the effects of stray radiation are minimized. A light emitting diode (LED) has been used as the light source because of its fixed wavelength, narrow emission profile, low current requirements, and low cost. The comparator has been designed for photometric determinations where it is desirable to know if the analyte concentration is within a certain range. The sample introduction system has been designed to accommodate microtiter wells such as those often used in routine immunoassay procedures as the cuvettes. The unit has been designed to be operated by non-technically oriented persons. It can be battery powered for field use or operated from ac power.

## DEDICATION

To my Grandparents,  
my Parents, and  
my wife, Theresa.

## ACKNOWLEDGEMENTS

During my accumulated time at MSU I've made many friends, perhaps too many to acknowledge individually. However, several people do merit individual recognition. First, I'd like to express my thanks to Professor Stanley Crouch for his help and for teaching me that independent research can be a rewarding experience. I owe many thanks to Azure Fleetfang and Panther Solecat (a.k.a. Gene Ratzlaff and Chas Patton) for their assistance during my "formative years" when this all got started.

Pete Palmer deserves special mention for helping me to retain a much needed level of insanity, and for friendship above and beyond the call of duty. I'll never forget our excursions at the P.B. and discussions about the Hobbit/Lord of the Rings (!). Other folks which deserve special thanks are Bob, Pete W., Adrian, Chris, Cheryl, Norm, June, Jon and Karen to mention a few. The many other friends I've made while at MSU will not be forgotten.

Many thanks to Marty "Electric Bicycleman" Rabb for being patient with my endless questions regarding electronic circuits and for the biking lessons. The men of the machine shop, Russ Geyer, Dick Menke, and Deak Watters deserve acknowledgment for construction of countless items and repairs.

On the lighter side, I'd like to thank Dr. Loran Bieber for his friendship and the fishing trips during which he never failed to remind the crew to keep the rod tip up! That's what life is all about.

A very special acknowledgment is extended to my wife, Theresa, for her faith in me and for putting-up with me through a very difficult time. Without Theresa I might not have persevered!

And finally, to those people whose mere existence seemed to make life miserable, I tip my "Social Statement Cap!" (with acknowledgments to Bob R.).

## TABLE OF CONTENTS

<u>Chapter</u>	<u>Page</u>
List of Tables	viii
List of Figures	ix
I. INTRODUCTION	1
A. References	4
II. MOLECULAR LUMINESCENCE in SOLUTION	5
A. Absorption of light	5
B. Fluorescence	9
Fluorescence Lifetimes	10
Quenching of Fluorescence	13
C. Phosphorescence	15
Phosphorescence Lifetimes	17
Oxygen Quenching	18
Heavy Atom Effect in Phosphorescence	19
D. References	21
III. ROOM-TEMPERATURE PHOSPHORESCENCE	22
A. Introduction to Room Temperature Phosphorescence	22
B. Solid Surface RTP	24
C. Sensitized RTP	26
D. Microcrystalline and Colloidal RTP	27
E. Cyclodextrin Enhanced RTP	28
F. Micelle-Stabilized RTP	31
G. Deoxygenation methods	37
Inert Gas Purging	37
Vacuum Degassing	38
Freeze-Pump-Thaw	38
Semipermeable Membranes	38
Chemical Scavenging	39
Chromium(II)	39
Zinc Column	40
Sodium Sulfite	41
H. References	42
IV. FLOW INJECTION ANALYSIS	45
A. Principles of Flow Injection Analysis	46
B. Related Applications of Flow Injection Analysis	50
Stopped-Flow in FIA	50
Luminescence Detection in FIA	50
C. References	52

V.	<b>INSTRUMENTATION</b>	55
	A. Home-Built Microcomputer-Controlled Luminescence Spectrometer	55
	Twin Bus Microcomputer System	56
	Home-Built Luminescence Spectrometer	59
	Microcomputer/Spectrometer Interface	59
	Experimental Determination of the Dominant Noise Source	67
	B. Perkin-Elmer Model LS-5 Luminescence Spectrometer	70
	C. References	71
VI.	<b>LUMINESCENCE SPECTRA</b>	72
	A. Reagents	72
	B. Fluorescence Spectra	74
	C. RTP Spectra	76
	MS-RTP Spectra	76
	CD-RTP Spectra	85
	D. Phosphorescence Lifetimes	90
	E. References	95
VII.	<b>ROOM TEMPERATURE PHOSPHORESCENCE with FLOW INJECTION ANALYSIS SAMPLE INTRODUCTION</b>	96
	A. Flow Injection System	96
	B. Carrier Study	98
	C. Deoxygenation of Flowing Streams	100
	Chromium (II)/Zn(Hg) Oxygen Scavenging	100
	Vacuum Deoxygenation	108
	Sodium Sulfite Deoxygenation	110
	D. RTP/FIA Calibration Curves	112
	E. References	128
VIII.	<b>WHAT'S NEXT?</b>	129
	A. References	132
IX.	<b>PORTABLE DUAL BEAM FIBER OPTIC-BASED PHOTOMETRIC COMPARATOR</b>	133
	A. Introduction	133
	B. Experimental	135
	Optical Arrangement	135
	Analytical Manifold	135
	Circuit Description	137
	C. Results and Discussion	140
	D. References	143
X.	<b>APPENDIX: FORTH SOURCE CODE LISTING</b>	144

## LIST of TABLES

<u>Table</u>	<u>Title</u>	<u>Page</u>
Table 5.1	Modules with their Principal Integrated Circuits	57
Table 5.2	Effect of Radiant Power on the S/N	69
Table 7.1	Comparison of Static and Flow Cell in Perkin-Elmer LS-5	97
Table 7.2	Comparison of Static and Flow Cell in Home-Built Instrument	98
Table 7.3	Fluorescence Enhancement Factors	105
Table 7.4	Results of Weighted Linear Regression for Naphthalene Calibration Curve	114
Table 7.5	Results of Weighted Linear Regression for 2-Bromonaphthalene Calibration Curve	117
Table 7.6	Results of Weighted Linear Regression for Biphenyl Calibration Curve	121
Table 7.7	Parameters for Pyrene fit to Exponential Rise in RTP	124
Table 7.8	Results of Weighted Linear Regression for Pyrene Calibration Curve	127
Table 9.1	Components of Comparator Circuit	139

## LIST of FIGURES

<u>Figure</u>	<u>Title</u>	<u>Page</u>
Figure 2.1	Generalized Jablonski diagram. A, absorbance; F, fluorescence; P, phosphorescence; VR, vibrational relaxation; IC, internal conversion; ISC, intersystem crossing; S <sub>0</sub> , S <sub>1</sub> , and S <sub>2</sub> are the ground and excited singlet states, respectively, and T <sub>1</sub> is the excited triplet state.	7
Figure 3.1.	Simplified representation of a cyclodextrin molecule.	29
Figure 3.2.	A) Simplified representation of a surfactant monomer. B) Anionic micelle in aqueous solvent. C) Reverse micelle.	33
Figure 4.1	Simplified representation of a flow injection system. The reagent R is pumped through the manifold where the sample S is injected by a sample injection valve. The product is monitored by the flow-through detector FC. The product is then vented to waste W.	47
Figure 4.2	Laminar flow with molecular diffusion: (a) the sample plug, (b) under conditions of laminar flow, (c) laminar flow with molecular diffusion, (d) Gaussian peak profile resulting from molecular diffusion.	48
Figure 5.1	Block diagram of home-built luminescence spectrometer showing orientation of the components. Key: S, radiation source; L, lens; C, optional chopper; Mex, excitation monochromator; SC, sample chamber; PD, photodiode with amplifier circuitry; Mem, emission monochromator; I/V, current amplifier.	60
Figure 5.2	Schematic of transistor driver circuit used to amplify current supplying power to chopper motor.	62
Figure 5.3	Timing diagram depicting the three types of phasing: A, chopper signal lags source signal; B, chopper signal leads source signal; and C, signals are in phase.	64
Figure 5.4	Photodiode amplifier circuit. R <sub>1</sub> = 1 MΩ, R <sub>2</sub> = 2.2 MΩ, and R <sub>in</sub> = 680 Ω.	65

Figure 6.1	Excitation and fluorescence emission spectra of naphthalene. A) excitation scan taken on Perkin-Elmer LS-5 with $\lambda_{em} = 330$ nm. B) emission scan taken on LS-5 with $\lambda_{ex} = 276$ nm. C) emission scan taken on home-built instrument with $\lambda_{ex} = 280$ nm. See text for explanation of peaks above 450 nm.	75
Figure 6.2	Excitation and fluorescence emission spectra of 2-bromonaphthalene. A) excitation scan from LS-5 with $\lambda_{em} = 315$ nm. B) emission scan from LS-5. C) emission scan from home-built instrument.	77
Figure 6.3	Excitation and fluorescence emission spectra of pyrene. A) excitation scan taken on home-built instrument with $\lambda_{em} = 395$ nm. B) excitation scan taken on LS-5 with. See text for explanation in peak intensities. C) emission scan taken on LS-5, $\lambda_{ex} = 335$ nm.	78
Figure 6.4	Excitation and fluorescence emission spectra of biphenyl taken on LS-5. A) excitation scan with $\lambda_{em} = 315$ nm. B) emission scan with $\lambda_{ex} = 260$ nm.	79
Figure 6.5	Fluorescence emission of naphthalene taken on home-build instrument with $\lambda_{ex} = 280$ nm and 16 nm bandpasses. A) 0.10 M SDS, and B) 0.10 M SDS with 25 mM $TiNO_3$ added. See text for explanation.	80
Figure 6.6	Luminescence spectra of naphthalene in 0.10 M SDS with 25 mM $TiNO_3$ (dotted line), and deoxygenated solution (solid line).	82
Figure 6.7	Phosphorescence spectrum of naphthalene in 0.10 M SDS with 25 mM $TiNO_3$ and 10 mM $Na_2SO_3$ . Delay time after HI-to-LO transition of chopper is 10 $\mu s$ .	83
Figure 6.8	Rise in phosphorescence intensity for two concentrations of surfactant. A) 0.15 M 30/70 TI/Na DS. B) 0.10 M 30/70 TI/Na DS. Phosphorescence intensity is in arbitrary units.	84
Figure 6.9	MS-RTP spectrum of 2-bromonaphthalene in 0.15 M 30/70 TI/Na DS with 10 mM $Na_2SO_3$ . A) home-built instrument, and B) Perkin-Elmer LS-5.	86
Figure 6.10	MS-RTP spectrum of pyrene in 0.15 M 30/70 TI/Na DS with 10 mM $Na_2SO_3$ . A) home-built instrument, and B) Perkin-Elmer LS-5.	87
Figure 6.11	MS-RTP spectrum of biphenyl in 0.10 M 30/70 TI/Na DS with 10 mM $Na_2SO_3$ .	88
Figure 6.12	CD-RTP spectrum of 2-bromonaphthalene in 0.01 M $\beta$ -cyclodextrin with 0.58 M DBE.	89

Figure 6.13	Phosphorescence decay of naphthalene. Data from, A) Perkin-Elmer LS-5, B) home-built instrument. Curve through data points represents the best fit to data as determined by the single exponential decay of equation 6-1.	92
Figure 6.14	Phosphorescence decay of pyrene. Data from home-built instrument. Curve represents best fit of data to single exponential decay.	94
Figure 7.1	A) fluorescence peak profile of pyrene obtained with water as the carrier, and B) SDS carrier.	99
Figure 7.2	Characteristic fluorescence peak profiles obtained with A) water, B) SDS, C) NaCl, D) NaBr, E) NaC <sub>2</sub> H <sub>3</sub> O <sub>2</sub> , and F) LiCl.	101
Figure 7.3	Concentric tube dialyzer used for deoxygenation with Cr(II).	103
Figure 7.4	FIA manifold used for deoxygenation with concentric tube dialyzer	104
Figure 7.5	A) Fluorescence peak profiles obtained for pyrene by FIA. Sample concentrations from left to right are 20, 15, 12, 10, 7, 5, 2, and 1 $\mu$ M, respectively. B) Calibration curve using average maximum peak intensity obtained from A.	106
Figure 7.6	Absorbance spectra of A) pyrene in 0.15 M SDS, B) Chromium deoxygenating solution, and C) pyrene waste solution showing contamination of pyrene sample by chromium.	107
Figure 7.7	Vacuum deoxygenation apparatus.	109
Figure 7.8	FIA manifold used for RTP determinations.	111
Figure 7.9	Rise in RTP observed for RTP/FIA system.	113
Figure 7.10	Rise in RTP for naphthalene observed with RTP/FIA system for A) 140 $\mu$ M, B) 100 $\mu$ M, C) 30 $\mu$ M, D) 10 $\mu$ M, E) 3 $\mu$ M, and F) 1 $\mu$ M solutions. Time is relative to injection of sample.	115
Figure 7.11	Calibration curve for naphthalene by RTP/FIA. RTP intensity is in arbitrary units.	116
Figure 7.12	Calibration curve for 2-bromonaphthalene by RTP/FIA. RTP intensity is in arbitrary units.	118
Figure 7.13	Rise in RTP observed for 100 $\mu$ M biphenyl.	119
Figure 7.14	Fit of rise in RTP for 100 $\mu$ M biphenyl to an exponential equation.	120

Figure 7.15	Calibration curve for biphenyl by RTP/FIA. Intensity of 100 $\mu\text{M}$ sample obtained from equation 7-4. RTP intensity is in arbitrary units.	122
Figure 7.16	Rise in RTP for pyrene observed with RTP/FIA system for A) 200 $\mu\text{M}$ , B) 100 $\mu\text{M}$ , C) 30 $\mu\text{M}$ , D) 10 $\mu\text{M}$ , E) 3 $\mu\text{M}$ , and F) 1 $\mu\text{M}$ solutions. Time is relative to injection of sample.	123
Figure 7.17	Fit of rise in RTP for pyrene samples to equation 7-4. See text for explanation. Curves correspond to A) 200 $\mu\text{M}$ , B) 100 $\mu\text{M}$ , C) 30 $\mu\text{M}$ , D) 10 $\mu\text{M}$ , E) 3 $\mu\text{M}$ , and F) 1 $\mu\text{M}$ pyrene sample concentrations.	125
Figure 7.18	Calibration curve for pyrene by RTP/FIA. RTP intensities are obtained from fit of data in Figure 7.17 to equation 7-4.	126
Figure 9.1.	Manifold of the optical comparator showing configuration of the source, fiber optic, and photodiodes. The grooved tracks minimize scratches in the bottom of the analysis cups.	136
Figure 9.2.	Circuit schematic for optical comparator circuit. Light from LED4 illuminates photodiodes PD1 and PD2 through the bifurcated fiber optic.	138

## CHAPTER I

### INTRODUCTION

This dissertation presents work performed on two vastly different projects. The main topic of this research is room temperature phosphorescence (RTP) spectrometry. Phosphorescence is traditionally performed in glasses at 77 K to avoid collisional deactivation of the excited molecule. RTP was first reported for molecules adsorbed on a solid support. Schulman and Walling [1,2] are commonly attributed with the discovery of RTP. Since then, the pioneering work of Winefordner [3] has developed RTP into a viable analytical technique. Recently, several other RTP methods have been reported which enable phosphorescence measurements to be made in fluid solutions. These techniques can be automated easily because of the fluid sample matrix employed. The research on RTP in this dissertation focuses on the development of an automated system for performing RTP in fluid solution. Flow injection analysis is used for sample introduction because of its versatility, speed, and the simplicity of the equipment required.

Chapter II is a fundamental background of molecular luminescence in solution. The chapter is divided into three main categories: absorption of light, molecular fluorescence, and molecular phosphorescence. These are described to provide basic principles which can then be assumed in subsequent chapters.

Room temperature phosphorescence is discussed in Chapter III. A brief historical survey traces the development of several RTP techniques. These techniques are then discussed individually. Methods commonly used to deoxygenate solutions prior to RTP analysis are then introduced.

Chapter IV describes the technique of flow injection analysis (FIA). The underlying principles of FIA, sample injection, controlled dispersion, and reproducible timing, are described. Two related applications of FIA, stopped-flow and luminescence detection, are then discussed. This discussion provides a background for techniques applied in later chapters.

The instrumentation used in this research is described in Chapter V. The development of a home-built spectrofluorometer is described first. Studies performed to characterize the dominant source of noise in the instrument are then discussed. A Perkin-Elmer model LS-5 spectrofluorometer was also used in this research and is described in this chapter.

Chapter VI presents spectra of the compounds used in this research. Fluorescence spectra are obtained to determine the optimum excitation wavelength for each compound. RTP spectra of these compounds are also described. The spectra obtained are presented to show the characteristic phosphorescence emission bands. These spectra are then used to determine the emission wavelength which yields the maximum phosphorescence intensity. Phosphorescence lifetimes of selected compounds are determined as a means to confirm the presence of RTP.

Experiments tracing the development of a system used for RTP with FIA sample introduction are described in Chapter VII. Studies to determine the best carrier to use in the flow system are discussed along with experiments to test various deoxygenation methods. These studies resulted in the development of a system for performing RTP by FIA. Ideas for future projects are given in Chapter VIII.

The second project presented in this dissertation is the development of a dual beam fiber optic-based photometric comparator. This work was performed as a consulting project for a local business. This instrument was developed as an alternative to optical comparison of reference and sample solutions. The instrument performs a direct comparison of reference and sample solutions and indicates if the transmittance

of the sample is less than, greater than, or approximately equivalent to the reference.  
The comparator was designed to be used by non-technically oriented persons.

**CHAPTER I REFERENCES**

1. Schulman, E.M.; and Walling, C., *Science*, **1972**, *178*, 53
2. Schulman, E.M.; and Walling, C., *J. Phys. Chem.*, **1973**, *77*, 902
3. Paynter, R.A.; Wellons, S.L.; and Winefordner, J.D., *Anal. Chem.*, **1974**, *46*, 736

## CHAPTER II

### MOLECULAR LUMINESCENCE IN SOLUTION

This chapter is a discussion of the photophysical processes that lead to molecular luminescence in solution. These are described here so that familiarity with these topics can be assumed in subsequent chapters. Three topics are discussed; absorption of light, molecular fluorescence, and phosphorescence. The absorption of light by a molecule is one way which the molecule can be excited to a higher energy level.

Fluorescence is a radiative transition from an excited energy level to the ground state. Equations are derived which show the relationship between the fluorescence intensity and the concentration of the analyte. The lifetime of a fluorescent molecule is then described as are methods for determining fluorescent lifetimes. The effect of quenchers on fluorescence and two mechanisms of quenching are presented.

The photophysical processes which lead to phosphorescence are introduced in the final section. This section deals primarily with cryogenic phosphorescence. Equations relating phosphorescence intensity to analyte concentration are derived. Finally, the quenching effect of molecular oxygen and the heavy atom effect in phosphorescence are discussed.

#### Absorption of Light

Molecular luminescence spectroscopy is based on the emission of light by electronically excited molecules. The excitation process involves the interaction of the electric field associated with the exciting radiation with the loosely bound  $\pi$  or nonbonded electrons of the absorbing molecule. Through this interaction the electronic

distribution of the absorbing molecule is distorted which causes energy to be absorbed from the electric field of the excitation beam. The energy necessary for absorption depends on the types of bonds available in the molecule. From the standpoint of organic molecular spectroscopy, the most important element in the absorption of radiation in the ultra-violet and visible region is the C=C double bond. If a molecule absorbs a photon, an electron in the  $\pi$  cloud of this bond can be promoted to the  $\pi$  anti-bonding orbital ( $\pi \rightarrow \pi^*$ ).

Because of the quantization of molecular energy levels, excitation of a molecular species will occur only if the energy associated with the excitation radiation corresponds to the difference in energy between the ground electronic state and an electronically excited state of the absorbing molecule. The intensity of radiation absorbed by the molecule ( $I_a$ ) can be calculated by the Beer-Lambert law:

$$I_a = I_0 - I_t = I_0(1 - e^{-\epsilon b C}) \quad (2-1)$$

where  $I_0$  and  $I_t$  are the incident and transmitted light intensities, respectively,  $\epsilon$  is the molar absorptivity of the molecule, and  $C$  is the molar concentration of the absorber in pathlength  $b$  of the sample. The energy of radiation required to excite the species from one energy level to an excited energy level ( $\Delta E$ ) is given by the Planck frequency relation:

$$\Delta E = h\nu = \frac{hc}{\lambda} \quad (2-2)$$

where  $\nu$  is the frequency of the light of wavelength  $\lambda$ , and  $c$  is the velocity of light. In molecules, each electronic state has several associated vibrational levels (Figure 2.1). In the ground electronic state, virtually all molecules occupy the lowest vibrational level at room temperature. Most polyatomic molecules in the ground state have an even number of electrons with their spins paired. The spin of the electron,  $s$ , can be equal to  $+1/2$  or  $-1/2$ . When the electron spins are paired, this is termed a singlet electronic state. The lowest electronic singlet state is the  $S_0$  state. When a molecule absorbs radiation of sufficient energy it can be excited vibrationally as well as electronically to energy level

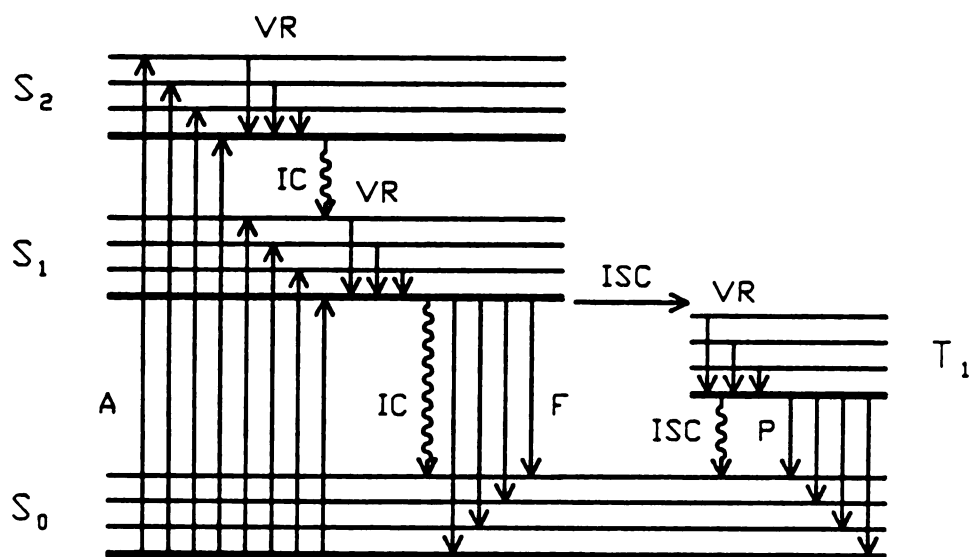


Figure 2.1

Generalized Jablonski diagram. A, absorbance; F, fluorescence; P, phosphorescence; VR, vibrational relaxation; IC, internal conversion; ISC, intersystem crossing;  $S_0$ ,  $S_1$ , and  $S_2$  are the ground and excited singlet states, respectively, and  $T_1$  is the excited triplet state.

$S_n$ ; the value of  $n$  refers to the electronic states 1, 2, etc. This transition occurs in approximately  $10^{-15}$  s. Most absorption transitions originate from the lowest vibrational level of the ground electronic state. This ground-to-excited singlet transition is responsible for the ultraviolet and visible absorption spectra observed for molecules.

During the time that the molecule is in the excited state, some energy in excess of the lowest vibrational energy level of that excited state can be rapidly dissipated by a radiationless process known as vibrational relaxation. This excess energy is absorbed by the solvent molecules in inelastic collisions with the excited molecule which occurs in  $10^{-11}$  to  $10^{-10}$  s. The excited molecule also can undergo a second type of radiationless transition from an upper electronic state to a lower one by a process known as internal conversion. This process can occur when a highly excited vibrational level of a lower singlet overlaps the occupied level. Internal conversion occurs generally in  $10^{-12}$  s.

If the excess energy of the excited state is not dissipated by collisions with other molecules, the electron may return to the ground electronic state with the emission of radiant energy. This transition,  $S_1 \rightarrow S_0$ , is known as fluorescence and occurs in  $10^{-10}$  to  $10^{-6}$  s following excitation. The emission usually results from the lowest excited electronic state  $S_1$ . This is known as Kasha's rule [1].

Intersystem crossing is another pathway which competes with fluorescence for deactivation of the excited singlet state. Intersystem crossing necessitates a change in the spin angular momentum which can occur when spin-orbital coupling is present. This change results in parallel electron spins, thereby causing the molecule to be in a triplet state ( $T_n$ ). Molecules in upper vibrational levels of the triplet state undergo vibrational relaxation and internal conversion to the lowest vibrational level of the lowest triplet state,  $T_1$ . These molecules can then return to the ground state by triplet-singlet intersystem crossing (quenching) or by the emission of light. This emission of light accompanying the  $T_1 \rightarrow S_0$  transition is termed phosphorescence. This process is a "spin forbidden" transition and is characterized by lifetimes on the order of  $10^{-4}$  to 10 s. The

two radiative transitions from excited energy levels,  $S_1$  and  $T_1$ , to the ground state,  $S_0$ , are discussed in more detail below.

### Fluorescence

Fluorescence is the radiative transition between an excited ( $S_n$ ) and ground ( $S_0$ ) singlet state. This transition is between two levels of the same spin multiplicity and occurs  $10^{-10}$  to  $10^{-6}$  s after excitation. The fluorescence most commonly observed in solutions is called Stokes fluorescence. The photons emitted are less energetic than the absorbed photons because of vibrational relaxation and internal conversion processes.

If thermal energy is applied to an excited state molecule, population of higher energy vibrational levels will result. Emission at a higher energy than the absorbed photons may then be observed. This is anti-Stokes fluorescence which is often observed in dilute gases at elevated temperatures. Because of the large energy difference between  $S_0$  and  $S_1$ , essentially no fluorophores will populate  $S_1$  as a result of thermal energy.

Resonance fluorescence occurs when the energy of the emitted radiation is the same as the absorbed energy. This type of fluorescence is not normally observed in solutions because of intense Rayleigh scattering at the excitation wavelength. However, it does occur in gases and crystals.

The fluorescence intensity observed ( $I_f$ ) can be derived from the Beer-Lambert law, (eq. 2-1):

$$I_f = I_0 \phi_f (1 - e^{-\epsilon b C}) f(\theta) g(\lambda), \quad (2-3)$$

where  $f(\theta)$  represents a geometrical factor that is determined by the solid angle of the fluorescing radiation viewed by the detector, and  $g(\lambda)$  defines the efficiency of the detector as a function of wavelength of the fluorescence incident on it. The fluorescence quantum yield,  $\phi_f$ , is the fraction of absorbed photons converted to fluorescence photons. This quantity is also related to the rate constants for fluorescence and competitive deactivation processes,  $k_f$  and  $k_d$ , respectively, by

$$\phi_f = \frac{k_f}{k_f + k_d} \quad (2-4)$$

The fluorescence quantum yield may approach unity in unique cases.

The exponential term in equation 2-3 can be expanded by the series approximation to yield

$$I_0 \phi_f (1 - e^{-\epsilon b C}) f(\theta) g(\lambda) = I_0 \phi_f (\epsilon b C - \frac{(\epsilon b C)^2}{2!} + \frac{(\epsilon b C)^3}{3!} - \dots + \frac{(\epsilon b C)^n}{n!}) f(\theta) g(\lambda) \quad (2-5)$$

For dilute solutions where the absorbance,  $\epsilon b C$  is small, equation 2-5 reduces to

$$I_f = I_0 \phi_f f(\theta) g(\lambda) \epsilon b C \quad (2-6)$$

or

$$I_f = \phi_f K C \quad (2-7)$$

where  $K = I_0 f(\theta) g(\lambda) \epsilon b$ . Therefore, at low analyte concentrations, where the absorbance of the solution is less than 0.005 in a 1 cm pathlength cell, the fluorescence intensity is linearly related to the analyte concentration to within a 1% deviation [5]. At higher concentrations, scattering at the emission wavelength as well as the inner-filter effect cause deviations from linearity. The inner-filter effect is caused by significant absorption of the excitation radiation, or by significant absorption of the emitted fluorescence when these processes occur within the volume element of illumination and observation of the cell.

### ***Fluorescence Lifetimes***

The lifetime of the lowest excited singlet state ( $\tau_f$ ) is also an important property of fluorescing molecules. The fluorescence lifetime is defined as

$$\tau_f = 1/(k_f + k_d) \quad (2-8)$$

and is the time required for the fluorescence intensity to fall to 1/e of its initial intensity.

The fluorescence intensity is related to the lifetime,  $\tau_f$ , by

$$I_f = I_f^0 (e^{-t/\tau_f}), \quad (2-9)$$

where  $t = 0$  is defined as the end of the excitation pulse and  $I_f^0$  is the fluorescence intensity at the time the excitation source is turned off. The fluorescence quantum yield and  $\tau_f$  are related by

$$\tau_f = \phi_f \tau_{N, f} \quad (2-10)$$

where  $\tau_{N, f} = 1/k_f$  is the natural lifetime of the excited state. This represents the lifetime of the fluorescing molecule if fluorescence were the sole pathway for deactivating the lowest singlet state.

The decay of fluorescence emission is predicted to be an exponential as shown in equation 2-9. Information that is useful in fundamental studies of energy transfer and quenching can be provided by lifetime measurements. The luminescence lifetime can be used to enhance selectivity or facilitate multicomponent determinations.

The primary goal of an experimental approach to lifetime determination is to obtain data reflecting the time dependence of the decay of the luminescence. For a sample consisting of only one fluorescing compound, the time-decay profile is described by equation 2-9. This equation can be linearized by taking the natural logarithm of both sides to obtain

$$\ln(I_f) = \ln(I_f^0) - t/\tau_f \quad (2-11)$$

Therefore, a plot of  $\ln(I_f)$  vs  $t$  should yield a slope of  $-1/\tau_f$ . This is called the *log slope method* and assumes that the luminescence signal decays to zero at infinite time [3]. The contributions of the dark signal, background luminescence, and electronic offsets are assumed to be negligible with respect to the analyte luminescence signal.

If the dark current term is not negligible, the *Guggenheim method* [4] may be used to accurately linearize first-order kinetic data. In this method, the natural logarithm of the difference in luminescence signals between pairs of data points along the decay curve, separated by a constant time interval, are plotted against time.

$$\ln(I_f' - I_f) = -t/\tau_f + \text{constant} \quad (2-12)$$

where  $I_f'$  is the fluorescence intensity made at time  $t + \Delta$ , and  $\Delta$  is a constant time increment. For best results,  $\Delta$  should be two to three lifetimes. The lifetime of the analyte is obtained from the negative reciprocal of the slope.

The *pulse excitation method* involves monitoring the luminescence decay after the analyte is excited with a short duration radiative pulse. If a pulsed source is not used the radiation from a continuous source must be gated with an external modulator. The true decay of the luminescence is observed if the excitation pulse width is much shorter than the luminescence lifetime [5]. Otherwise deconvolution methods must be used to obtain the luminescence decay.

*Time-correlated single-photon counting* is a widely used method for lifetime measurements. The time between the excitation pulse and the arrival of the first fluorescence photon is measured. The time of photon emission, although random, is weighted according to the decay kinetics of the lumiphore. Measuring the emission time for a large number of excitation pulses enables the fluorescence decay curve to be reconstructed. A true decay curve is obtained when the probability of observing more than a single luminescence photon per excitation pulse is very small. An average count rate of 0.01 - 0.05 photons emitted per excitation pulse is used. Although this technique has a resolution of about 0.2 ns, the low repetitive rate of the pulsed source and the large number of counts that must be accumulated require several hours to accumulate data.

Another class of lifetime measurements is based on the use of a continuous, sinusoidally modulated excitation source and phase sensitive detection apparatus [6]. This is called the *Phase Shift Method*. The finite lifetime of the excited state causes the modulated emission to be shifted in phase by an angle  $\phi$  relative to the excitation. The fluorescence lifetime  $\tau_f$  can be calculated from the phase shift and angular modulation frequency  $\omega$  ( $\omega = 2\pi f$  where  $f$  is the linear modulation frequency)

$$\tau_f = \omega^{-1} \tan(\phi) \quad (2-13)$$

or from the angular modulation frequency and the demodulation factor  $m$  ( $m = \cos(\phi)$ ),

$$\tau_f = \omega^{-1} \sqrt{(m^{-2} - 1)} \quad (2-14)$$

The quantities  $\phi$  and  $m$  can be measured relative to a signal from a scattering solution. In this case,  $m$  is the ratio of the modulation depth of the ac waveform of the fluorophore to that of the scattering solution [5]. Alternatively,  $\phi$  and  $m$  can be measured relative to a reference fluorophore of known lifetime.

### ***Quenching Effects on Fluorescence***

Quenching is the reduction of the fluorescence by competing deactivation processes. This results from interactions between a fluorophore and another species present in the system. Two types of quenching are recognized: static and dynamic quenching.

Static quenching occurs when an interaction takes place between the potentially fluorescent molecule, which is in the ground state, and the quenching species to form a nonfluorescent complex [7]. The efficiency of this process is governed by the formation constant of the complex as well as the concentration of the quencher. The association constant for the formation of the complex is given by

$$K_s = \frac{[FQ]}{[F][Q]} \quad (2-15)$$

where  $[FQ]$  is the concentration of the complex,  $[F]$  is the concentration of the non-complexed fluorophore, and  $[Q]$  is the concentration of the quencher. Since the complex species is nonfluorescent, the fraction of fluorescence which remains is given by  $f = I_f/I_{f,0}$ , where  $I_{f,0}$  is the fluorescence intensity in the absence of quencher. The total concentration of the fluorophore  $[F]_0$  is given by

$$[F]_0 = [F] + [FQ], \quad (2-16)$$

If equation 2-16 is substituted into equation 2-15 and fluorescence intensities are used instead of fluorophore concentrations, the result is

$$I_{f,0}/I_f = 1 + K_s[Q] \quad (2-17)$$

It can be seen from equation 2-17 that there is a linear relationship between the ratio of fluorescence intensities, in the absence and presence of quencher, and the concentration of the quencher.

Dynamic quenching occurs when the quenching species and the excited molecule collide, and energy is transferred with no resulting radiation. This effect is summarized in the Stern-Volmer equation:

$$\phi/\phi_0 = \frac{1}{1 + k_q\tau_0[Q]} \quad (2-18)$$

where  $k_q$  is the bimolecular quenching constant,  $\phi_0$  and  $\phi$  are the quantum yields of fluorescence in the absence and presence of the concentration of quencher, respectively, and  $\tau_0$  is the lifetime of the fluorophore in the absence of the quencher. This equation can be expressed as

$$I_{f,0}/I_f = 1 + k_q\tau_0[Q] = 1 + K_D[Q]. \quad (2-19)$$

where  $K_D = k_q\tau_0$  is the Stern-Volmer quenching constant. Quenching data are often presented as a plot of  $I_{f,0}/I_f$  versus  $[Q]$  since equation 2-19 predicts a linear relationship. In such a plot the y intercept is unity and the slope is equal to  $K_D$ . A linear Stern-Volmer plot generally indicates a single class of fluorophores, all of which are accessible to the quencher [8].

It must be noted that the dependence of  $I_{f,0}/I_f$  on  $[Q]$  is identical for both static and dynamic quenching, equations 2-17 and 2-19. Fluorescence quenching data obtained from intensity measurements alone cannot determine whether static or dynamic quenching is occurring. Fluorescence lifetime measurements are the most definitive method for distinguishing the quenching mechanism. In static quenching the complexed fluorophores are nonfluorescent, and the only fluorescence observed is from the non-complexed fluorophore. Therefore, the observed lifetime is unaffected by the quencher. However, in dynamic quenching, the lifetime will decrease because quenching is an additional process which depopulates the excited state without the emission of radiation.

It can be seen from equation 2-17 that there is a linear relationship between the ratio of fluorescence intensities, in the absence and presence of quencher, and the concentration of the quencher.

Dynamic quenching occurs when the quenching species and the excited molecule collide, and energy is transferred with no resulting radiation. This effect is summarized in the Stern-Volmer equation:

$$\phi/\phi_0 = \frac{1}{1 + k_q\tau_0[Q]} \quad (2-18)$$

where  $k_q$  is the bimolecular quenching constant,  $\phi_0$  and  $\phi$  are the quantum yields of fluorescence in the absence and presence of the concentration of quencher, respectively, and  $\tau_0$  is the lifetime of the fluorophore in the absence of the quencher. This equation can be expressed as

$$I_{f,0}/I_f = 1 + k_q\tau_0[Q] = 1 + K_D[Q]. \quad (2-19)$$

where  $K_D = k_q\tau_0$  is the Stern-Volmer quenching constant. Quenching data are often presented as a plot of  $I_{f,0}/I_f$  versus  $[Q]$  since equation 2-19 predicts a linear relationship. In such a plot the y intercept is unity and the slope is equal to  $K_D$ . A linear Stern-Volmer plot generally indicates a single class of fluorophores, all of which are accessible to the quencher [8].

It must be noted that the dependence of  $I_{f,0}/I_f$  on  $[Q]$  is identical for both static and dynamic quenching, equations 2-17 and 2-19. Fluorescence quenching data obtained from intensity measurements alone cannot determine whether static or dynamic quenching is occurring. Fluorescence lifetime measurements are the most definitive method for distinguishing the quenching mechanism. In static quenching the complexed fluorophores are nonfluorescent, and the only fluorescence observed is from the non-complexed fluorophore. Therefore, the observed lifetime is unaffected by the quencher. However, in dynamic quenching, the lifetime will decrease because quenching is an additional process which depopulates the excited state without the emission of radiation.

Absorption spectra can also be used to distinguish static and dynamic quenching of the fluorophore. Collisional quenching only affects the excited states of the fluorophore; therefore, no changes in the absorption spectra are predicted. However, complexation by static quenching will result in perturbations in the absorption spectrum of the fluorophore [8].

Dynamic and static quenching also can be distinguished by the effect of temperature on the fluorescence intensity. Because dynamic quenching depends upon molecular diffusion, higher temperatures will result in larger diffusion coefficients which will decrease the observed fluorescence. In contrast, increased temperatures are likely to decrease the stability of the fluorophore-quencher complex in static quenching. This will then lower the value of the static quenching constant and result in an increased fluorescence intensity being observed at higher temperatures.

### **Phosphorescence**

As was mentioned earlier, phosphorescence is the radiation emitted when a molecule in the lowest vibrational level of the first excited triplet state returns to the ground singlet state,  $T_1 \rightarrow S_0$ . Population of the triplet state occurs via intersystem crossing from an excited singlet state (see Figure 2.1). Once the molecule is in the triplet state it will undergo vibrational relaxation and internal conversion to the lowest vibrational level. This is also consistent with Kasha's rule.

In the ground state of unsaturated organic compounds, two  $\pi$  electrons with antiparallel spins occupy the orbitals of lowest energy. When a molecule is raised to an excited energy level, an electron is promoted to an orbital that was previously unoccupied. In this instance, the spin-angular momenta of the two electrons are no longer restricted by the Pauli principle and their spins may be either antiparallel (singlet state) or parallel (triplet state). At the instant of excitation, only electrons are reorganized; the heavier nuclei keep their ground state geometry. This is a result of the

Franck-Condon principle which states that electronic transitions occur without a change in position of the nuclei.

Intersystem crossing can be made favorable when there is strong spin-orbital coupling in which the orbital motion of the electron induces a magnetic field that interacts with its spin magnetic moment. This interaction "flips" the spin of the electron [9]. This effect is very weak unless the electron has a high probability density near the nucleus. Typically only atoms with high nuclear charges (heavy atoms) exhibit appreciable spin-orbital coupling. This heavy atom effect is partially responsible for the population of the triplet state which leads to phosphorescence. Because of the spin forbidden nature of the  $T_1 \rightarrow S_1$  transition, the lifetime of the triplet state can be quite long and is typically  $10^{-4}$  to 10 s. Because of this long lifetime, the triplet state is readily quenched by collision with solvent molecules or dissolved oxygen. However, in a rigid matrix it can survive for longer periods of time and lose energy only by the emission of radiation.

In phosphorescence there are many nonradiative processes which compete for deactivation of the triplet state. The probability of radiative or nonradiative transitions can be described by their corresponding rate constants: rate constant for fluorescence,  $k_f$ ; rate constant for fluorescence quenching,  $k_{fq}$ ; rate constant for intersystem crossing,  $k_{isc}$ ; rate constant for phosphorescence,  $k_p$ ; and rate constant for phosphorescence quenching,  $k_{pq}$ . The efficiency for triplet state formation from  $S_1$  is

$$f_T = \frac{k_{isc}}{k_{isc} + k_f + k_{fq}} \quad (2-20)$$

Therefore, the phosphorescence quantum efficiency can be defined as

$$\phi_p = f_T \frac{k_p}{k_p + k_{pq}} \quad (2-21)$$

or

$$\phi_p = \frac{k_{isc}}{k_{isc} + k_f + k_{fq}} \frac{k_p}{k_p + k_{pq}} \quad (2-22)$$

The relatively long lifetime of the triplet state renders it quite susceptible to the many deactivations processes competing with phosphorescence. In the gas phase and in solution  $k_{pq} \gg k_p$ , the phosphorescence yield is subsequently very low and  $\phi_p$  becomes vanishingly small. Low temperature rigid matrices, high viscosity solvents, or solid substrates can be used to decrease the quenching processes and consequently increase the phosphorescence yield.

The relationship between the phosphorescence intensity and the concentration of the phosphor is similar to that obtained for fluorescence (see eq. 2-7):

$$I_p = K' \phi_p C \quad (2-23)$$

where  $K' = I_0 f(\theta) g(\lambda) \epsilon b$ . Therefore, the phosphorescence intensity is linearly related to the concentration of the phosphor.

### ***Phosphorescence Lifetimes***

The phosphorescence lifetime is defined similarly to that of fluorescence

$$\tau_p = 1/(k_p + k_d) \quad (2-24)$$

and is the time required for the phosphorescence intensity to decrease to  $1/e$  of its original intensity following excitation. The rate constant  $k_d$  represents the summation of all nonradiative rate constants. The phosphorescence intensity at time  $t$  is related to  $\tau_p$  by

$$I_p = I_p^0 (e^{-t/\tau_p}) \quad (2-25)$$

where  $I_p$  is the phosphorescence intensity at time  $t$  and  $I_p^0$  is the phosphorescence intensity at  $t = 0$ .

Phosphorescence can be differentiated from fluorescence by its longer lifetime. Fluorescence lifetimes of organic molecules are on the order of  $10^{-10}$  to  $10^{-6}$  s whereas phosphorescence lifetimes range from  $10^{-4}$  s to 10 s. This difference is the basis of the time- and phase-resolved techniques that are used to differentiate components of a mixture exhibiting similar spectra, but different lifetimes.

### ***Oxygen Quenching***

The triplet nature of the ground state of molecular oxygen contributes significantly to the collisional deactivation of phosphorescence [10]. Several theoretical models pertaining to the effect of oxygen on phosphorescence have been proposed. McGlynn, Azumi, and Kinoshita have treated the effect of oxygen as an intermolecular exchange interaction [9]. A mechanism has been described by Murrell by which the enhanced ground state to triplet state absorption intensity is borrowed from a charge-transfer transition of the aromatic-O<sub>2</sub> complex [11]. The concept of a "contact charge transfer" mechanism has been developed by Tsubomura and Mulliken [12]. In this mechanism the interaction between oxygen and the aromatic compound can occur in the absence of definite complex formation. A theoretical study of the quenching of the triplet state by molecular oxygen was performed by Kawaoka et al. where it was concluded that the most likely quenching mechanism deactivates the molecule from the triplet state to the ground singlet state while oxygen undergoes a transition from its ground triplet state to an excited singlet state [13].

The long triplet lifetime of phosphorescence induces an excessive oxygen quenching effect. Although oxygen quenches fluorescence, the effect is not nearly so dramatic as is observed in phosphorescence. The collisional quenching mechanism can be described by the Stern-Volmer equation for phosphorescence (see eqns. 2-18, 2-19). For a given quenching process with a quenching rate constant  $k_q = 10^8 \text{ mol L}^{-1} \text{ s}^{-1}$ , a quencher concentration  $[Q] = 10^{-3} \text{ M}$  and a fluorescent lifetime  $\tau_f = 10^{-8} \text{ s}$ , the emitted fluorescence intensity will decrease by only 0.1%. Under the same conditions, with a phosphorescence lifetime of  $\tau_p = 10^{-1} \text{ s}$ , the emitted phosphorescence intensity will suffer a decrease of 99.9%. Therefore, for oxygen sensitive systems following the Stern-Volmer equation, it is essential that the sample be deoxygenated prior to the phosphorescence intensity measurement.

### ***Heavy Atom Effect in Phosphorescence***

It has already been noted that the heavy atom effect is the mechanism by which the probability of the  $S_1 \rightarrow T_1$  intersystem crossing is enhanced. The heavy atom effect was first reported by Kasha where a mixture of two colorless pure liquids,  $\alpha$ -chloronaphthalene and ethyl iodide, produced a yellow color with no chemical reaction occurring [14]. The color effect was due to the development of the  $S_1 \rightarrow T_1$  absorption band. He attributed this effect to collisional perturbation of spin-orbital coupling. This phenomenon, which is known as the "external heavy atom effect," is distinguished from the "internal heavy atom effect" in which the heavy atoms are chemically bonded with the compound [15]. The external heavy atom effect is not as pronounced as internal heavy atom coupling which is expected [16,17]. The internal heavy atom effect increases the phosphorescence emission by increasing the  $S_1 \rightarrow T_1$  intersystem crossing rate and also by reducing collisional deactivation due to decreased phosphorescence lifetimes.

The external heavy atom effect generally produces the following effects [9]: an increase in the  $S_0 \rightarrow T_1$  absorption, a decrease in the phosphorescence lifetime, a decrease in the fluorescence quantum yield,  $\phi_f$ , and an increase in the phosphorescence quantum yield,  $\phi_p$ . Although the heavy atom effect increases the rates of both  $T_1 \rightarrow S_0$  intersystem crossing and  $T_1 \rightarrow S_0$  phosphorescence, the effect is usually greater on the latter producing a net increase in  $\phi_p$  [18].

Two major coupling mechanisms have been proposed to explain the external heavy atom effect for aromatic compounds. Robinson [19] proposed an "exchange mechanism" in which the perturbed triplet state borrows radiative intensity from a spin-forbidden transition that is usually localized on the heavy atom. The extent of mixing of the heavy atom triplet states depends on the extent of exchange interaction between the triplet electron pair of the aromatic molecule and the electrons associated with an excited triplet state of the heavy atom. Murrell [20] and Tsubomura and Mulliken [12] proposed

a "charge-transfer" mechanism which involves interaction of the excited triplet states with the charge-transfer-excited singlet state of the aromatic-heavy atom complex.

A major disadvantage of using alkyl halides to obtain the heavy atom effect is that they begin to absorb strongly in the region from 300-350 nm. Therefore, they can absorb a substantial fraction of the energy required to promote the formation of the  $T_1$  state which leads to phosphorescence.

## CHAPTER II REFERENCES

1. Kasha, M., *Diss. Far. Soc.*, **1950**, *9*, 14
2. Wehry, E.L.; in Guilbault, G.G., *Practical Fluorescence: Theory, Methods, and Techniques*; Marcel Dekker: NY, 1973, Chapter 3
3. Demas, J.N., *Excited State Lifetime Measurements*, Academic Press; NY, 1983, p. 75
4. Guggenheim, E.A., *Philos. Mag.*, **1926**, *2*, 538
5. Ingle, J.D.; Crouch, S.R., *Spectrochemical Analysis*, Prentice-Hall, 1988; Chapter 12
6. Lakowicz, J.R. *Principles of Fluorescence Spectroscopy*; Plenum Press: NY, 1983, Chapter 3
7. Schulman, S.G. in *Molecular Luminescence Spectroscopy: Methods and Applications: Part I*; Elving, P.J.; Winefordner, J.D.; Kolthoff I.M., Editors, John Wiley & Sons, NY, 1985
8. Lakowicz, J.R., *op. cit.*, Chapter 9
9. McGlynn, S.P.; Azumi, T.; Kinoshita *Molecular Spectroscopy of the Triplet State*, Prentice-Hall, Englewood Cliffs, N.J., 1969
10. Birks, J.B. *Photophysics of Aromatic Molecules*, Wiley-Interscience, London, 1970, pp. 499-504
11. Murrell, J.N., *Mol. Phys.*, **1960**, *3*, 319
12. Tsubomura, H.; Mulliken, R.S., *J. Am. Chem. Soc.*, **1960**, *82*, 5966
13. Kawaoda, K.; Khan, A.U.; Kearns, P.R., *J. Chem. Phys.*, **1967**, 1842
14. Kasha, M., *J. Chem. Phys.*, **1952**, *20*, 71
15. McClure, D., *J. Chem. Phys.*, **1949**, *17*, 905
16. McGlynn, S.P.; Sunseri, R.; Christodouleas, J., *J. Chem. Phys.*, **1962**, *37*, 1818
17. Nag-Chaudhuri, J.; Stoessel, L.; McGlynn, S.P., *J. Chem. Phys.*, **1963**, *38*, 2027
18. Giachino, G.G.; Kearns, D.R., *J. Chem. Phys.*, **1970**, *52*, 2964
19. Robinson, G.W., *J. Chem. Phys.*, **1967**, *46*, 572
20. Murrell, J.N., *Mol. Phys.*, **1960**, *3*, 319

## **CHAPTER III**

### **ROOM-TEMPERATURE PHOSPHORESCENCE**

This chapter is an introduction to room temperature phosphorescence (RTP). The various RTP techniques to provide a controlled microenvironment for the luminophore are introduced and discussed individually. These RTP techniques are solid-surface, sensitized, microcrystalline and colloidal, cyclodextrin-induced, and micelle-stabilized.

Following the discussion of the RTP techniques, the methods of deoxygenation commonly used with RTP are introduced: inert gas purging, freeze-pump-thaw, vacuum preparation, the use of semi-permeable membranes, and chemical scavenging.

#### **Introduction to Room Temperature Phosphorescence**

Traditionally phosphorescence is performed in rigid media at liquid nitrogen temperature (77 K) to minimize the effects of quenchers in solution. The lack of widespread use of low temperature phosphorescence (LTP) can be attributed to the need for cryogenic equipment and the problems involved with introducing the sample into the phosphorimeter. Sample preparation involves lowering a long quartz capillary cell into a quartz Dewar flask filled with liquid nitrogen. The rate of cooling of the sample cell and the chemical nature and composition of the solvent system will determine whether the cooled matrix will be a clear glass, a cracked glass, or a snow. Thus, the selection of the proper solvent is critical; it should form a clear glass at 77 K and have a low phosphorescence background. The analyte should be readily soluble in the solvent at 77 K. The most common solvent for nonpolar compounds is a mixture of ethanol,

isopentane, and diethyl ether in a volume proportion of 2:5:5. This solvent mixture is commonly known as EPA [1]. The solvents should be purified to remove compounds that phosphoresce.

The major advantages of LTP are the low detection limits (in the nanomolar range), the linearity of calibration curves (linear over several decades of concentration), and the high degree of selectivity. This selectivity results from the choice of excitation and emission wavelengths and temporal discrimination which can be used to distinguish phosphorescence from fluorescence and analyte phosphorescence from that of other phosphorescent molecules.

The time required for sample preparation for LTP measurements and the equipment required for working at cryogenic temperature has prompted interest in RTP techniques. Perhaps the first observation of RTP was made by Millson in 1944 [2]. He noted that various cottons, and many other fibers, phosphoresced at room temperature when "bone dry". In 1958 Brown [3] observed RTP of naphthiminazole on a paper chromatogram. The brilliant yellow phosphorescence lasted for several seconds after the removal of the excitation radiation. This report may have been overlooked in the literature because this observation was incidental to the main topic of his paper and was not mentioned in the summary. In 1967 Roth [4] reported a study of the RTP of more than 18 compounds adsorbed on several supporting media. The phosphorescence of all phosphorescent molecules lasted for several seconds after withdrawal of the excitation radiation. It is possible that other phosphorescent molecules were overlooked either because of their shorter lifetimes or because the excitation wavelength was inappropriate for the low-pressure mercury lamp used as a light source. In this paper, Roth emphasized the value of the technique as a simple, selective, and non-destructive detection method for paper chromatography and electrophoresis. Although Roth appears to be the first to recognize the generality of RTP in an analytical context [5], credit for the discovery of RTP of molecules adsorbed on a solid support is attributed to

Schulman and Walling in 1972 [6,7]. They reported RTP emission from salts of a wide variety of polynuclear carboxylic or sulfonic acids, phenols, and amines adsorbed on paper, silica, alumina and other supports. The phosphorescence was observed only with ionic compounds. The technique is oxygen insensitive but requires thorough drying. The emission and excitation spectra are very similar to those observed at 77 K, although the spectra did exhibit a loss of fine structure and the lifetimes were shorter.

Recently, several different RTP methods have been discovered and developed into analytical techniques. Of these, solid-surface RTP [8], micelle-stabilized RTP [9], and cyclodextrin-induced RTP [10] all employ an interaction of the analyte with its immediate environment (the substrate to which the analyte is adsorbed, or the micelle or cyclodextrin cavity). This minimizes the quenching pathways which normally deactivate the triplet state at room temperature by radiationless means. A fourth RTP method, sensitized RTP, uses the energy transfer from a donor analyte to an acceptor molecule which readily phosphoresces at room temperature [11]. Biacetyl and 1,4-dibromonaphthalene are two commonly used acceptor molecules. A fifth RTP technique has been reported which employs microcrystalline or colloidal suspensions [12,13]. These techniques are discussed individually below.

### **Solid-Surface RTP**

In 1974 Winefordner et al. [8] initiated a broad research effort to establish the general use of RTP as an analytical technique. This group reported the first analytical studies of solid-surface RTP and found that the limits of detection for various naphthalene sulfonic acids on filter paper were competitive with other methods. The linear dynamic ranges for many of the compounds were found to be limited because the filter paper used as a solid substrate exhibited a phosphorescence background; this raised the limit of detection and lowered the linear dynamic range of the compounds.

The number of ionic sites on a molecule is an important factor in producing solid-surface RTP [14]. Although 2-naphthol has a polar hydroxyl group, RTP was not observed for this compound adsorbed on paper. However, intense RTP was observed for its ionic form, sodium 2-naphthoxide [15,16]. The ratio of RTP to LTP was found to be less than one for all compounds tested, but the ratio was the highest for doubly charged species in 1 M NaOH [14]. Uncharged species such as sulfguanidine and 5-acetyluracil showed the lowest RTP/LTP ratios. This was interpreted to indicate that hydrogen bonding was an active force in immobilizing the analyte [17]. This theory was supported by the discovery that the RTP signal was proportional to the surface concentration of -OH groups. Phosphorescence emission was drastically decreased for some compounds spotted on smooth, chemically inert substrates such as polyethylene fiber, borosilicate fiber, or silanized paper. The silanization process reduces the number of hydroxyl groups on the paper which diminishes the extent of hydrogen bonding between the analyte and the support. The addition of sugars to the support paper to enrich the hydroxyl concentration provided a substantial enhancement in the phosphorescence signal and lengthened the observed lifetime [18]. This was supported by the discovery that the lifetime increased when the sample was prepared from a basic solution causing it to be deposited as the salt which can be more tightly bound.

Background luminescence has been one of the major drawbacks of solid-surface RTP. Attempts to reduce the background emission from paper have been described by Ward et al. [19]. Attempts at washing the contaminants from the paper have met with little success [20,21]. Bateh and Winefordner [20] attempted to photobleach the lignins or hemicelluloses believed to be the source of the background. They then concluded that such a pretreatment improved the adsorption characteristics of the filter paper but did not significantly reduce the phosphorescence background.

Nonuniformity in the surface of the filter paper substrate may also contribute to systematic and random errors in the phosphorescence measurement. Bateh and

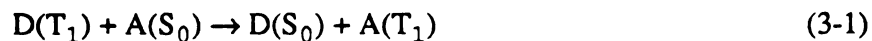
Winefordner [20] conducted a comparison of various lots of filter paper and found that the quality was sufficiently consistent for use in RTP applications. Lot-to-lot variation with paper is seldom noticed since one RTP assay requires such a small amount of paper (0.6 cm diameter circle) that it takes a very large number of measurements to use up an entire lot.

The heavy atom effect has been found to significantly enhance the RTP signals of polynuclear aromatic hydrocarbons [22]. The observed trend is  $Tl^+ > Ag^+ > Pb^{2+} > Hg^{2+}$ ; thallium ion also produced enhancements on several spectral features of the emission bands. The addition of 1.0 M NaI increased the RTP emission from naphthalene sulfonates adsorbed on filter paper approximately 50-fold while decreasing the fluorescence by about 95% [23,24]. A remarkable enhancement of solid-surface RTP by 1.0 M NaI was observed for tryptophan (455-fold), its methyl ester (340-fold), and for indole (370-fold) [25]. For a more comprehensive discussion of the external heavy atom effect on solid-surface RTP the reader is referred to a recent monograph by Vo-Dinh [26].

Other substrates used for solid-surface RTP include paper lint, ion exchange paper, alumina, silica gel, asbestos, sodium acetate, sucrose, starch, chalk, inorganic substrates, and polymer-salt mixtures. Since filter paper appears to be the most favorable substrate [27], these other supports will not be discussed here.

### Sensitized RTP

In sensitized RTP the analyte is detected indirectly via the phosphorescence of an acceptor in liquid solution at room temperature. After excitation, the weakly (or non-) phosphorescent analyte acts as an energy donor and transfers its triplet state energy to an acceptor [28];



In this equation D is the donor, A is the acceptor, and  $T_1$  and  $S_0$  are the triplet and ground states, respectively. A suitable acceptor should have a high phosphorescence quantum efficiency in liquid solutions, a triplet energy lower than that of the donor, and a low molar absorptivity at the excitation wavelength of the donor. Commonly used acceptors are biacetyl and 1,4-dibromonaphthalene. The role of the absorption spectrum of the acceptor molecule in sensitized RTP has prompted interest in biacetyl as an acceptor because of its very low molar absorptivity over a large wavelength region [28].

The intensity of sensitized RTP in liquid due to a donor-acceptor couple is given by

$$P(\text{sens}) = kI_{\text{ex}}(2.3\epsilon^{\text{D}}[D]l)\theta_{\text{ISC}}^{\text{D}}\theta_{\text{t}}^{\text{DA}}\theta_{\text{p}}^{\text{A}}S_{\text{p}}^{\text{A}} \quad (3-2)$$

where  $P(\text{sens})$  is the photomultiplier output for uncorrected spectra,  $k$  is an instrumental constant independent from the excitation and emission wavelengths,  $I_{\text{ex}}$  is the intensity of the excitation light source at the excitation wavelength,  $\epsilon^{\text{D}}$  is the molar absorptivity of the donor D at the excitation wavelength,  $[D]$  is the donor concentration,  $l$  is the optical pathlength,  $\theta_{\text{ISC}}^{\text{D}}$  is the intersystem crossing efficiency of the donor,  $\theta_{\text{t}}^{\text{DA}}$  is the energy transfer efficiency,  $\theta_{\text{p}}^{\text{A}}$  is the phosphorescence efficiency of the acceptor, and  $S_{\text{p}}^{\text{A}}$  is a dimensionless parameter related to the wavelength dependence of the detector [28].

Sensitized RTP is an indirect method in which only the excitation characteristics of the analyte play a role. Direct excitation of the acceptor must be avoided since it would lead to a background phosphorescence. All analyte compounds are detected at the characteristic wavelength of the acceptor molecule. Thus, effects of stray light and fluorescence background are reduced [28].

### Microcrystalline and Colloidal RTP

Colloidal or microcrystalline RTP was discovered during the course of characterizing microcrystalline suspensions [29,30]. This effect was observed initially

for biphenyl. These systems are produced by adding the solute as a concentrate dissolved in a water-miscible solvent. With rapid addition a uniform dispersion is obtained which can remain suspended for several weeks in a glass container. This method requires minimal sample preparation; deaeration to remove oxygen is not required.

The microcrystals appear to act in a manner analogous to interactions in solid-surface RTP in that the quenching pathways normally observed at room temperature are minimized. The microcrystals act as their own substrates and provide stability to the triplet state. The lifetimes observed were shorter than for analogous solutions at 77 K or for micelles [29,30]. However, the analytical utility of this phenomenon appears to be limited as the concentration dependence of the RTP was found to be non-linear.

### **Cyclodextrin Enhanced RTP**

Cyclodextrins (CDs) are macrocyclic carbohydrates produced by the bacterial degradation of starch. They are used in biochemistry research to mimic enzymes [31]. The cyclodextrin molecules consist of six, seven, or eight glucose monomers arranged in a torus and are denoted as  $\alpha$ -,  $\beta$ -, and  $\gamma$ -cyclodextrin, respectively. The CD has a rigid conical molecular structure with a hollow interior. The inner diameters are 6 Å for  $\alpha$ -CD, 8 Å for  $\beta$ -CD, and 10 Å for  $\gamma$ -CD [32]. A simplified structural representation of a CD is shown in Figure 3.1.

The interior cavity of the CD, which is hydrophobic in nature, can contain one or more highly energetic water molecules. This situation is thermodynamically unfavorable partially because of the repulsive effect of the polarity of the water molecule(s) with the CD interior. Thus, when less polar species are introduced into the CD solution they will easily enter the cavity of the CD if they satisfy the size criterion of fitting at least partially into the CD interior. Water in the interior of the CD will then

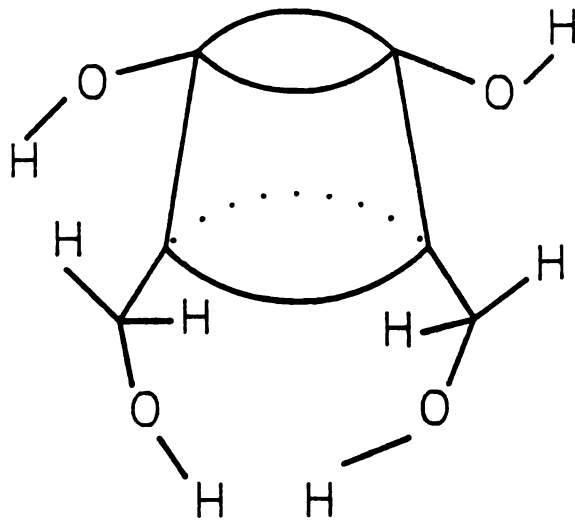


Figure 3.1. Simplified representation of a cyclodextrin molecule.

be expelled into the bulk phase. This will result in an inclusion complex of the less polar species and the CD. Typically, a one-to-one complex is formed [33-35].

The CD provides favorable microenvironment polarity and decreased degrees of freedom in molecular motion; it shields the excited state lumiphore from interferences from molecular oxygen and ionic species in the bulk solution. The first reports of cyclodextrin-enhanced RTP (CD-RTP) appeared in 1982. Turro reported that CD-RTP of 1-chloro and 1-bromonaphthalene was observed in deoxygenated solutions [36]. They found that the phosphorescence emission was substantially shielded from nitrite quenching, and the lifetimes were enhanced by the addition of 10% acetonitrile. Shortly thereafter, they observed CD-RTP of 4-bromo-1-naphthoyl in aqueous  $\gamma$ -CD under 1 atmosphere of oxygen [37].

It was at this time that CD-RTP caught the interest of Cline Loves's group who evaluated it for its analytical applications [38,39]. They reported CD-RTP for several non-heavy-atom containing polynuclear aromatic hydrocarbons and found that the addition of an external heavy atom was found to be necessary to obtain CD-RTP. In fluid solutions at room temperature, singlet emission is the dominant pathway for deactivation without a mechanism for enhanced spin orbital coupling and in the presence of oxygen. Cline Love and coworkers [38,39] obtained the external heavy atom effect in the aqueous cyclodextrin solutions by adding 1,2-dibromoethane (DBE). Apparently DBE is small enough to be able to fit easily into the CD cavity and sufficiently nonpolar that it partitions readily out of the polar aqueous phase into the CD. The proposed mechanism for CD-RTP involves the formation of a termolecular complex between the CD, the haloalkane, and the lumiphore [38].

Although other nonionic sources of bromine may be more effective in inducing CD-RTP, they were found not to be useful due to their limited water solubilities and/or their sizes [38]. The addition of DBE to a solution of phenanthrene in  $\beta$ -CD quenched over 90% of the fluorescence and allowed the phosphorescence to be observed. It

should be noted here that DBE is reported to be a known mutagen and potential carcinogen; it should be handled with extreme care [40].

Because the CD cavity has a specific volume, it is possible to discriminate against molecules of different sizes based on the steric requirement that the lumiphore must fit at least partially into the CD cavity. There must also be sufficient volume available for the inclusion of DBE to enhance the triplet emission. These criteria can be used as a selective means of analysis based on the molecules size and shape as well as its hydrophobicity. The volume of the CD must be such that the termolecular complex can be formed if CD-RTP is to be observed.

The ubiquitous nature of paramagnetic oxygen must be considered in fluid solutions where there is no rigid matrix. The lumiphore/CD inclusion complex shields the excited state from quenchers in solution. The effect of oxygen on the triplet state of a complexed molecule was first studied by Turro for brominated naphthalene derivatives [37]. Cline Love has shown that 10-40% of the RTP signal remains after the sample is aerated [38]. Therefore, CD-RTP is at least partially immune to the quenching effect of molecular oxygen.

### **Micelle-Stabilized RTP**

Surfactants are molecules having a hydrophobic group and a highly charged hydrophylic group. The word *surfactant* is a syncope of **surface active agents**. The hydrophobic backbone of the surfactant can vary in length from eight to twenty carbons and the hydrophylic portion can be a partially dissociable carboxylate, a fully ionized moiety such as anionic sulfate or cationic trimethyl ammonium plus a counterion, or an uncharged polar species such as polyethylene glycol. At low concentrations in solution the surfactant exists mostly as monomers, although dimers, trimers, etc. can also exist. As the concentration is increased a specific concentration is reached, the critical micelle concentration (CMC), at which point the monomers aggregate to form a micelle; for

sodium dodecyl sulfate (SDS), a typical surfactant used for micellar assemblies in RTP, the CMC has been found to be  $8.0 \times 10^{-3}$  M [41]. Micelles are roughly spherical in shape and consist typically of 60 - 100 monomers. The number of monomers incorporated into a micelle is the aggregate number; for SDS the aggregate number has been reported to be 71 [41]. The radius of the micelle is approximately equal to the length of a fully extended hydrophobic group, surrounded by an outer region containing the hydrated hydrophilic groups and bound water. As the concentration of the surfactant is increased above the CMC more micelles are formed. The concentration of the micelles in solution can be calculated by

$$[\text{micelle}] = \frac{[\text{surfactant}] - \text{CMC}}{\text{aggregate number}} \quad (3-3)$$

The macroscopic solution properties of micellar solutions approximate a truly homogeneous solution; they cannot be filtered using conventional methods, and they do not cause measurable light scattering in conventional spectrometry [42].

In aqueous solution, the hydrophobic region of the surfactant forms the interior of the micelle with the polar group oriented outward toward the polar solvent. In organic solvents a reverse micelle can be formed where the polar group of the surfactant forms the interior of the micelle. These moieties are represented in Figure 3.2.

The micelle is an organized assembly that is in dynamic equilibrium with the bulk solvent phase. The dissociation rate constant for surfactant monomers is on the order of  $10^5 - 10^9 \text{ s}^{-1}$  and is strongly dependent on the length of the hydrocarbon chain. The association rate constant is nearly diffusion controlled with a rate constant on the order of  $10^8 - 10^9 \text{ M}^{-1} \text{ s}^{-1}$  [43].

Aqueous micellar solutions in concentrations above their CMC can increase dramatically the solubility of hydrophobic compounds (probe molecules) which are normally nearly insoluble in aqueous solutions. For example, the solubility of pyrene is increased five orders of magnitude over its normal water solubility in a 0.1 M sodium dodecyl sulfate solution [42]. The probe is in the same phase as the micelle solution

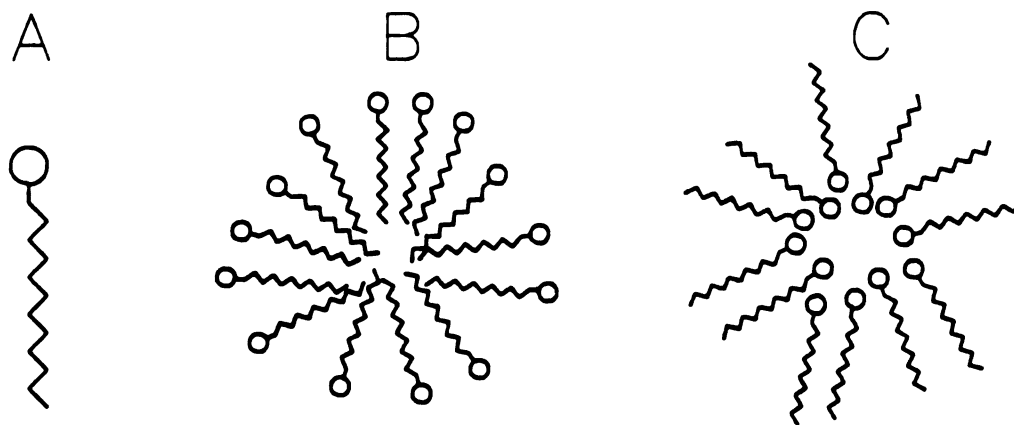


**Figure 3.2.** A) Simplified representation of a surfactant monomer.  
B) Anionic micelle in aqueous solvent.  
C) Reverse micelle.

which results in a thermodynamically stable system [44]. In general, the less soluble the probe is in water, the stronger its association with the micelle aggregate.

The micellar environment tends to shield the probe molecule located within the assembly from reaction with species located in the bulk aqueous phase [45]. The micelle provides sufficient protection for the triplet state of the probe molecule so that phosphorescence can be observed at room temperature. Kalyansundaram, Grieser, and Thomas [45] reported the first observation of RTP in micelles. They attributed the observation of Micelle-Stabilized RTP (MS-RTP) to the protective screening of the probe by the micelle assembly. The solutions were degassed by bubbling oxygen-free nitrogen gas through the samples for 30 minutes. Traces levels of oxygen ( $<10^{-6}$  M) were found to quench effectively the phosphorescence emission because oxygen readily penetrates the micelle. MS-RTP was reported for several ionic micelle systems and phosphorescent lifetimes in the millisecond range were observed.

Kalyansundaram, Grieser, and Thomas [45] also found that in anionic micelles, hydrophilic quenchers such as  $\text{Cu}^{2+}$  and  $\text{Tl}^{+}$  are located at the surface of the micelle. This promotes efficient quenching at the micelle-water interface. The cupric ion was found to reduce both the lifetime and the phosphorescence yield whereas the thallos ion decreased the lifetime while increasing the yield. The heavy-metal can act as a counterion to the anionic micelle and be held in close proximity to the negatively charged polar group. The micelle can therefore organize the reactants (the probe and the thallium heavy-metal) on a molecular scale which raises the effective concentration of the heavy-metal and increases the probability of spin orbital coupling [46]. Phosphorescence of halogenated compounds showed a less pronounced external heavy atom effect, which indicates that the halogen atom was operating as an internal heavy atom. Similar effects were observed by Turro et al. [47] and Humphry-Baker et al. [48]. Humphry-Baker et al. reported dramatic increases in the phosphorescence of pyrene and

naphthalene in anionic surfactant solutions with  $\text{Ag}^+$  as the counterion. This indicated that the silver counterion facilitated spin orbital coupling by the heavy atom effect.

Almgren, Grieser, and Thomas [41] used MS-RTP to study the dynamics of solubilization of biphenyl, naphthalene, and 1-methylnaphthalene in ionic micellar solutions. The exit rates for these compounds were found to be  $>5 \times 10^4 \text{ s}^{-1}$ . The exit rate of 1-bromonaphthalene from SDS was found to be  $2.5 \times 10^4 \text{ s}^{-1}$  and the diffusion-controlled entrance rate was  $5 - 8 \times 10^9 \text{ M}^{-1} \text{ s}^{-1}$ . They considered this to be a representative value for other arenes.

In 1980 Cline Love, Skrilec, and Habarta [9] demonstrated the first analytical application of MS-RTP in aqueous solution. They found linear dynamic ranges (LDRs) for pyrene, naphthalene and biphenyl in Na/Tl and Na/Ag mixed counterion lauryl sulfate micelles to be over 2 decades with limits of detection (LODs) comparable to those found in EPA at 77 K. Thallium counterions were found to give consistently higher signals and better sensitivities than the silver counterions. This parallels the observations found for solid-surface RTP. The RTP intensity peaked at  $\sim 30\% \text{ Tl}^+$  and  $\sim 30\% \text{ Ag}^+$ , but the enhancement due to the heavy atom effect was essentially complete by 20% metal ion concentration. Cline Love et al. used a total surfactant concentration of 0.15 M.

The effect of temperature on RTP intensities was investigated. A modest temperature coefficient was observed, being roughly a factor of one or two per  $10^\circ\text{C}$ . This indicates that modest temperature control is required for quantitative analysis.

Cline Love's group [49] also reported MS-RTP characteristics of functionally substituted aromatic molecules including ketones, aldehydes, alcohols, carboxylic acids, phenols, and amines. Once again, they observed LODs that were comparable to those obtained at 77 K. Thallium was used as the heavy atom counterion for the surfactant since it was determined previously that thallium is more sensitive than silver as an MS-RTP enhancer. In general, they found that the heavy atom quenched 75 - 99% of

the fluorescence. Phosphorescent lifetimes were found to range from 250  $\mu\text{s}$  to 1 ms for the compounds tested. The relative standard deviations (RSDs) for the lifetime determinations were found to be better than 10% with meticulous deoxygenation.

Following this work, Cline Love et al. [50] studied the dynamics of the analyte-micelle interaction in mixed micelles containing thallium as the counterion. The phosphorescence lifetime  $\tau_p$  in micellar solutions can be described by

$$1/\tau_p = k_- + k_{MP} - \frac{k_- k_+ [M]}{k_p + k_+ [M]} \quad (3-4)$$

where  $k_-$  is the rate constant for exit of the triplet probe from the micelle,  $k_{MP}$  is the deactivation from within the micelle,  $k_+$  is the reentry rate of the probe into the micelle,  $k_p$  is the rate of deactivation outside the micelle, and  $[M]$  is the concentration of the micelle as calculated by equation 3-3. This equation assumes that the concentration of internal and external quenchers are negligible and that heavy atoms are not treated explicitly as quenchers of the excited state probe. With these assumptions it can be seen that the observed lifetime depends on  $k_-$  and  $k_{MP}$  when the surfactant, and hence the micelle concentration is kept constant.

A background correction method that relies on the reversible chemically induced quenching of the excited triplet state by molecular oxygen has also been described by Cline Love et al. [51]. In this method, the luminescence intensities of the deaerated and aerated sample solutions are measured using the same instrumental parameters. The calculated difference in the two emission intensities then yields the signal and spectra due to the phosphorescence alone.

Woods and Cline Love investigated heavy atom and complexation effects on MS-RTP of pyridinic nitrogen molecules [52]. They observed greater RTP enhancement with 0.08 M 50/50  $\text{Ag}^+/\text{Na}^+$  lauryl sulfate than with the thallium counterion. Silver forms a strong complex through the nitrogen to keep the heavy atom in close proximity to the phosphorescent molecule.

Synchronous scanning MS-RTP was demonstrated by Femia and Cline Love for the simultaneous determination of mixtures [53]. They found that optimum results are obtained when the total analyte concentration is much less than  $5 \times 10^{-5}$  M because of triplet transfer causing errors in the measurements. The specific threshold value depends on the donor-acceptor system as well as the phosphorescent lifetimes of the molecules.

### **Deoxygenation Methods**

The high efficiency of molecular oxygen as a triplet quencher necessitates deoxygenation to observe RTP in fluid solutions. Several deoxygenation methods have been developed. Many of these methods were developed primarily for fluorescence or electrochemical detectors where dissolved oxygen either quenches the analyte signal or causes a high background current.

#### ***Inert Gas Purging***

Kalyanasundaram et al. [45] bubbled all solutions with nitrogen having an oxygen concentration less than 0.5 ppm for 30 minutes prior to phosphorescence measurements. This method saturates the solution with the inert gas so that dissolved oxygen is removed. Argon has also been used as an inert gas to deoxygenate solutions for polarographic analysis [54]. Although argon was found to be more efficient than nitrogen in this study, widespread use of argon is probably inhibited by its higher cost.

One obvious result of bubbling gases through a surfactant solution is foaming, which can cause a loss of solution due to overflow. If the flow rate of the deoxygenating gas is reduced to minimize foaming, inordinately long deoxygenation times are required. A gas bubbling system for use with surfactant solutions has been described by Buell and Demas [55]. This system uses a Teflon tube running down the center of a 60° funnel with a ground glass joint. The funnel, which fits into a long

necked cell, collects the bubbles forced out the glass tube by the purge gas. The Teflon tube acts as a wick to drain the fluid from ruptured bubbles back into the cell. The oxygen concentration from an oxygen saturated solution was reduced to less than  $10^{-5}$  M in about 13 minutes. This design enables higher purge gas flow rates to be used and decreases the deoxygenation time to 8 - 10 minutes since solutions are normally saturated with air rather than oxygen.

### ***Vacuum Degassing***

A degassing method based on evacuation has been described by Battino et al. [56]. Although this method has not been used explicitly in RTP, it was reported to be able to thoroughly degas 500 ml of liquid in 30 minutes or less.

### ***Freeze-Pump-Thaw***

Degassing solutions by freeze-pump-thaw cycles has been described by Takakubo and Faure [57]. This method is not time efficient because several cycles are required to successfully degas solutions. Solutions must also be allowed to equilibrate at room temperature since freezing causes some partitioning of the surfactant solution.

### ***Semipermeable Membranes***

A method has been described by Reim [58] for the continuous removal of dissolved oxygen from chromatographic effluents. The method is based on the use of tubular semipermeable membranes. Silicone rubber was used as the membrane because of its high oxygen permeability and chemical inertness. The membrane device was constructed from a plastic tube shell onto which polypropylene end caps were fitted with a double O-ring seal. One end cap contained a fitting for a vacuum pump connection and the second contained standard male chromatographic fittings through which a tubular silicone membrane was sealed with silicone rubber sealant. The gas flux across the membrane is proportional to the permeability of the membrane and the oxygen partial pressure difference across the membrane walls. It is inversely

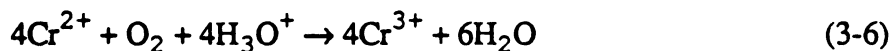
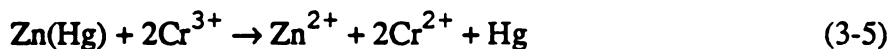
proportional to the thickness of the membrane wall. Several approaches to maximize oxygen transport across the membrane were considered. Purging the shell with an inert gas required large volumes of gas to rapidly flush the shell. Flushing the shell with alkaline-sulfite solution increased baseline peak-to-peak noise considerably due to the pulsing action of the pump employed. Although this method offered the maximum pressure difference across the membrane, it was found to have the lowest oxygen removal of the methods tested. This was believed to be due to the slow reaction kinetics at the outer membrane wall. (The sulfite reaction for oxygen removal is discussed later.) Evacuation of the shell was found to be the superior method. Residence times less than one minute were found to decrease the oxygen concentration to less than 0.1 ppm.

### ***Chemical Scavenging Methods***

Several deoxygenation methods based on chemical scavenging have been reported [59-62]. These methods reduce the oxygen dissolved in solution to water. These techniques are discussed below.

#### ***Chromium(II)***

Rollie, Ho, and Warner described a method based on the diffusion of oxygen across a permeable membrane into a solution of  $\text{Cr}^{2+}$ . The  $\text{Cr}^{2+}$  is formed by the reduction of  $\text{Cr}^{3+}$  by a Jones Reductor  $\text{Zn(Hg)}$ . The  $\text{Cr}^{2+}$  then reduces the oxygen to water. This technique is used to minimize the quenching of fluorescence in a flowing stream [59]. This method is based on the following reactions:



As oxygen diffuses across the membrane it is immediately reduced to water by  $\text{Cr}^{2+}$  (reaction 3-6). The  $\text{Cr}^{3+}$  formed by this reaction is then reduced by the Jones Reductor (reaction 3-5) to form  $\text{Cr}^{2+}$  which can be used in equation 3-6. Therefore, the

concentration of oxygen never reaches a level which would reduce the concentration difference across the membrane. This causes oxygen to continue to diffuse across the membrane until the analyte solution is oxygen free. Polyethylene tubing was used as the membrane because silicone tubing had the tendency to expand under the pressure of the flowing solvent. The greatest oxygen removal was obtained with a 90 minute equilibration time. Although this method has been proven effective, the inordinately long equilibration time precludes the usefulness of this method for routine analyses.

An automated on-line deoxygenator for luminescence was then described by Rollie, Patonay, and Warner [60]. This system reduces sample handling to a minimum because deoxygenation and luminescence analysis occur within a closed system. The deoxygenator consists of a 12-inch dialyzer with a 0.2-mil very low density polyethylene membrane. With this system samples could be deoxygenated in five minutes. Thus, the use of a low density membrane decreased dramatically the deoxygenation time to enable reproducible deoxygenations to be performed on-line.

### *Zinc Column*

A zinc oxygen-scrubber column for use in liquid chromatography has been described by MacCrehan and May [61]. This method employs a "reductor" column packed with zinc particles to reduce the oxygen to water by the following sequence of reactions:



The reductor column was found to have a finite lifetime since zinc is being oxidized in the process. The removal of oxygen by the zinc scrubber column is reported to compare favorably with the semipermeable membrane method discussed previously [58].

### *Sodium Sulfite*

A deoxygenation technique that uses sodium sulfite as an oxygen scavenger in micellar solutions was reported by Díaz García and Sanz-Medel [62]. This method reduces the oxygen in the micellar solution and does not rely on diffusion of oxygen across a membrane. Sodium sulfite has been used routinely in polarographic determinations to remove dissolved oxygen from alkaline and neutral supporting electrolytes [63]. The reduction of oxygen occurs according to



Reaction 3-9 reaches a steady state when the micellar phase becomes equilibrated with the oxygen in the headspace within the sample cell. The reaction time for the oxygen consumption is related to the surfactant concentration. Higher surfactant concentrations took longer to deoxygenate. The optimum sodium sulfite concentration with respect to deoxygenation time and phosphorescence intensity was determined to be 0.010 M for 0.1 M SDS solution [62]. This method is considerably easier than any aforementioned technique and requires no special apparatus. However, there are two immediate disadvantages of this technique that must be mentioned. The concentration of sodium ions from the sodium sulfite will have a counter-ion effect on micelles. This will alter the aggregate number and change the size of the micelle. It is possible that the sulfite ion will react with constituents in the sample. The effect this has on phosphorescence would have to be determined experimentally.

## CHAPTER III REFERENCES

1. Ingle, J.D.; Crouch, S.R., *Spectrochemical Analysis*, Prentice-Hall, 1988
2. Millson, H.E., *The Phosphorescence of Textile Fibers and Other Substances*, *Calco Tech. Bull*, American Cyanamid Co., 1944, 753
3. Brown, D.J., *J. Chem. Soc.*, 1958, 1974
4. Roth, M., *J. Chromatog.*, 1967, 30, 276
5. Llyod, J.B.F.; Miller, J.N., *Talanta*, 1979, 26, 180
6. Schulman, E.M.; and Walling, C., *Science*, 1972, 178, 53
7. Schulman, E.M.; and Walling, C., *J. Phys. Chem.*, 1973, 77, 902
8. Paynter, R.A.; Wellons, S.L.; and Winefordner, J.D., *Anal. Chem.*, 1974, 46, 736
9. Cline Love, L.J.; Skrilec, M.; Habarta, J.G., *Anal. Chem.*, 1980, 52, 754
10. Scypinski, S.; Cline Love, L.J., *Anal. Chem.*, 1984, 56, 322
11. Donkerbroek, J.J.; Gooijer, C.; Velthorst, N.H.; Frei, R.W.; *Anal. Chem.*, 1982, 54, 891
12. Weinberger, R.; Cline Love, L.J., *Spectrochimica Acta*, 1984, 40A, 49
13. Weinberger, R.; Cline Love, L.J., *Appl. Spectrosc.*, 1985, 39, 516
14. Wellons, S.L.; Paynter, R.A. ; Winefordner, J.D., *Spectrochim. Acta*, 1974, 30A, 2133
15. Parker, R.T.; Freedlander, R.S.; Dunlap, R.B., *Anal. Chim. Acta*, 1980, 119, 189
16. Parker, R.T.; Freedlander, R.S.; Dunlap, R.B., *Anal. Chim. Acta*, 1980, 120, 1
17. Schulman, E.M.; Parker, R.T., *J. Phys. Chem.*, 1977, 81, 1932
18. Niday, G.J.; Seybold, P.G., *Anal. Chem.*, 1977, 50, 1577
19. Ward, J.L.; Bateh, R.P.; Winefordner, J.D., *Analyst*, 1982, 107, 335
20. Bateh, R.P.; Winefordner, J.D., *Talanta*, 1982, 29, 713
21. Ward, J.L.; Bower, E.L.Y.; Winefornder, J.D., *Talanta*, 1981, 28, 119
22. Bower, E.L.Y.; Winefordner, J.D., *Anal. Chim. Acta.*, 1978, 102, 1
23. Seybold, P.G.; White, W., *Anal. Chem.*, 1975, 47, 1199

24. White, W.; Seybold, P.F., *J. Phys. Chem.*, **1977**, *81*, 2035
25. Meyers, M.L.; Seybold, P.G., *Anal. Chem.*, **1979**, *51*, 1609
26. Vo-Dinh, T., *Room Temperature Phosphorimetry for Chemical Analysis*; Wiley Interscience: New York, 1984, Chapter 2
27. Ward, J.L.; Walden, G.L.; Winefordner, J.D., *Talanta*, **1981**, *28*, 201
28. Donkerbroek, J.J.; Gooijer, C.; Velthorst, N.H.; Frei, R.W., *Anal. Chem.*, **1982**, *54*, 891
29. Weinberger, R.; Cline Love, L.J., *Spectrochimica Acta*, **1984**, *40A*, 49
30. Weinberger, R.; Cline Love, L.J., *Appl. Spectrosc*, **1985**, *39*, 516
31. Tabushi, I., *Acc. Chem. Res.*, **1982**, *15*, 66
32. Scypinski, S.; Cline Love, L.J., *Anal. Chem.*, **1984**, *56*, 322
33. Saenger, W., *Angew. Chem., Int. Ed. Engl.*, **1980**, *19*, 344
34. Bender, M.L.; Komiyama, M., *Cyclodextrin Chemistry*; Springer-Verlag, Berlin, 1978
35. Cramer, F.; Saenger, W.; Spatz, H-Ch., *J. Am. Chem. Soc.*, **1967**, *89*, 14
36. Turro, N.J.; Bolt, J.D.; Kuroda, Y.; Tabushi, I., *Photochem. Photobiol.*, **1982**, *35*, 69
37. Turro, N.J.; Cox, G.S.; Li, X., *Photochem. Photobiol.*, **1983**, *37*, 149
38. Scypinski, S.; Cline Love, L.J., *Anal. Chem.*, **1984**, *56*, 322
39. Scypinski, S.; Cline Love, L.J., *Anal. Chem.*, **1984**, *56*, 331
40. Second Annual Report on Carcinogens (NTP 81-43, December, 1981) pp. 112-114
41. Almgren, M.; Grieser, F.; Thomas, J.K., *J. Am. Chem. Soc.*, **1979**, *101*, 279
42. Cline Love, L.J.; Habarta, J.G.; Dorsey, J.G., *Anal. Chem.*, **1984**, *56*, 1133A
43. Aniansson, E.A.G.; Wall, S.N.; Almgren, M.; Hoffman, H.; Kielmann, I.; Ulbricht, W.; Zana, R.; Lang, J.; Tondre, C., *J. Phys. Chem.*, **1976**, *80*, 905
44. Rosen, M.J., *Surfactants and Interfacial Phenomena*, Wiley-Interscience, New York, 1978; Chapter 4
45. Kalyanasundaram, K.; Grieser, F.; Thomas, J.K., *Chem. Phys. Lett.*, **1977**, *51*, 501
46. Hurtubise, R.J., *Anal. Chem.*, **1983**, *55*, 699A

47. Turro, N.J.; Kou-Chang, L.; Ming-Fea, C.; Lee, P., *Photochem. Photobiol.*, **1978**, *27*, 523
48. Humphry-Baker, R.; Moroi, Y.; Grätzel, M., *Chem. Phys. Lett.*, **1978**, *58*, 207
49. Skrilec, M.; Cline Love, L.J., *Anal. Chem.*, **1980**, *52*, 1559
50. Cline Love, L.J.; Habarta, J.G.; Skrilec, M., *Anal. Chem.*, **1981**, *53*, 437
51. Cline Love, L.J.; Skrilec, M., *Anal. Chem.*, **1981**, *53*, 1872
52. Woods, R.; Cline Love, L.J., *Spectrochim. Acta, Part A*, **1984**, *40A*, 643
53. Femia, R.A.; Cline Love, L.J., *Anal. Chem.*, **1984**, *56*, 327
54. Lund, W.; Opheim, L.N., *Anal. Chim. Acta*, **1975**, *79*, 35
55. Buell, S.L.; Demas, J.N., *Rev. Sci. Instrum.*, **1982**, *53*, 1298
56. Battino, R.; Banzhof, M.; Bogan, M.; Wilhelm, E., *Anal. Chem.*, **1971**, *43*, 806
57. Takakubo, M.; Faure, J., *Photochem. Photobiol.*, **1983**, *38*, 137
58. Reim, R.E., *Anal. Chem.*, **1983**, *55*, 1188
59. Rollie, M.E.; Ho, C.-N.; Warner, I.M., *Anal. Chem.*, **1983**, *55*, 2445
60. Rollie, M.E.; Patonay, G.; Warner, I.M., *Anal. Chem.*, **1987**, *59*, 180
61. MacCrehan, W.A.; May, W.E., *Anal. Chem.*, **1984**, *56*, 625
62. Díaz García, M.E.; Sanz-Medel, A., *Anal. Chem.*, **1986**, *58*, 1436
63. Kolthoff, I.M.; Lingane, J.J., *Polarography*; Interscience, New York, 1952; Vol. 1

## CHAPTER IV

### FLOW INJECTION ANALYSIS

Continuous flow analysis is a technique in which the concentration of an analyte is measured in a continuously flowing stream of liquid or gas. Mixing and incubation of the solution takes place as it flows through a manifold consisting of interconnected tubing. Continuous flow analysis can be divided into two areas: segmented and non-segmented continuous flow analysis. Leonard Skeggs is accredited with the development of the segmented technique [1]. In this technique, commonly referred to as continuous flow analysis (CFA), the sample stream is segmented with air bubbles to prevent excessive dispersion of the sample by the natural dispersive nature of laminar flow. The air bubbles divide the flowing stream into a number of segments and therefore prevent excessive dilution of the sample. They also minimize carry-over and prevent excessive dispersion of the sample. The sample is introduced into the manifold by timed aspiration. The reaction time is determined by the length, the inner diameter, and the flow rate of the solutions. Within each segment nearly complete mixing takes place so that the signal obtained at the output approximates a rectangular shape as would be expected in the ideal case of a discrete sample plug. This system was later developed by Technicon Corporation and marketed commercially as the AutoAnalyzer.

Flow injection analysis (FIA) was developed several years later by two separate groups. Stewart, Beecher, and Hare [2] developed FIA as an outgrowth of liquid chromatography, while Jaromir Ruzicka and Elo Hansen [3] approached FIA as an alternative to CFA. Ruzicka and Hansen coined the generic name for this non-segmented continuous flow technique and are commonly given credit for inventing FIA.

### Principles of Flow Injection Analysis

FIA involves the injection of a small, but precisely known, volume of sample into a continuously flowing stream of reagent. The sample zone then mixes with the carrier stream on the way to the flow-through detector. The simplest flow injection analyzer, shown in Figure 4.1, consists of a pump, that propels the carrier stream through a polymeric tube, a method of sample injection, such as a multiport valve, and a flow-through detector. The sample is injected as a discrete zone and then disperses and reacts with the components of the carrier stream to form a species which is sensed by the flow-through detector and recorded. Conditions are such that laminar flow is predominant, which results in a parabolic velocity profile of the sample zone. This gives rise to dispersion of the sample along the axis of the polymeric tube. This dispersion can be controlled by judicious choice of tubing length and inner diameter, and the type of flow cell used. The carrier stream flow-rate and sample volume also affect the dispersion of the sample zone. A sample with an initial concentration of  $C^0$  is injected into the carrier stream. As the sample zone travels through the manifold, axial and radial mixing occur. These combined effects result in a predominantly Gaussian-shaped peak profile. The effect of laminar flow and molecular diffusion which results in the Gaussian-shaped peak is shown in Figure 4.2. Dispersion and molecular diffusion dilute the sample so that the maximum concentration sensed at the detector is  $C^{\max}$ , which is some fraction of  $C^0$ . The ratio of  $C^0$  to  $C^{\max}$  provides an empirical method by which dispersion,  $D$ , can be measured [4]:

$$D = \frac{C^0}{C^{\max}} = \frac{k'H^0}{k''H} \quad (4-1)$$

For most applications, the analytical readout is based on the measurement of the peak height,  $H$ . The conversion factors between instrumental readout and the concentration are  $k'$  and  $k''$ . The heights of the sample peaks before and after dispersion has taken place are  $H^0$  and  $H^{\max}$ , respectively. Under conditions where the Lambert-Beer law is obeyed, the two proportionality constants are equivalent. Ruzicka and Hansen [4] have

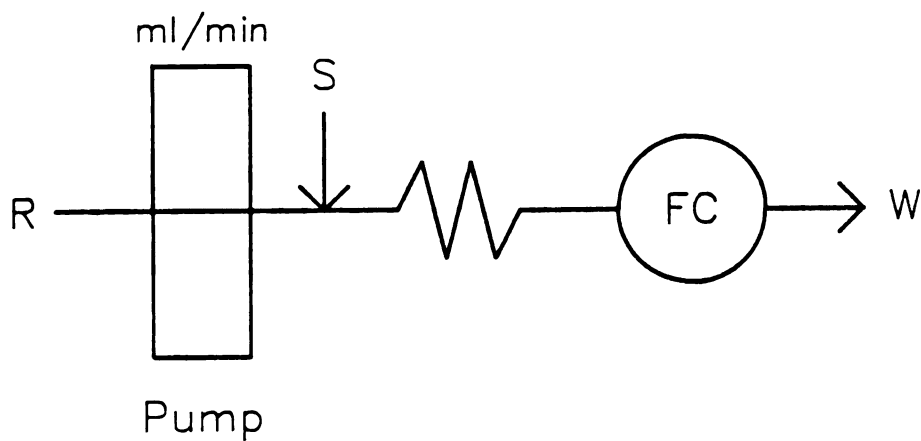
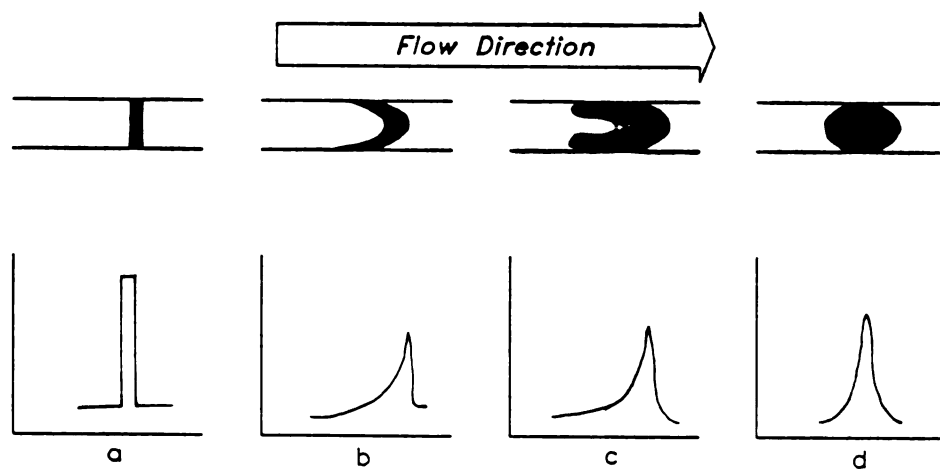


Figure 4.1

Simplified representation of a flow injection system. The reagent R is pumped through the manifold where the sample S is injected by a sample injection valve. The product is monitored by the flow-through detector FC. The product is then vented to waste W.



**Figure 4.2** Laminar flow with molecular diffusion: (a) the sample plug, (b) under conditions of laminar flow, (c) laminar flow with molecular diffusion, (d) Gaussian peak profile resulting from molecular diffusion.

classified dispersion in FIA as limited ( $D = 1-3$ ), medium ( $D = 3-10$ ), and large ( $D > 10$ ). The type of dispersion used depends on the application for which it is intended. Limited dispersion will maintain sample integrity for applications where mere transport of the sample is desired. When a chemical reaction between the sample and the carrier must take place medium or large dispersion is desirable.

The type of manifold used is one method of controlling the dispersion of the sample zone. Ruzicka and Hansen have reported the results of a comparison of various types of FIA manifolds [5]. Relatively large amounts of dispersion are obtained with straight open tubular reactors (OTRs). Coiled tubes decrease the amount of dispersion due to secondary flow, flow that is perpendicular to the axis of the reactor. The extent of secondary flow increases as the diameter of the coil decreases and the mean velocity of the carrier increases. Dispersion can be minimized by using packed reactors rather than OTRs. Although the pressure drop across a reactor packed with small diameter particles may preclude the use of an inexpensive low-pressure pump, such as a peristaltic pump, reactors packed with solid glass spheres with diameters slightly less than that of the tube (60% to 80%) yield a pressure drop slightly greater than a coiled OTR [6]. These single bead string reactors (SBSRs) decrease the dispersion by breaking up the parabolic velocity profile.

Sample volume and manifold length also influence the dispersion obtained in systems where the flow rate and tubing diameter are held constant. Increasing the sample volume and decreasing the manifold length both decrease the amount of dispersion obtained. For further information on the theory and applications of FIA the reader is referred to the monograph by Ruzicka and Hansen [4] and a recent monograph by Valcarcel and Luque de Castro [7].

### **Related Applications of Flow Injection Analysis**

Although applications of FIA are quite numerous, several specific applications have been used throughout the course of this research: luminescence and stopped-flow. These techniques will now be discussed briefly.

#### ***Stopped-Flow in FIA***

The stopped-flow mode can be used for two different purposes: to increase the sensitivity of a measurement by increasing the residence time, or to measure the rate of a reaction. An increase in the residence time will allow a reaction to increase the yield of the measured species. The appropriate choice of the stop period will gain reaction time without increasing the length of the manifold which would increase the dispersion of the sample zone due to laminar flow. Therefore, dispersion will become independent of time (with the exception of the very small contribution from molecular diffusion).

If the flow is stopped while the sample zone is within the flow cell, it is possible to record the progress of the reaction. In this technique, the flow of the carrier must come to a complete standstill such that the same section of the sample zone is held reproducibly within the flow cell for measurement. This can be best achieved by an electronic timer activated by the injection valve and connected to the pump. Injection of the sample triggers the timer to count a delay time. Once the timer has delayed for the predetermined time, the pump is turned off to stop the flow. After the reaction has been monitored for the desired time, the pump is turned on to rinse the flow-cell and to prepare for the next sample. The delay time and reaction time are chosen to suit the particular chemistry.

#### ***Luminescence detection in FIA***

Luminescence detectors monitor the radiation emitted by an excited state analyte as it returns to the ground state. In chemiluminescence the molecule is excited through a chemical reaction. In this technique, no radiation source is required and therefore

filters or monochromators are not required for wavelength isolation. The detection system consists of a radiation transducer and a readout.

In fluorescence and phosphorescence, however, the analyte is excited by radiation of a specific wavelength, and the radiation resulting from the return to the ground state is monitored at a specific emission wavelength. Therefore, a suitable source of radiation is required with a wavelength isolation device to excite the analyte molecule. The wavelength isolation device can be a filter or monochromator. Typically, the emitted radiation is monitored at 90° relative to the excitation beam. With this arrangement, the flow cell must have windows oriented on adjacent sides of the flow cell. The windows of the cell are commonly quartz or sapphire so that they will transmit the ultra-violet radiation used for sample excitation. As with the excitation radiation, the emitted luminescence radiation is isolated with either a filter or a monochromator. The emitted luminescence is then detected by the radiation transducer and monitored by the readout.

The flow cells used are typically low-pressure flow-through cells with low volumes. Large volume flow-through cells will increase the dispersion of the sample zone. Cells with a wide variety of volumes and pathlengths are available which can be selected to suit the particular needs of the analysis.

To date, there have been many applications of fluorescence detection in FIA [8-44]. A literature search of applications of RTP in flowing streams (flow injection analysis and chromatographic systems) has resulted in few manuscripts being found [45-49]. These applications are all based on the sensitized RTP of biacetyl. Two methods were found that are based on the quenched RTP of biacetyl by a suitable analyte [49,50]. None of these RTP techniques employs a direct measurement of the phosphorescence of an analyte.

## CHAPTER IV REFERENCES

1. Skeggs, L., *Am. J. Clin. Pathol.*, **1957**, *13*, 451
2. Stewart, K.K.; Beecher, G.R.; Hare, P.E., *Fed. Proc.*, **1974**, *33*, 1439
3. Ruzicka, J.; Hansen, E., *Anal. Chim. Acta*, **1975**, *78*, 145
4. Ruzicka, J.; Hansen, E., *Flow Injection Analysis*, John Wiley & Sons: New York, **1981**; Chapter 2
5. Ruzicka, J.; Hansen, E., *Anal. Chim. Acta*, **1984**, *161*, 1
6. Reign, J.M.; van der Linden, W.E.; Poppe, H., *Anal. Chim. Acta*, **1981**, *123*, 229
7. Valcarcel, M.; Luque de Castro, M.D., *Flow Injection Analysis: Principles and Applications*, John Wiley & Sons: New York, **1987**
8. Kina, K.; Shiraiishi, K.; Ishibashi N., *Talanta*, **1978**, *25*, 295
9. Braithwaite, J.I.; Miller, J.N., *Anal. Chim. Acta*, **1979**, *106*, 395
10. Lim, C.S.; Miller, J.N.; Bridges, J.W., *Anal. Chim. Acta*, **1980**, *114*, 183
11. Ishibashi, N.; Kina, K.; Goto, Y., *Anal. Chim. Acta*, **1980**, *114*, 325
12. Imasaka, T.; Harada, T.; Ishibashi, N., *Anal. Chim. Acta*, **1981**, *129*, 195
13. Kelly, T.A.; Christian, G.D., *Anal. Chem.*, **1981**, *53*, 2110
14. Playle, R.; Gleed, J.; Jonasson, R.; Kramer, J.R., *Anal. Chim. Acta*, **1982**, *134*, 369
15. Kelly, T.A., *Diss. Abstr. Int.*, **1981**, *42*, 2356
16. Mori, K.; Imasaka, T.; Ishibashi, N.; Jin, C.; Kokubu, N., *Bunseki Kagaku*, **1982**, *31*, 103
17. Kelly, T.A.; Christian, G.D., *Anal. Chem.*, **1982**, *54*, 1444
18. Rydevik, U.; Nord, L.; Ingman, F., *Int. J. Sports Med.*, **1982**, *3*, 47
19. Harris, J.M., *Anal. Chem.*, **1982**, *54*, 2337
20. Stewart, K.K.; Rosenfeld, A.G., *Anal. Chem.*, **1982**, *54*, 2368
21. Petty, R.L.; Michel, W.C.; Snow, J.P.; Johnson, K.S., *Anal. Chim. Acta*, **1982**, *142*, 299
22. Kelly, T.A.; Christian, G.D., *Talanta*, **1982**, *29*, 1109

23. Abdullahi, G.L.; Miller, J.N.; Sturley, H.N.; Bridges, J.W., *Anal. Chim. Acta*, **1983**, *145*, 109
24. Karlsson, J.; Jacobs, I.; Sjödin, B.; Tesch, P.; Kaiser, P.; Sahl, O.; Karlberg, B., *Int. J. Sports Med.*, **1983**, *4*, 52
25. Elliott, C.B., *Diss. Abstr. Int.*, **1983**, *43*, 3966
26. Motomizu, S.; Oshima, M.; Toei, K., *Bunseki Kagaku*, **1983**, *32*, 458
27. Kusube, K.; Abe, K.; Hiroshima, O.; Ishiguro, Y., *Chem. Pharm. Bull.*, **1983**, *31*, 3589
28. Weicker, H., *LaborPraxis*, **1984**, *8*, 300
29. Weiker, H.; Haegele, H.; Kornes, B.; Werner, A., *Int. J. Sports Med.*, **1984**, *5*, 47
30. Boza, F.L.; Luque de Castro, M.D.; Valcarcel, M., *Analyst*, **1984**, *109*, 333
31. Motomizu, S.; Mikasa, H.; Oshima, M.; Toei, K., *Bunseki Kagaku*, **1984**, *33*, 116
32. Aoki, T.; Uemura, S.; Munemori, M., *Bunseki Kagaku*, **1984**, *33*, 505
33. Neubert, P.; Reiff, K., *Fresenius Z. Anal. Chem.*, **1981**, *305*, 277
34. Valcarcel, M.; Luque de Castro, M.D.; Lazaro, F., *Anal. Proc.*, **1983**, *20*, 313
35. Miller, J.N., *Anal. Proc.*, **1983**, *20*, 487
36. Lazaro, F.; Luque de Castro, M.D.; Valcarcel, M., *Anal. Chim. Acta*, **1984**, *165*, 177
37. Lazaro, F.; Luque de Castro, M.D.; Valcarcel, M., *Fresenius Z. Anal. Chem.*, **1985**, *320*, 128
38. Aihara, M.; Arai, M.; Tomitsugu, T., *Anal. Lett.*, **1986**, *19*, 1907
39. Masoom, M.; Worsfold, P.J., *Anal. Chim. Acta*, **1986**, *179*, 217
40. Hwang, J.; Dasgupta, P.K., *Anal. Chem.*, **1986**, *58*, 1521
41. Kelly, T., In *Enzyme-Mediated Immunoassay*; Ngo, T.T., Lenhoff, H.M., Eds.; Plenum: New York, 1985; pp 191-201
42. Maeda, M.; Tsuji, A., *Analyst*, **1985**, *110*, 665
43. Linares, P.; Luque de Castro, M.D.; Valcarcel, M., *Anal. Chem.*, **1985**, *57*, 2101
44. Hult, K.; Fuchs, R. Peraica, M.; Plestina, R. Ceovic, S., *J. Appl. Toxicol.*, **1984**, *4*, 326
45. Donkerbroek, J.J., Van Eikema Hommes, N.J.R.; Gooijer, C.; Velthorst, N.H.; Frei, R.W., *Chromatographia*, **1983**, *15*, 218

46. Donkerbroek, J.J., Van Eikema Hommes, N.J.R.; Gooijer, C.; Velthorst, N.H.; Frei, R.W., *J. Chromatogr.*, **1983**, *255*, 581
47. Donkerbroek, J.J.; Veltkamp, A.C.; Praat, A.J.J.; Gooijer, C.; Frei, R.W.; Velthorst, N.H., *Appl. Spec.*, **1983**, *37*, 188
48. Baumann, R.A.; Gooijer, C.; Velthorst, N.H.; Frei, R.W., *Anal. Chem.*, **1985**, *57*, 1815
49. Gooijer, C.; Velthorst, N.H.; Frei, R.W., *TrAC - Trends Anal. Chem.*, **1984**, *3*, 259
50. Donkerbroek, J.J.; Veltkamp, A.C.; Gooijer, C.; Velthorst, N.H.; Frei, R.W., *Anal. Chem.*, **1983**, *55*, 1886

## CHAPTER V

### LUMINESCENCE INSTRUMENTATION

This chapter describes the instrumentation that was used throughout the course of this research. The initial studies were done with a microprocessor-controlled luminescence spectrometer designed and constructed in our laboratory. Later, a commercial instrument (Perkin-Elmer Model LS-5 Spectrofluorometer with a Model 3600 Data Station) became available. This instrument was used for most of the later studies. Although the commercial instrument offers optimized optics and source correction, the home-built instrument can be more readily programmed by the user. Data acquired on the home-built instrument can also be transmitted serially to a Digital Equipment Corporation LSI 11/23 minicomputer for graphical display, statistical evaluation, and mass storage. This option gives the locally designed instrument more data analysis veratility than is available with the Perkin-Elmer Data Station.

#### **Home-Built Microcomputer-Controlled Luminescence Spectrometer**

The home-built luminescence spectrometer is controlled by a modular twin bus microcomputer system designed by Newcome and Enke [1]. This microcomputer is interfaced to a custom-designed spectrofluoromter. A mechanical chopper is included in the design of this spectrofluorometer so that time-resolved phosphorescence measurements can be performed. The microcomputer, luminescence spectrometer, and interface are discussed individually below.

### ***Twin Bus Microcomputer System***

The version of the microcomputer used was constructed in this laboratory and is based on the Intel 8088 microprocessor (Intel Corp., Santa Clara, CA). The modular design of the microcomputer increases its flexibility and adaptability. Thus, a custom-tailored computer system can be created from a standard set of modules. Modules used in the microcomputer with their principal integrated circuits are listed in Table 5.1. Some of the unique features of the microcomputer are: the programmable interrupt controller, which expands the processors interrupt capacity and capabilities; the dual USART, which consists of two RS232 ports that are assigned to the user's terminal and the LSI 11/23; and the chip select, which allows addressing of other modules while eliminating unnecessary redundancy of decoding circuits.

Two other modules are of particular interest and deserve special mention: a counter/timer II, based on the AM9513 (Advanced Micro Devices, Sunnyvale, CA) and a sample/hold multiplexer (S/H-MUX). Both of these modules, as well as the 12-bit analog-to-digital converter (ADC) were designed by Ratzlaff [2]. The 9513 counter/timer contains five, 16-bit, individually programmable counters. Several applications of interest include time-of-day clocking, real-time program independent clocking, count up/down, polled or interrupt timing for data collection sequencing or peripheral servicing, programmable waveform generation, and event count accumulation.

The sample/hold multiplexer is a module containing four identical differential input inverting sample-and-hold (S/H) circuits (SHM-IC-1, Datel Intersil Inc., Mansfield, MA) which act as the first stages of the analog input circuit. With this design, only one analog-to-digital converter (ADC) is required. The S/H-MUX module is included to provide interfacing to more than one experimental apparatus at a given time and to allow multi-channel data acquisition. Each of the four S/Hs have independent digital control, which permits flexible operation initiated by software or

Table 5.1

## Modules with their Principal Integrated Circuits

Module	Principal Integrated Circuit
Central Processing Unit	8088
32k RAM/ROM	2716, 2016
Interrupt Controller	8259A-5
Dual USART	8251A
Parallel Input/Output	8255A-5
8k RAM	2114
Chip Select	<sup>a</sup>
Counter/Timer II	AM9513
Dual 8-bit DAC	AD558
12-bit DAC	AD565
Multiplexer	<sup>a</sup>
12-bit ADC	AD574
SASI Interface	<sup>a</sup>

<sup>a</sup> 74LS series TTL integrated circuits

asynchronous events. The four S/Hs are multiplexed by a 8-channel multiplexer (MX-808, Datel Systems Inc., Mansfield, MA) with a buffered output to maintain transfer accuracy. This output is used as the ADC input. For a more in-depth discussion of the counter/timer II, S/H-MUX, and ADC modules, the reader is referred to Ratzlaff's thesis [2].

The microcomputer has a single 8 in. floppy disk drive to facilitate program and data storage and to ease programming. Serial transmission of data to and from the LSI-11/23 is made possible by the program FORTHPIP [3]. This program serves as a means of communication between the microcomputer's operating environment and files on the minicomputer. Serial transmission is a slow process and is failure prone during heavy usage on the minicomputer. Downloading to the microcomputer from the floppy diskette saved considerable time over the serial link to the LSI-11/23. The same is true for the uploading process.

The microcomputer runs under the polyFORTH operating environment (FORTH, Inc., Hermosa Beach, CA). FORTH is a stack oriented, threaded interpreter. It was designed to provide power, ease, and flexibility in interfacing with instruments. A unique feature of FORTH is that it does not compile, but rather links programs or subroutines into new programs or subroutines. A FORTH programmer begins with a subset of useful subroutines called "words". Programming entails creating new words by linking previously defined words. Judicious choice of words should, theoretically, make a program in FORTH read like a sentence and therefore be easy to understand. However, it is the author's experience that this threaded nature makes complex programs quite difficult to decipher. FORTH excels in speed for high level mathematical calculations because of its use of fixed point rather than floating point math [4]. Some of the criticisms of FORTH are its lack of file structure, and its requirement that words be named uniquely. The version of FORTH used in this microcomputer uses the first three characters and the length of the word as a test for

word uniqueness. Therefore, one must be creative in assigning names so that each word remains exclusive.

### ***Home-Built Luminescence Spectrometer***

A typical fluorometer consists of a radiation source to excite the sample, an excitation and an emission wavelength selector (filters or monochromators), a radiation transducer, a signal processor, and a readout device. A block diagram of the microcomputer controlled spectrofluorometer is shown in Figure 5.1. The source of radiation for this instrument is a 150 W high pressure Xe arc lamp (CA-150 Light Source, Illumination Industries, Sunnyvale, CA). Radiation from this source is focused onto the entrance slit of the excitation monochromator (ISA H-10, Instruments SA Inc., Metuchen, NJ) by a quartz lens. The excitation and emission monochromators are mounted at 90° around a sample chamber designed and constructed in our laboratory. The emission beam is selected by the emission monochromator (ISA H-10). These monochromators have a linear dispersion of 8 nm/mm and a focal length of 100 mm with a F/3.5 aperture. The radiation transducer is a photomultiplier tube (PMT, model R-928, Hamamatsu, Bridgewater, NJ) The PMT photocurrent is amplified and converted to voltage by a commercial amplifier (Model 427 Current Amplifier, Keithley Instruments Inc., Cleveland, OH). The current amplifier output is digitized by the ADC module in the microprocessor. At present, the monochromators must be scanned manually.

Temporal discrimination is provided by a rotating disk chopper which is placed between the source and the entrance slit of the excitation monochromator. Its construction and use are described in more detail below.

### ***Microcomputer/Spectrometer Interface***

The microcomputer controls several components of the spectrofluorometer and peripherals associated with experiments performed on this instrument. These include

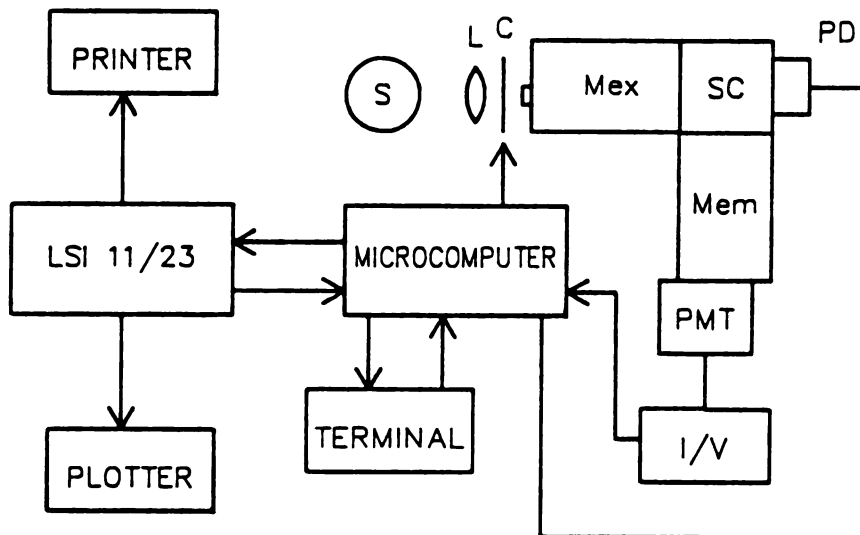


Figure 5.1

Block diagram of home-built luminescence spectrometer showing orientation of the components. Key: S, radiation source; L, lens; C, optional chopper; Mex, excitation monochromator; SC, sample chamber; PD, photodiode with amplifier circuitry; Mem, emission monochromator; I/V, current amplifier.

the rotating disk chopper and a peristaltic pump and sample injection valve for flow injection work. The chopper consists of a 10 cm diameter disk with 8 slots cut at equal intervals. This disk is mounted to the shaft of a 12 Vdc hobby motor. The rotation speed of the motor is controlled through one of the 9.95 Vdc full scale 8-bit digital-to-analog converters (DACs). Since the motor requires approximately 100 mA, which is more current than the DAC can supply, a transistor driver circuit was used to provide the necessary current. The power transistor is powered by an external power supply (Model EU-801-11, Heath Corp., Benton Harbor, MI). This circuit is shown in Figure 5.2. The voltage follower with gain was included to buffer the load on the DAC and to increase the supply voltage to the motor. This then allows slightly higher rotation speeds (which affects the chopping frequency) to be obtained by increasing the maximum transistor input to 12 Vdc.

To monitor the chopping frequency, an opto-interrupter is placed so that the blades of the rotating disk pass between the source and receiver. As the disk rotates, the opto-interrupter encodes information about the chopper status such as, is the motor turning?, what is the position of the blade? (is the source blocked?), what is the chopping frequency? The output of the phototransistor in the opto-interrupter is passed through a Schmitt trigger to provide noise discrimination. This ensures a reliable TTL signal from the opto-interrupter. With this arrangement, the opto-interrupter must be "phased" so that the TTL signal reflects correctly the status of the excitation radiation entering the sample chamber. Phasing is accomplished by placing a phototransistor inside the sample chamber such that it is exposed to the excitation radiation. The output of this phototransistor is also passed through a Schmitt trigger. Signals from both phototransistors are displayed concurrently on a dual-trace oscilloscope. The position of the opto-interrupter is then adjusted physically until both traces on the oscilloscope are in phase. If the opto-interrupter is not phased correctly, the sample will or will not be exposed to the excitation radiation as indicated by the opto-interrupter signals.

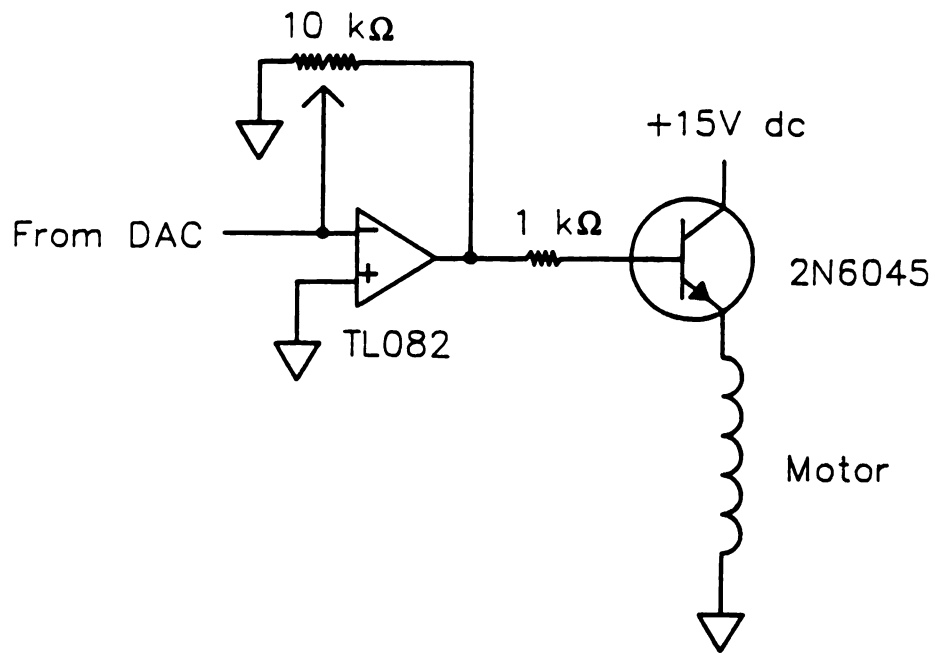


Figure 5.2

Schematic of transistor driver circuit used to amplify current supplying power to chopper motor.

Three examples of opto-interrupter/source phasing are shown in Figure 5.3. Early phasing occurs when the sample chamber HI-to-LO transition occurs before the opto-interrupter status indicates this transition. Late phasing occurs when the sample chamber HI-to-LO transition occurs after the opto-interrupter HI-to-LO transition. The opto-interrupter is phased correctly when the two transitions occur concurrently.

Although this opto-interrupter arrangement worked satisfactorily, phasing had to be performed prior to each experiment as motor vibrations had the tendency to disrupt the phasing of the opto-interrupter. The opto-interrupter was discarded and a second approach was taken to eliminate this phasing problem. An ultra-violet enhanced photodiode (model UV-040BQ, EG & G Photon Devices, Salem, MA) was situated in the sample chamber opposite the entrance slit. With this arrangement, the photodiode yields a direct indication of the source chopping with respect to the sample. The circuit used in this application is shown in Figure 5.4. The first stage amplifier is a current-to-voltage converter with gain. The second stage amplifier is an inverting voltage follower with gain. This two stage amplifier design is necessary because of the low responsivity of the photodiode near the excitation wavelengths used in luminescence. The responsivity of the photodiode at 254 nm is 0.14 A/W, compared to 0.62 A/W at 900 nm [4]. The output of this amplifier is then passed through a Schmitt trigger to obtain a TTL signal.

The microcomputer is able to monitor the status of the chopper through the 8255A parallel peripheral interface. The 8255A contains three 8-bit ports, A, B, and C. In the mode used for basic input/output, each port can be configured individually. The output of the Schmitt trigger on the photodiode circuit serves as the input to the input port C0 on the 8255A. It is through bit 0 of the port C status byte that the microcomputer can determine if the source is blocked or not. If the bit is set to 1, the excitation radiation is viewed by the sample; conversely, if the bit is set to 0 the source

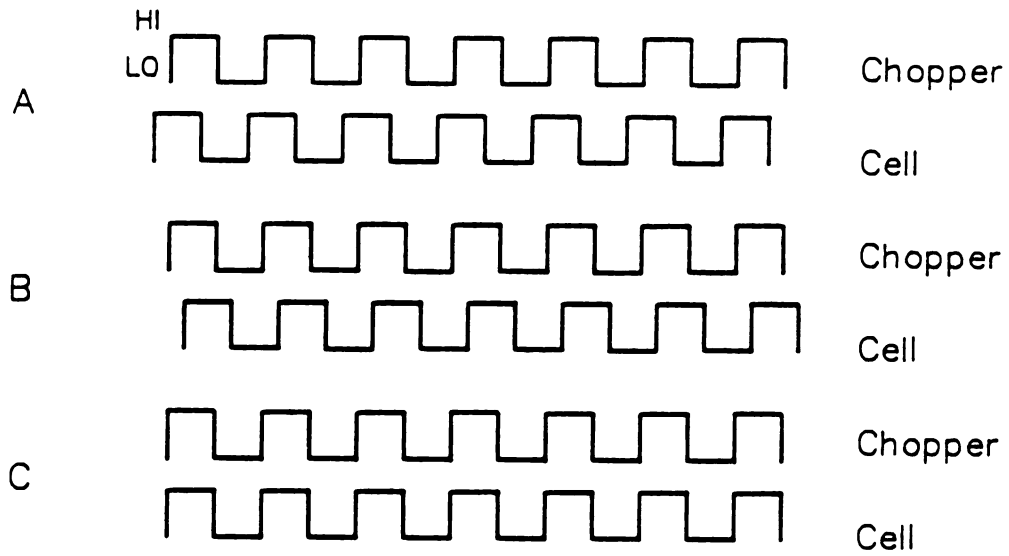


Figure 5.3

Timing diagram depicting the three types of phasing: A, chopper signal lags source signal; B, chopper signal leads source signal; and C, signals are in phase.

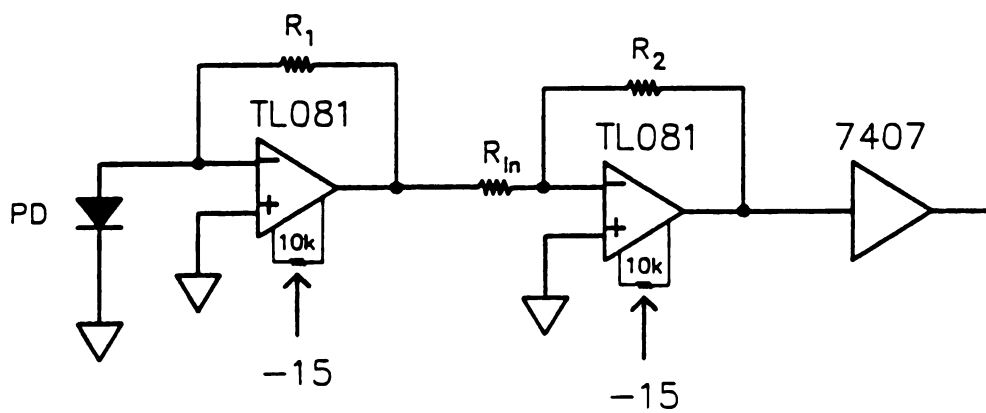


Figure 5.4 Photodiode amplifier circuit.  $R_1 = 1\text{ M}\Omega$ ,  $R_2 = 2.2\text{ M}\Omega$ , and  $R_{in} = 680\ \Omega$ .

is blocked. The FORTH word ?STAT checks the status of port C0 through the address of port C, ".CPIO". (See code in block number 160 in Appendix A.)

The chopping frequency is adjusted by the voltage applied to the motor rotating the masking disk. The frequency of oscillation is determined by programming the counter/timer to count the number of HI to LO transitions per unit time. A program, ?FREQ, was written to count the number of transitions in 1 s and then report the frequency in Hertz. (See Appendix A, block number 161, 162.) This program uses two of the counters on the 9513. Counter 1 is programmed to count the number of LO to HI transitions and accumulate the sum while the counter is active. This counter is active only while counter 2 is active. Counter 2 is programmed to wait for the first LO to HI transition and then delay for 1 s. The delay period is adjustable to 10 s with the word 10SEC, and back to 1 s with 1SEC. With these programs it is possible to determine the chopping frequency accurately.

For experiments in flow injection analysis, two other peripheral devices were interfaced to the microcomputer: a peristaltic pump (model IP-12, Brinkmann Instruments, Westbury, NY), and a pneumatically actuated Teflon rotary sample injection valve (Rheodyne type 50, Anspec Co. Inc., Ann Arbor, MI). The pump is supplied with connections to be used for remote functions through a 5-pin male plug (Switchcraft model 05BL5M or equivalent). Speed control of the pump is accomplished by supplying 0-5.5 Vdc to pole 3 and grounding pole 2. The variable voltage supply is obtained by connecting a voltage divider to the second 8-bit DAC which limits the voltage maximum to 5.5 Vdc. The pump speed is changed on the pump with a digital setting between 0 and 99. The desired digital setting is passed to the program PUMP (see Appendix A, block number 24) which calculates the data value for the DAC to obtain the corresponding pump speed from the desired pump digital setting. The relationship between the DAC output and the actual pump speed was determined

experimentally by measuring the voltage supplied to the pump motor for various digital settings.

The direction of the pump is controlled through bit 0 of port B on the 8255A. This pin is connected to pole 4 on the pump and pole 2 is connected to ground. Setting bit B0 to 0 should cause the pump to change directions. However, the pump loaded the 8255A output and was not able to sink the current. Therefore, a 7407 HEX buffer was added between the 8255A and the pump. The FORTH words FWRD and RVRS set the direction of the pump to forward and reverse, respectively.

The sample injection valve is controlled through bit 0 of port A. The output of the port is used to control a photo-isolated, zero-voltage switching relay (Magnavox model W3PCX-1, Newark Electronics, Grand Rapids, MI). This relay controls the 120 Vac pneumatic actuator. A zero-voltage switching relay is used to minimize rf switching noise which had the tendency to "crash" the microcomputer.

### ***Experimental Determination of the Dominant Noise Source***

This section describes experiments which were performed to determine the dominant noise source(s) in the home-built instrument. Knowledge of the major noise sources could indicate modifications in the instrumental design to improve the signal-to-noise ratio. The signal-to-noise ratio (S/N) is defined as the ratio of the mean value of the analytical signal divided by the rms noise,  $S/N = E/\sigma_E$  [5]. The rms noise is the standard deviation of the analytical signal derived from n measurements. There are several different types of noise. Random noise is unpredictable in its sign and magnitude of deviation from the mean signal. The sign and magnitude of the deviation for nonrandom noise can be correlated in time to some event.

Noise can also be classified as fundamental or nonfundamental. Fundamental noise arises from the particle nature of light and electricity and cannot be completely eliminated. Nonfundamental noise is due to imperfect components and instrumentation. This noise can be eliminated through careful instrument design.

The noise observed in a signal is due to the summation of the fluctuations emanating from random and nonrandom noise sources. As this section is not intended to be a discussion of signal-to-noise ratio theory, the reader is referred to a recent text by Crouch and Ingle for a more thorough discussion [6].

There are three limiting cases of noise: dark current noise, which is independent of the source radiation flux,  $\Phi$ ; shot noise, with a standard deviation ( $\sigma_E$ ) proportional to  $\sqrt{\Phi}$ ; and flicker noise, with  $\sigma_E$  proportional to  $\Phi$ .

Photons arrive randomly at the photocathode of the radiation transducer because of the random emission of photons from the excitation source or analyte. The signal ( $E$ ) from photoanodic current ( $i_a$ ) of the PMT is

$$E = Gi_a = mGR(\lambda)\Phi \quad (5-1)$$

where  $G$  is the current-to-voltage converter gain,  $m$  is the PMT gain, and  $R(\lambda)$  is the PMT cathodic responsivity. For the Shot noise-limited case

$$\sigma_E = [2e\Delta f(1+\alpha)mGE]^{1/2} \quad (5-2)$$

where  $\Delta f = 1/(4RC)$  is the noise bandpass of the electronics,  $\alpha$  is the secondary emission or multiplication noise factor, and  $e$  is the charge on an electron. The signal-to-noise ratio determined from equations 5-1 and 5-2 reduces to

$$S/N = E/\sigma_E = \sqrt{\Phi}/k \quad (5-3)$$

where  $k = [2e\Delta f(1+\alpha)]^{1/2}$  and is a bandwidth constant proportional to  $\Delta f$  [5]. Therefore, equation 5-3 indicates that the  $S/N$  increases as the square root of  $\Phi$ . Shot Noise is reflected in the readout because all conversions following the photocathode multiply the signal and noise by linear factors. Equation 5-3 indicates that a plot of  $\log(S/N)$  vs  $\log(\Phi)$  should yield a slope of 1/2. Since flicker noise is proportional to  $\Phi$ , a plot of  $\log(S/N)$  vs  $\log(\Phi)$  should yield a slope of unity. Because the dark current noise is independent of  $\Phi$ , a  $\log(S/N)$  vs  $\log(F)$  plot will have a slope of zero. This was tested experimentally by varying the monochromator slit width and measuring the  $S/N$ . This experiment was performed under conditions normally used for fluorescence and

phosphorescence work in this research since the signal level will change the dominant source of noise. For a continuum source, the radiant power passed by the monochromator is proportional to the square of the slit width provided the entrance and exit slits are of equal size [6]. In fluorescence spectroscopy,  $I_f$  is a linear function of  $\Phi$ . Therefore, any increase in  $\Phi$  will increase  $I_f$ . The fluorescence intensity of 0.1  $\mu\text{M}$  quinine sulfate in 0.2 M sulfuric acid was monitored at 450 nm with an excitation wavelength of 365 nm for three different slit widths. Data from this experiment are shown in Table 5.2. Since the signal  $E$  is proportional to  $\Phi$ , a plot of  $\log(S/N)$  vs  $\log(E)$  is equivalent to a plot of  $\log(S/N)$  vs  $\log(\Phi)$ . Results from a linear regression yield a slope of 0.468 with a correlation coefficient of 0.993. This is only a 6.4% deviation from the value of 0.500 expected for shot noise. Therefore, photocurrent shot noise can be assumed to be the limiting noise in this instrument under these conditions.

Table 5.2  
Effect of Radiant Power on the S/N

Slit Width (mm)	Signal (ADC counts) <sup>a</sup>	$\sigma_n$	S/N
2.	3600	52	69
2.	3700	52	71
1.	230	9	26
1.	230	10	23
0.5	17	3	6
0.5	17	3	6

<sup>a</sup>average of 100 analog-to digital conversions

### Perkin-Elmer Model LS-5 Luminescence Spectrometer

The model LS-5 luminescence spectrometer is a microprocessor controlled instrument with digital display. The source of radiation is 9.9 W xenon discharge lamp which is pulsed at 60 Hz. The source pulses have a full width at half maximum of less than 10  $\mu$ s. Wavelength isolation is facilitated by two F/3 monochromators. These monochromators are stepper motor driven and can be scanned independently. The excitation monochromator covers the wavelength range of 230-720 nm while the emission monochromator covers 250-650 nm. The range of the emission monochromator can be extended to 800 nm with a red sensitive PMT. Both monochromators are capable of isolating the grating zero order. The spectral bandpasses of the monochromators are selectable with nominal values of 3, 5, 10, and 15 nm for excitation and 3, 5, 10, and 20 nm for emission.

The LS-5 instrument includes an excitation/correction system that uses a quantum counter (rhodamine B) in front of a reference PMT. The reference PMT is matched to the sample PMT. Rhodamine B has a fluorescence quantum efficiency that is nearly independent of the excitation wavelength. The ratioing system of the LS-5 corrects source spectral distribution and the wavelength dependence of the excitation monochromator and optics.

The LS-5 is capable of gating the detector which allows phosphorescence measurements to be made. The delay and gate times of the PMT are selectable in increments of 10  $\mu$ s not to exceed a total of 13ms.

A Perkin-Elmer model 3600 data station is connected to the LS-5 through a RS232C interface for instrument control and external data manipulation. The data station also includes software for data manipulation, graphical display, and mass storage on floppy diskette.

**CHAPTER V REFERENCES**

1. Newcome, B.H.; Enke, C.G., *Rev. Sci. Instrum.*, **1984**, *55*, 2017
2. Ratzlaff, E.H., Ph.D. Thesis, Michigan State University, East Lansing, MI, **1982**
3. Philip Hoffman, private communication, January, 1982
4. Brodie, L., *Starting FORTH*; Prentice-Hall: Englewood Cliffs, NJ, 1981
5. Malmstadt, H.V.; Enke, C.G.; Crouch, S.R., *Electronics and Instrumentation for Scientists*; Benjamin/Cummings: Menlo Park, CA, 1981
6. Crouch, S.R.; Ingle, J.D., *Spectrochemical Analysis*; Prentice-Hall, 1988; Chapter 5.

## CHAPTER VI

### LUMINESCENCE SPECTRA

This chapter describes an experimental approach to obtaining RTP. First, the purification and preparation of the reagents required are discussed. Like fluorescence, phosphorescence arises from intersystem crossing of the excited singlet state to the triplet state. Hence, the absorption transition leading to phosphorescence is identical to that leading to fluorescence. This chapter discusses the fluorescence excitation and emission spectra of selected compounds. Solutions of these compounds were then prepared for RTP and phosphorescence spectra obtained.

#### Reagents

All luminescence studies described were performed with solutions. The analyte microenvironment for this work was provided by either micellar assemblies or cyclodextrin inclusion complexes. The surfactant used for micelles was sodium dodecyl sulfate (SDS, also known as sodium lauryl sulfate, Aldrich Chemical Co. Inc., Milwaukee, WI). This surfactant was 98% pure and is used without purification. The  $\beta$ -cyclodextrin (CD) was also used without additional purification (Aldrich). As discussed in Chapter III, a heavy atom is normally required to obtain phosphorescence. For the CD solutions the heavy atom was 1,2-dibromoethane (99+% Gold Label, DBE, Aldrich) and was used as supplied. All water used in these studies was obtained from a Corning Mega-Pure system. House distilled water first passes through deionizing columns to remove organics. The water is then distilled which results in a resistance of at least 50 k $\Omega$  cm.

For micellar solutions, thallium(I) ion is the preferred heavy atom to increase the phosphorescence yield. A high purity thallium nitrate (99.999%, Gold Label, Aldrich) was used. To avoid unnecessarily high ionic concentration in these solutions, thallium(I) dodecyl sulfate (TIDS) was prepared by a previously reported method [1]. This method involves mixing approximately stoichiometric quantities of SDS and thallium(I) nitrate solutions prepared in warm water. The precipitate was allowed to form overnight. The TIDS was then doubly recrystallized from water and dried overnight in a vacuum oven at 40°C. Stock solutions of SDS and CD were prepared with a concentration of 0.50 M. Working solutions with concentrations of 0.10-0.15 M were prepared from these stock solutions. Because of the limited solubility of TIDS, a 0.10 M stock solution of this reagent was prepared. However, even at this concentration, some precipitation occurred. Therefore, the solution was warmed slightly and mixed thoroughly prior to preparation of working solutions.

Deoxygenation of all solutions for phosphorescence measurements was performed by the addition of sodium sulfite. Sodium sulfite was purified by double recrystallization from cold water. The precipitate was then dried in a vacuum desiccator for several days. Stock solutions (0.10 M) were prepared in water just prior to preparation of working solutions to minimize the loss of sulfite because of reaction with ubiquitous oxygen. Once working solutions were prepared, the ground glass fittings on the sample volumetric flasks were sealed with Parafilm laboratory film (American Can Co., Greenwich, CT) to ensure an air-tight seal.

The analytes used in this research, naphthalene, pyrene, and biphenyl, were all doubly recrystallized from absolute ethanol and dried in a vacuum desiccator for several days. 2-Bromonaphthalene (97%, Aldrich) was used as received. Stock solutions of these compounds for use in micelles were prepared by dissolving the analyte in absolute ethanol. An aliquot of this ethanolic solution was pipetted into a clean, dry volumetric flask. The ethanol was evaporated with dry nitrogen gas. The residue was then

dissolved in 0.50 M SDS by ultra-sonification of the solution. The solution was then diluted to the mark with water. The stock analyte solution was prepared with a concentration of 1.0 mM. The surfactant concentration was either 0.50 or 0.10 M.

Although early work in solution RTP [1,2] suggested that all glassware be baked at 1000 K prior to being used for the first time for RTP work, this was not done in these studies. All glassware was cleaned scrupulously and rinsed with 20% nitric acid. The glassware was then rinsed with copious amounts of water. The same volumetric flasks were used throughout.

### **Fluorescence Spectra**

Fluorescence excitation and emission spectra of naphthalene, 2-bromonaphthalene, pyrene, and biphenyl, are presented in this section. The excitation wavelength for each analyte was determined by setting the emission monochromator to the zero order and scanning the excitation monochromator. The excitation monochromator was then set at the wavelength yielding the greatest relative fluorescence intensity. The emission monochromator was scanned to determine the emission wavelength. A final excitation spectrum was then obtained with the emission monochromator set at the wavelength yielding the greatest relative fluorescence intensity.

The excitation and emission spectra for naphthalene in 0.15 M SDS are shown in Figure 6.1. Spectra A and B were obtained on the Perkin-Elmer LS-5 spectrofluorometer with 5 nm bandpass on both the excitation and emission monochromators. These spectra show an absorbance band centered at 276 nm and a fluorescence band at 330 nm. Spectrum C was taken on the home-built system with 16 nm bandpasses on both monochromators. The luminescence intensities are given in arbitrary units. The peak at ~505 nm seen in spectrum C is believed to be due to

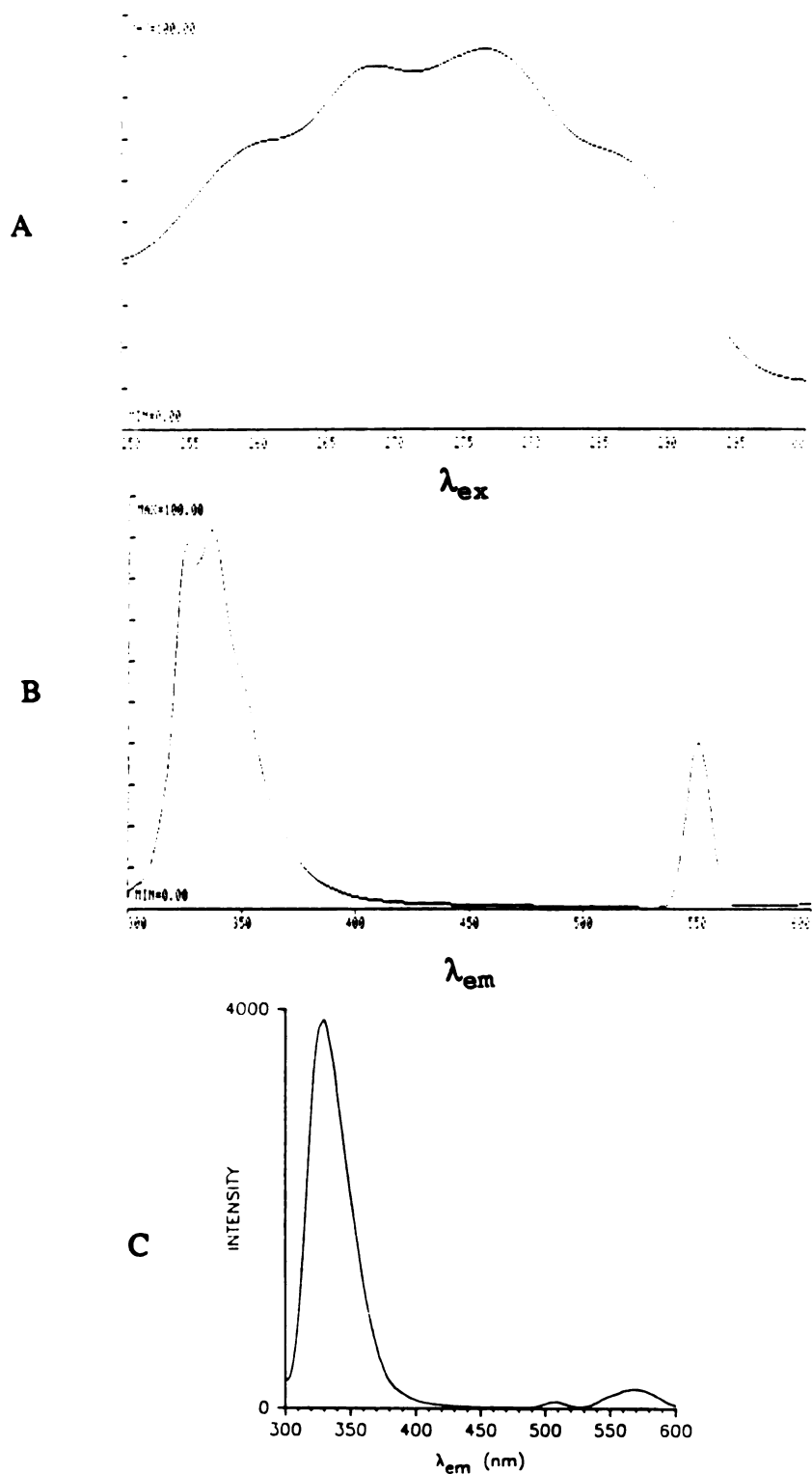


Figure 6.1

**Excitation and fluorescence emission spectra of naphthalene.**  
 A) excitation scan taken on Perkin-Elmer LS-5 with  $\lambda_{em} = 330$  nm.  
 B) emission scan taken on LS-5 with  $\lambda_{ex} = 276$  nm. C) emission scan taken on home-built instrument with  $\lambda_{ex} = 280$  nm. See text for explanation of peaks above 450 nm.

impurities in the quartz cell used. The peak at ~560 nm in spectrum B and C is due to scattered source radiation in the second order.

With the same instrument parameters, the excitation and emission spectra of 2-bromonaphthalene were obtained, as shown in Figure 6.2. The excitation band is centered at 286 nm with a fluorescence band at 316 nm.

Figure 6.3 shows the excitation spectrum for pyrene taken with an emission wavelength of 395 nm on both instruments. These spectra differ because the spectrum taken on the Perkin-Elmer LS-5 is corrected, while that taken on the home-built instrument system is uncorrected. The higher resolution of Figure 6.3 B is due to the narrower bandpasses of the monochromators. The fluorescence spectrum of pyrene in Figure 6.3 C has an emission band at 395 nm.

Spectra of biphenyl were acquired solely on the Perkin-Elmer LS-5, as shown in Figure 6.4. The absorption band is centered at 260 nm with the fluorescence emission at 472 nm. The bandpasses of both monochromators were 5 nm.

### **RTP Spectra**

The goal of this research was to develop a system for automating RTP measurements by introducing samples via flow injection analysis (FIA). This requires working with solutions. Therefore, for direct measurement of analyte phosphorescence, only two techniques for obtaining RTP are applicable, micelle stabilized RTP (MS-RTP) and cyclodextrin induced RTP (CD-RTP). Phosphorescence spectra obtained using these techniques are presented below.

#### ***MS-RTP Spectra***

MS-RTP cannot be obtained by simply preparing a sample in a soap solution. There must be a mechanism for spin-orbital coupling, and the sample solution must be deoxygenated. Figure 6.5 is the fluorescence spectrum of naphthalene in 0.10 M SDS and in 0.10 M SDS with 25 mM  $\text{TlNO}_3$ . Notice that the addition of the thallium ion

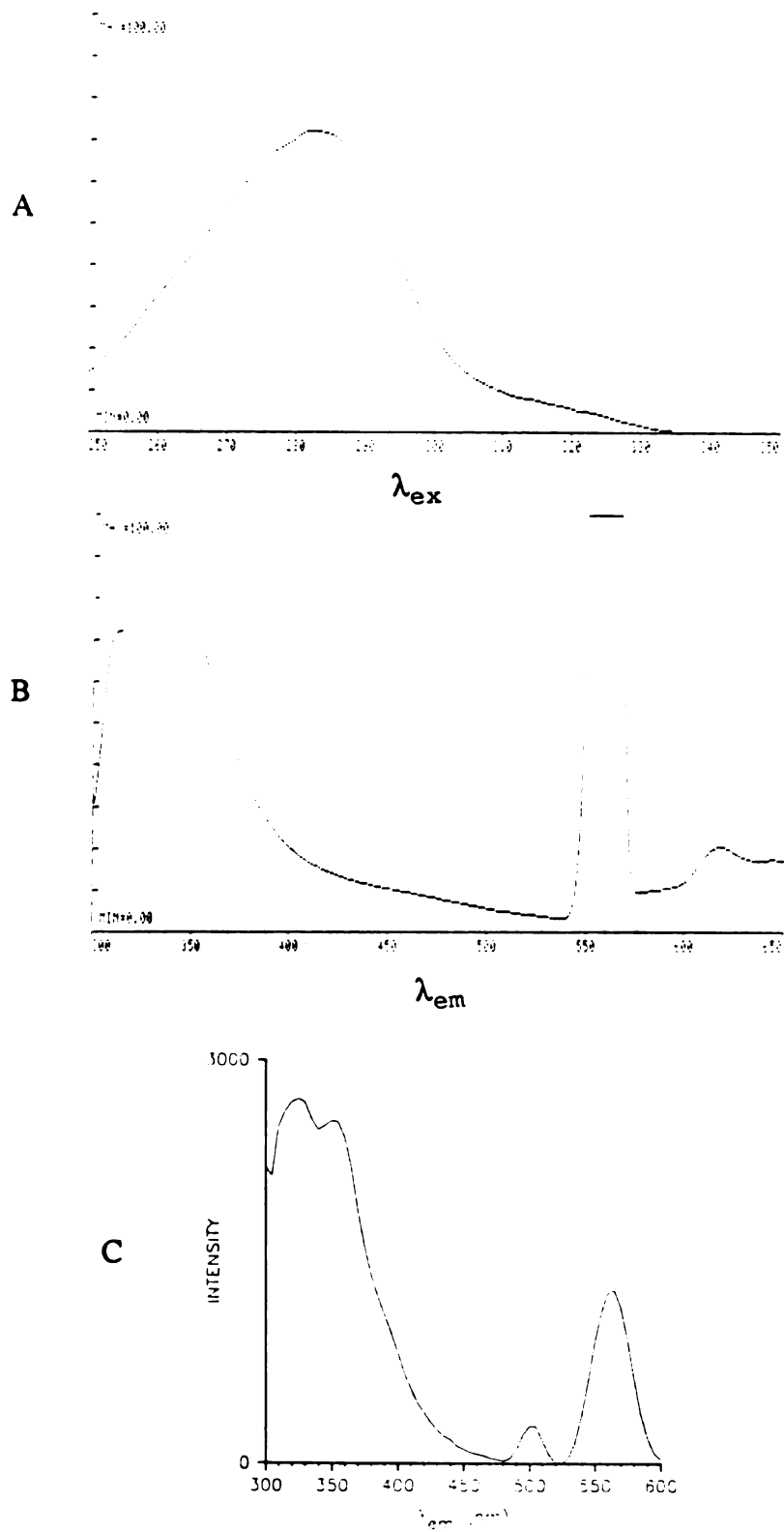


Figure 6.2 Excitation and fluorescence emission spectra of 2-bromonaphthalene. A) excitation scan from LS-5 with  $\lambda_{em} = 315$  nm. B) emission scan from LS-5. C) emission scan from home-built instrument.

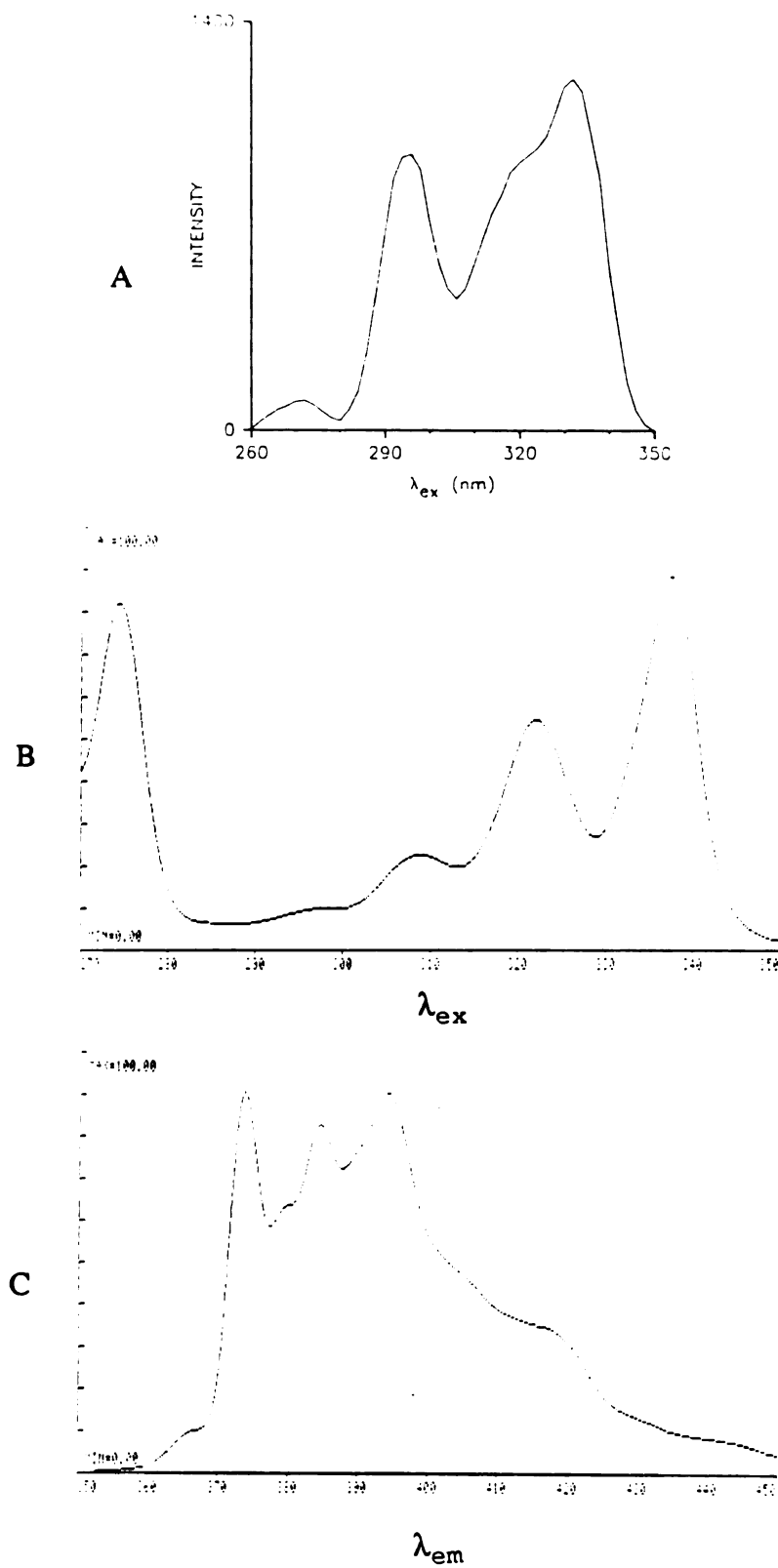


Figure 6.3

Excitation and fluorescence emission spectra of pyrene. A) excitation scan taken on home-built instrument with  $\lambda_{em} = 395$  nm. B) excitation scan taken on LS-5 with. See text for explanation in peak intensities. C) emission scan taken on LS-5,  $\lambda_{ex} = 335$  nm.

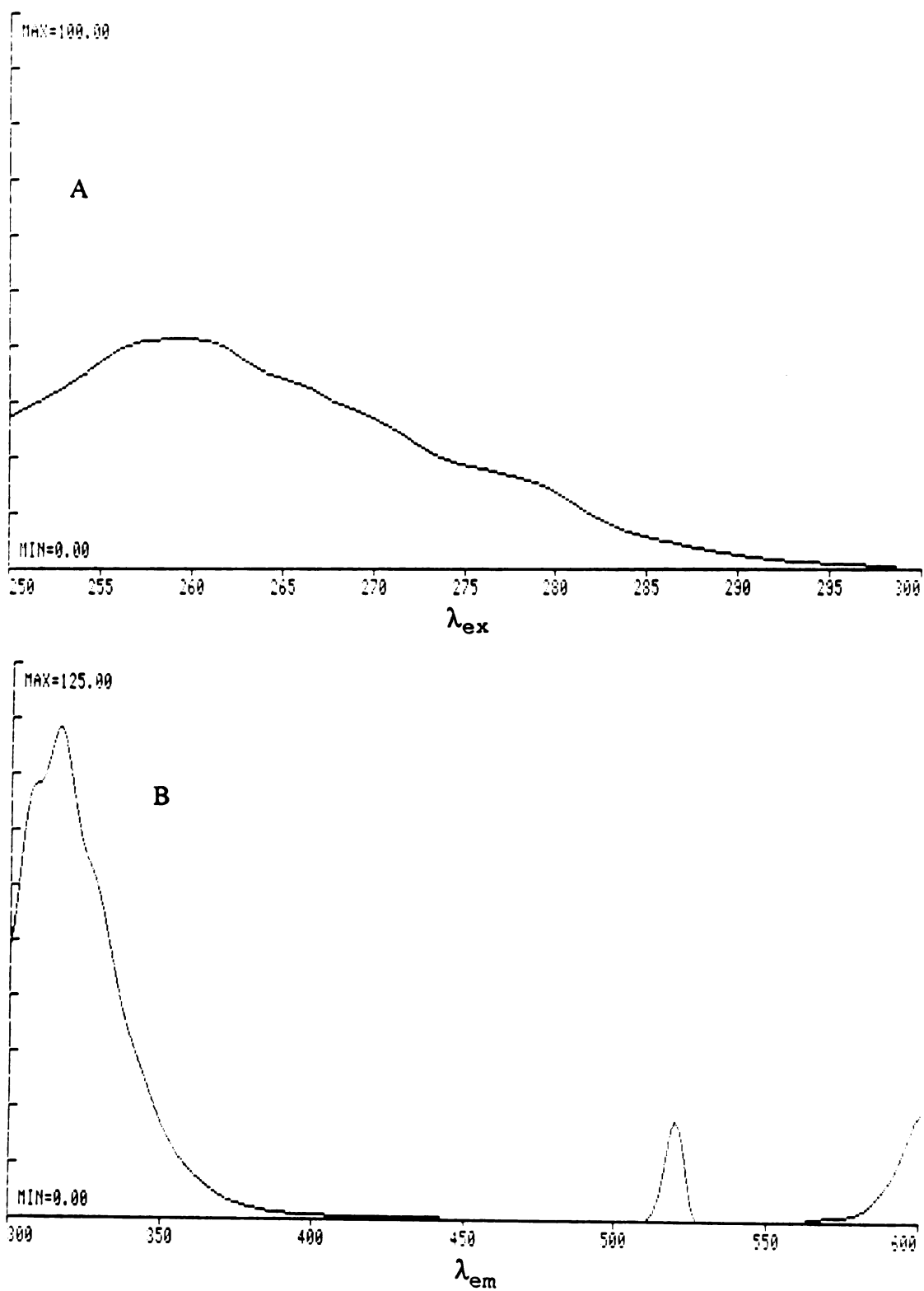


Figure 6.4 Excitation and fluorescence emission spectra of biphenyl taken on LS-5. A) excitation scan with  $\lambda_{em} = 315$  nm. B) emission scan with  $\lambda_{ex} = 260$  nm.

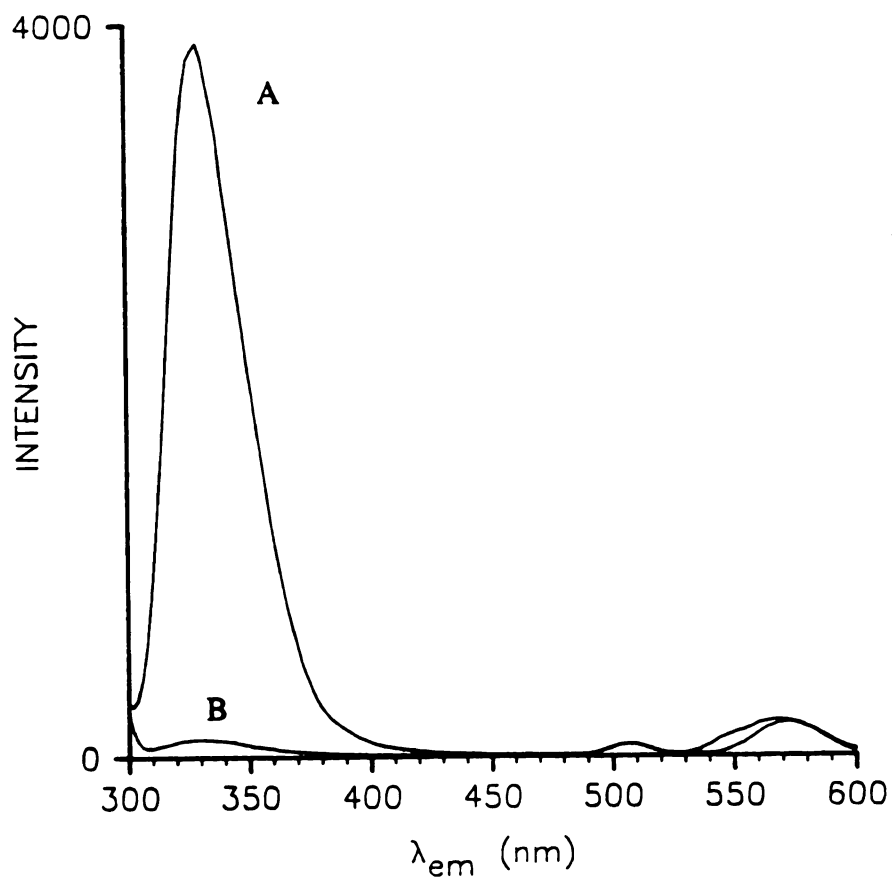


Figure 6.5

Fluorescence emission of naphthalene taken on home-build instrument with  $\lambda_{ex} = 280$  nm and 16 nm bandpasses. A) 0.10 M SDS, and B) 0.10 M SDS with 25 mM  $TlNO_3$  added. See text for explanation.

markedly decreases the observed fluorescence intensity. This is due to an enhanced probability of the excited singlet-to-triplet transition. The triplet state non-radiatively decays because of quenchers, such as molecular oxygen, in the solution. The peak observed at 570 nm is due to scatter excitation radiation of 286 nm in the second order. The peak at ~505 nm is believed to be due to an an impurity in the quartz cell [4].

Deoxygenation of the heavy-atom containing solution removes the quencher inhibiting the radiative triplet-to-ground state transition. The solution was deoxygenated by adding sodium sulfite. Figure 6.6 shows the spectra of the deoxygenated and non-deoxygenated heavy-atom containing solutions. The deoxygenated solution has a shoulder present at 485 nm. Also, the peak at 505 nm has increased in intensity and shifted to 510 nm. A phosphorescence spectrum of the deoxygenated, heavy-atom containing solution is shown in Figure 6.7. The peak at 330 nm is due to delayed fluorescence, and phosphorescence peaks are observed at 480, 510, and 560 nm. The peak at 560 nm is due partially to scattered excitation radiation in the second order. Therefore, to observe RTP, the analyte must have a mechanism to enhance the singlet-to-triplet transition, and the solutions must be deoxygenated.

All solutions for MS-RTP measurements were prepared by dilution of the stock analyte solution in SDS. The working solution contained 0.10-0.15 M 30/70 TI/Na DS with 10 mM sodium sulfite to reduce oxygen. The sample cell used in these experiments was a standard  $1 \text{ cm}^2$  fluorescence cell modified so that a rubber stopper may be used to form an air-tight seal. This minimizes diffusion of oxygen into the solutions once they have been deoxygenated. The deoxygenation reaction of sulfite ion was discussed in Chapter III.

The concentration of the surfactant influences the time for deoxygenation of the solution [3]. Figure 6.8 shows the rise in the RTP of 2-bromonaphthalene for two surfactant concentrations, 0.15 and 0.10 M 30/70 TI/Na DS. These plots were obtained with the home-built instrument used in phosphorescence mode. The instrument was

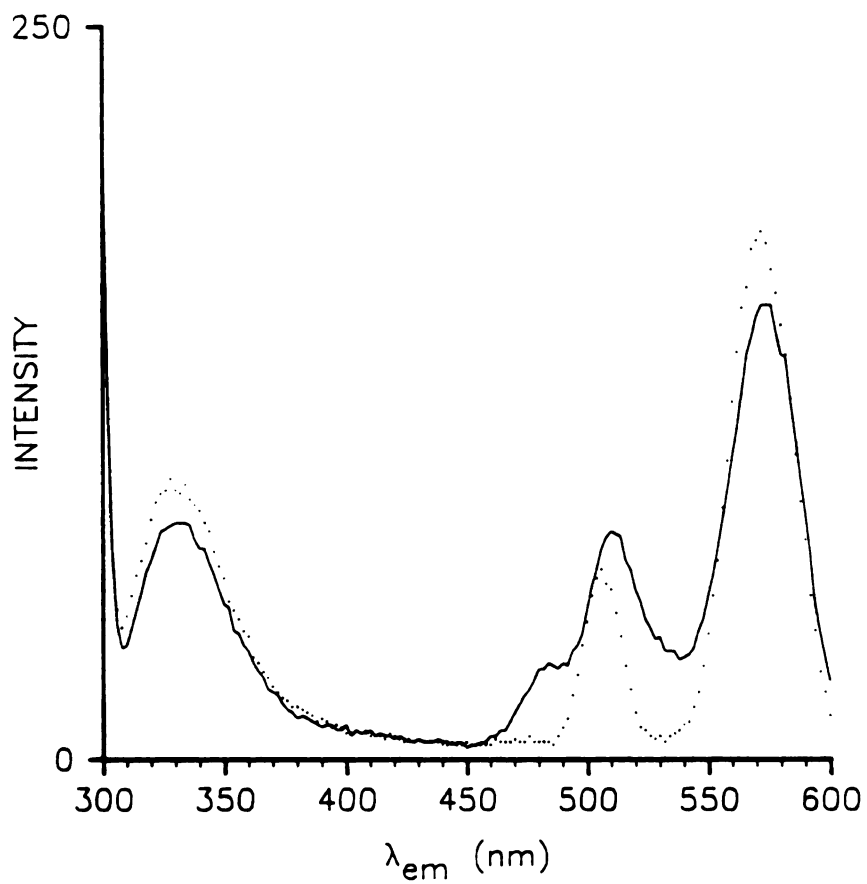


**Figure 6.6** Luminescence spectra of naphthalene in 0.10 M SDS with 25 mM  $TiNO_3$  (dotted line), and deoxygenated solution (solid line).

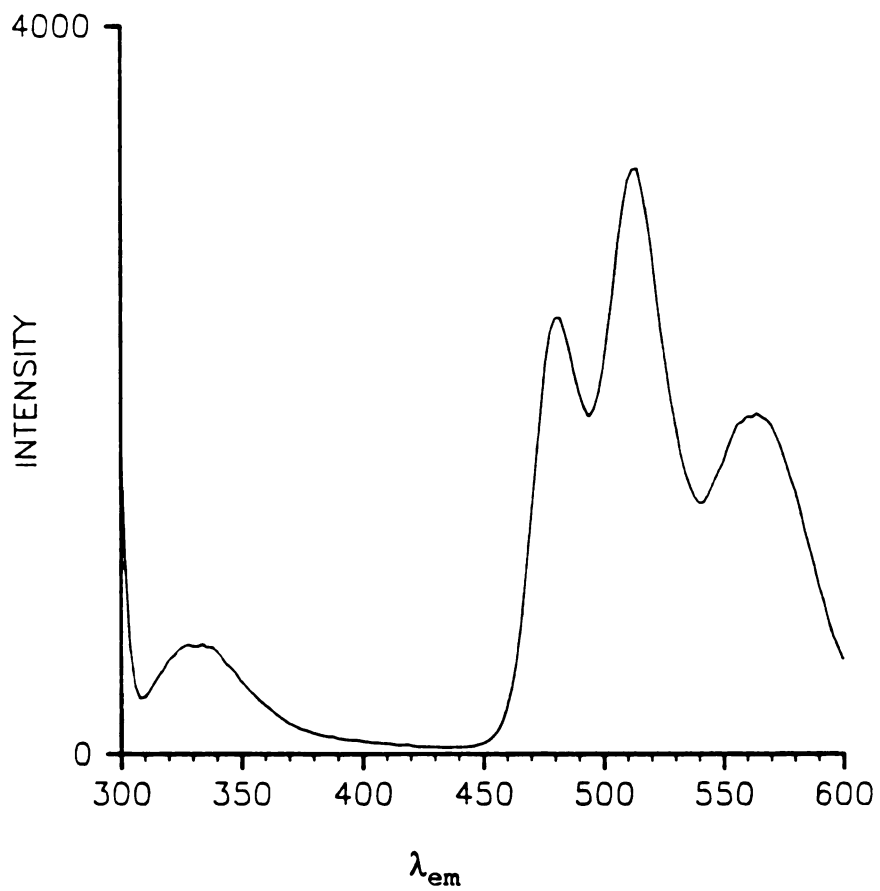


**Figure 6.7** Phosphorescence spectrum of naphthalene in 0.10 M SDS with 25 mM  $\text{TiNO}_3$  and 10 mM  $\text{Na}_2\text{SO}_3$ . Delay time after HI-to-LO transition of chopper is 10  $\mu\text{s}$ .

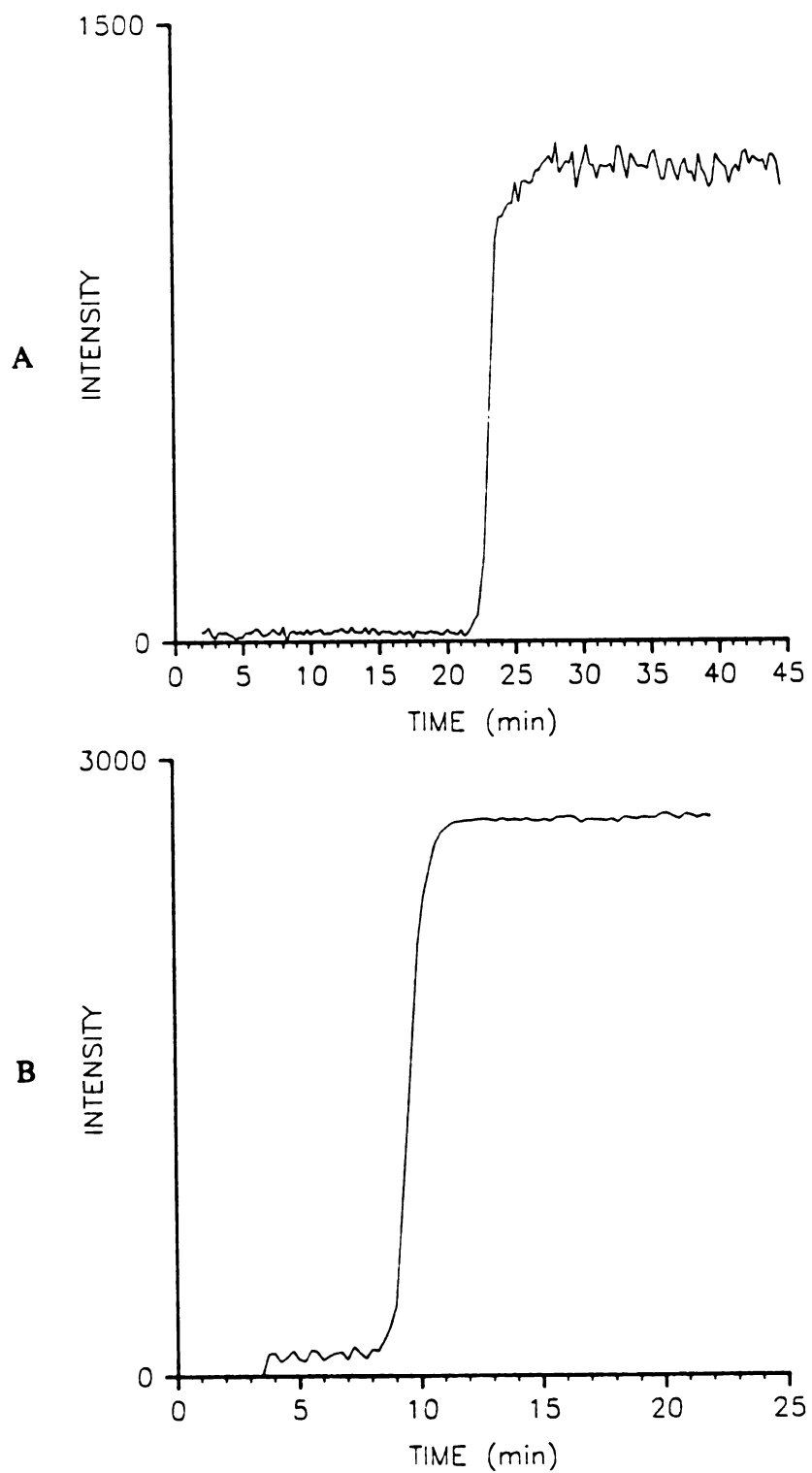


Figure 6.8

Rise in phosphorescence intensity for two concentrations of surfactant. A) 0.15 M 30/70 TI/Na DS. B) 0.10 M 30/70 TI/Na DS. Phosphorescence intensity is in arbitrary units.

programmed to sample the phosphorescence intensity every 15 s for 45 min. These studies showed that for 0.15 M surfactant solutions, approximately 23 min. should be allowed for deoxygenation in order to observe RTP. For 0.10 M surfactant this time is reduced to 10 min. Although decreasing the surfactant concentration decreases the time required for solution deoxygenation, low surfactant concentrations should be avoided because this decreases the micelle concentration. Low micelle concentrations will increase the number of analyte molecules located within a micelle. If two analyte molecules are located in the same micelle, triplet-triplet annihilation or excimer formation can become the principal deactivation mechanism at room temperature [5]. This can be a cause of curvature in MS-RTP calibration curves [1].

The MS-RTP spectra of 2-bromonaphthalene, pyrene, and biphenyl are shown in Figures 6.9, 6.10, and 6.11, respectively. These spectra all show phosphorescence peaks red-shifted relative to their fluorescence peaks. 2-Bromonaphthalene has RTP peaks at 485, 515 and 565 nm. This latter peak is due partially to second-order scattered excitation radiation. Pyrene has a low intensity peak at 520 nm with two more intense peaks at 595 and 650 nm. Characteristic RTP peaks for biphenyl are at 443 and 471 nm.

### ***CD-RTP Spectra***

The potential advantage of CD-RTP is due to its partial immunity to phosphorescence quenching by oxygen. This would simplify greatly sample preparation by eliminating the most difficult step. A solution of 2-bromonaphthalene in 0.01 M CD was prepared with 0.58 M DBE. Sodium sulfite was added to deoxygenate the solution to maximize the RTP intensity obtained. The CD-RTP spectrum of this solution is shown in Figure 6.12. This spectrum compares favorably with the MS-RTP spectrum in Figure 6.9. However, although a "cloudiness in the solution" was noted by Scypinski and Cline Love [6], considerable precipitation was observed here due to the addition of DBE. This abundant precipitate is a spectroscopists nightmare and

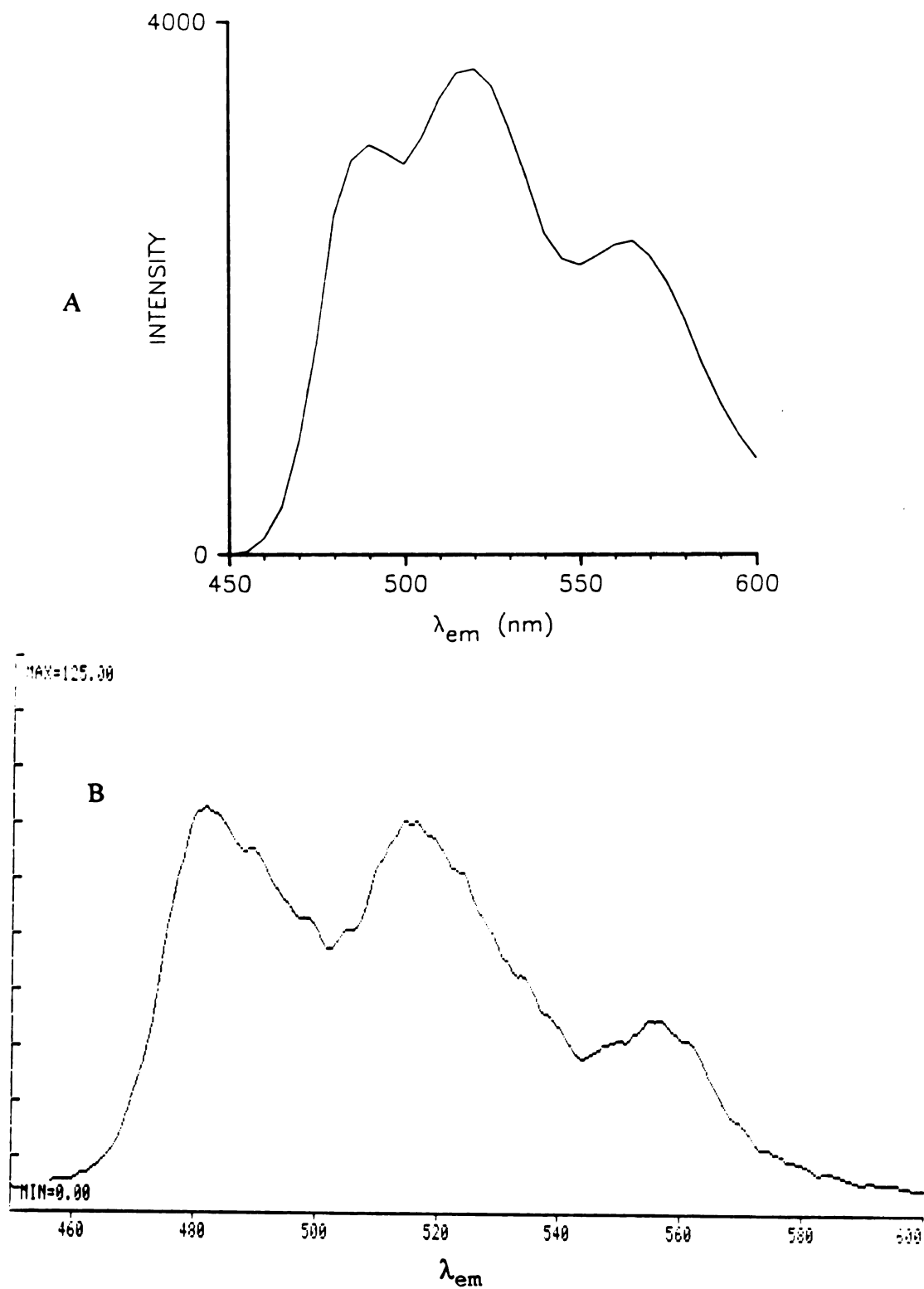


Figure 6.9 MS-RTP spectrum of 2-bromonaphthalene in 0.15 M 30/70 TI/Na DS with 10 mM Na<sub>2</sub>SO<sub>3</sub>. A) home-built instrument, and B) Perkin-Elmer LS-5.

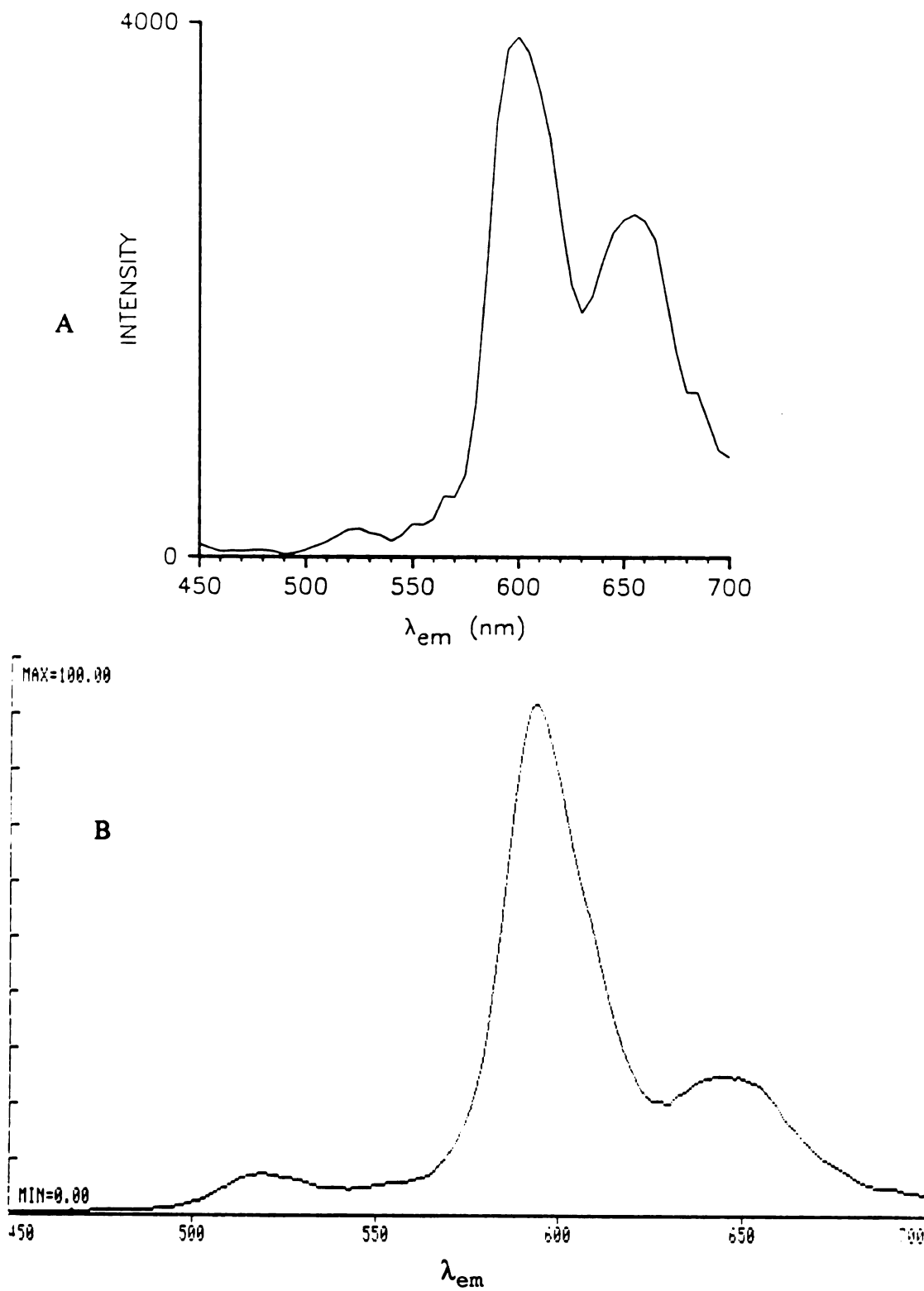
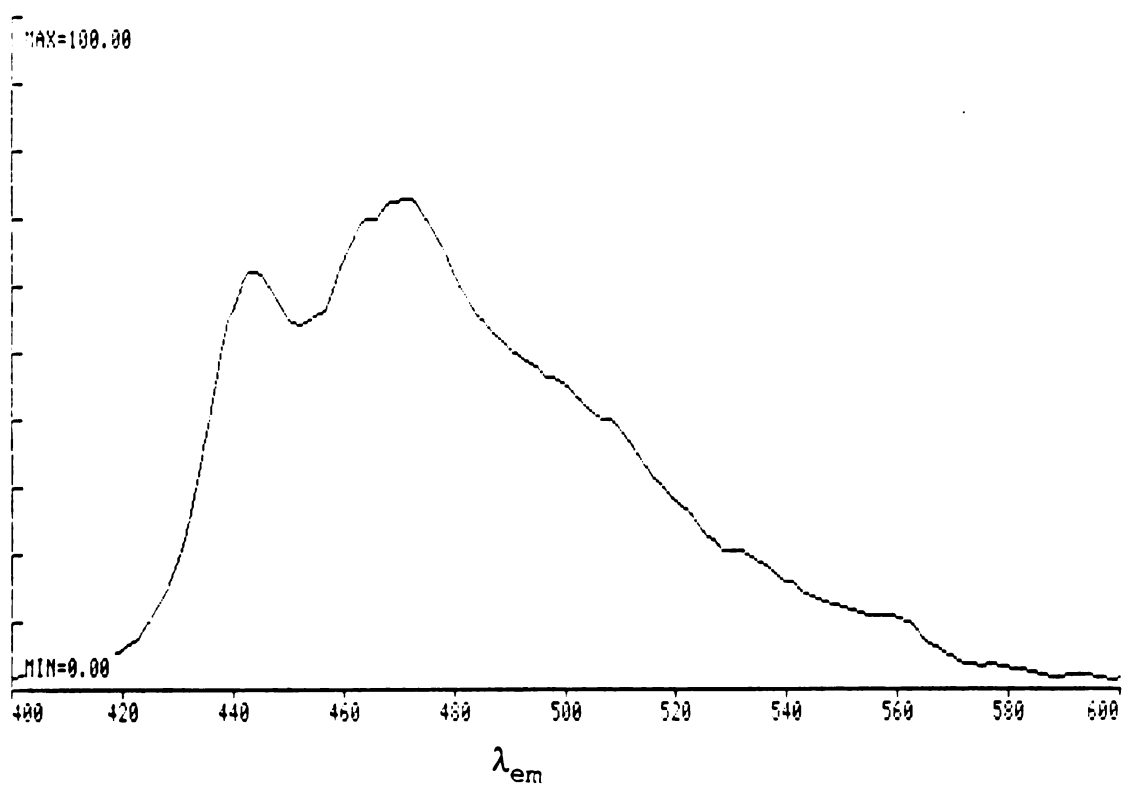
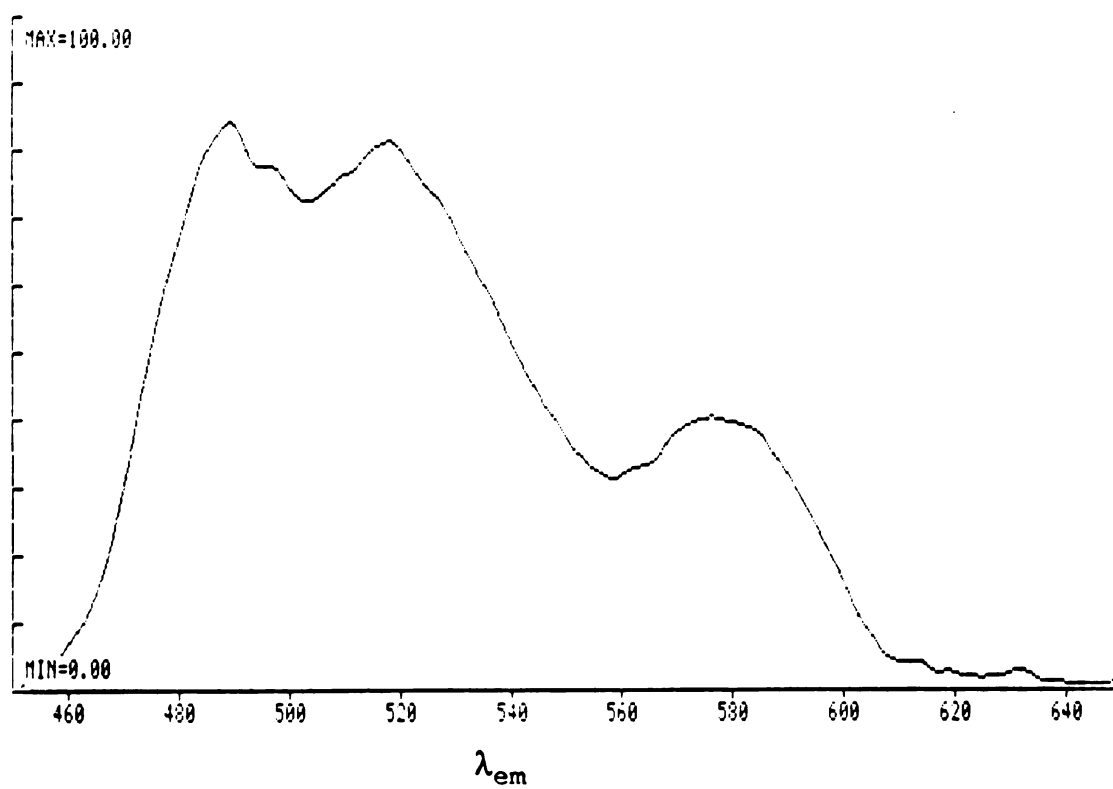


Figure 6.10 MS-RTP spectrum of pyrene in 0.15 M 30/70 TI/Na DS with 10 mM  $\text{Na}_2\text{SO}_3$ . A) home-built instrument, and B) Perkin-Elmer LS-5.



**Figure 6.11** MS-RTP spectrum of biphenyl in 0.10 M 30/70 TI/Na DS with 10 mM  $\text{Na}_2\text{SO}_3$ .



**Figure 6.12** CD-RTP spectrum of 2-bromonaphthalene in 0.01 M  $\beta$ -cyclodextrin with 0.58 M DBE.

precludes the use of CD-RTP in a flowing stream where the particles could plug the tubing and flow cell. Therefore, MS-RTP was chosen as the only viable method at present for direct analyte phosphorescence measurements in a flowing stream.

### **Phosphorescence Lifetimes**

Lifetime data are presented here only as a means of confirming the presence of RTP. It must be noted here that since many of the compounds used in this research were not purified meticulously, phosphorescence lifetimes obtained in these experiments will not necessarily compare well with values found in the literature. The phosphorescence lifetime of a compound is dependent on many factors such as the concentration and type of the heavy-atom species, the micelle concentration, and the presence of any contaminants and quenchers that may be found in the analytical solution. Equation 3-4 relates the phosphorescence lifetime to the rates of radiative and non-radiative deactivation and the micellar concentration. Since neither instrument has the capability for thermostating the sample chamber, variations in ambient temperature will also influence the observed phosphorescence lifetime.

The phosphorescence lifetime of naphthalene was obtained in 0.15 M 30/70 TI/Na DS. This solution was deoxygenated with 10 mM sodium sulfite. The FORTH program DECAY (blocks 70-72, Appendix A) was used to obtain the data for the lifetime determination on the home-built instrument. This program uses the counter/timer to count a delay time in  $\mu\text{s}$  after the HI-to-LO transition of the chopper. At the end of this count, the ADC is sampled and the data point is stored in memory. For each delay time, the user selects the number of ADC outputs to be averaged. The delay time is then incremented by a predetermined amount, and the process is repeated over a range of delay times. The data are then stored on floppy disk and transmitted serially to the LSI-11/23 for analysis and graphical presentation.

The phosphorescence decay is predicted to follow a single exponential decay. A simplex fitting routine, XYFIT, written by Wentzell [7] is used to fit the data to the following equation:

$$I_p(t) = I_0(e^{-kt}) + B \quad (6-1)$$

In this equation,  $I_p(t)$  is the phosphorescence intensity observed at time  $t$ ,  $k = 1/\tau_p$ , and  $B$  is included to account for any electrical and phosphorescence background in the signal.

The phosphorescence lifetime was also determined on the Perkin-Elmer LS-5 with the program OBEY DECAY on the Model 3600 Data Station. This program measures the phosphorescence intensity at six user selected delay times and uses a Guggenheim algorithm to calculate the lifetime. One immediate disadvantage of this system is that only six delay times can be used to calculate the lifetime, whereas the home-built instrument is not limited in this respect.

Phosphorescence decay curves of naphthalene acquired on both instruments are shown in Figure 6.13. The phosphorescence emission is monitored at 485 nm with an excitation wavelength of 280 nm on both instruments. The Perkin-Elmer DECAY OBEY program determined the lifetime to be 2.03 ms with a correlation coefficient of 0.9996, and a standard deviation of 0.062. These data were then fit to equation 6-1 with XYFIT. This determination resulted in a lifetime of 1.72 ms ( $I_0 = 818$ ,  $B = 50.5$ ) with a standard deviation of 1.13 for 6 points.

Results obtained on the home-built instrument yield a lifetime of 1.92 ms ( $I_0 = 2547$ ,  $B = -90$ ) with a standard deviation of .009 for 60 points. Bearing in mind that there was no temperature control through this series of experiments, the results from both instruments agree quite favorably. The phosphorescence lifetime of naphthalene found in the literature is 0.45 ms [8]. It is interesting to note that this lifetime is considerably shorter than observed in this laboratory. The Stern-Volmer equation predicts that quenchers and contaminants in the solution matrix will shorten

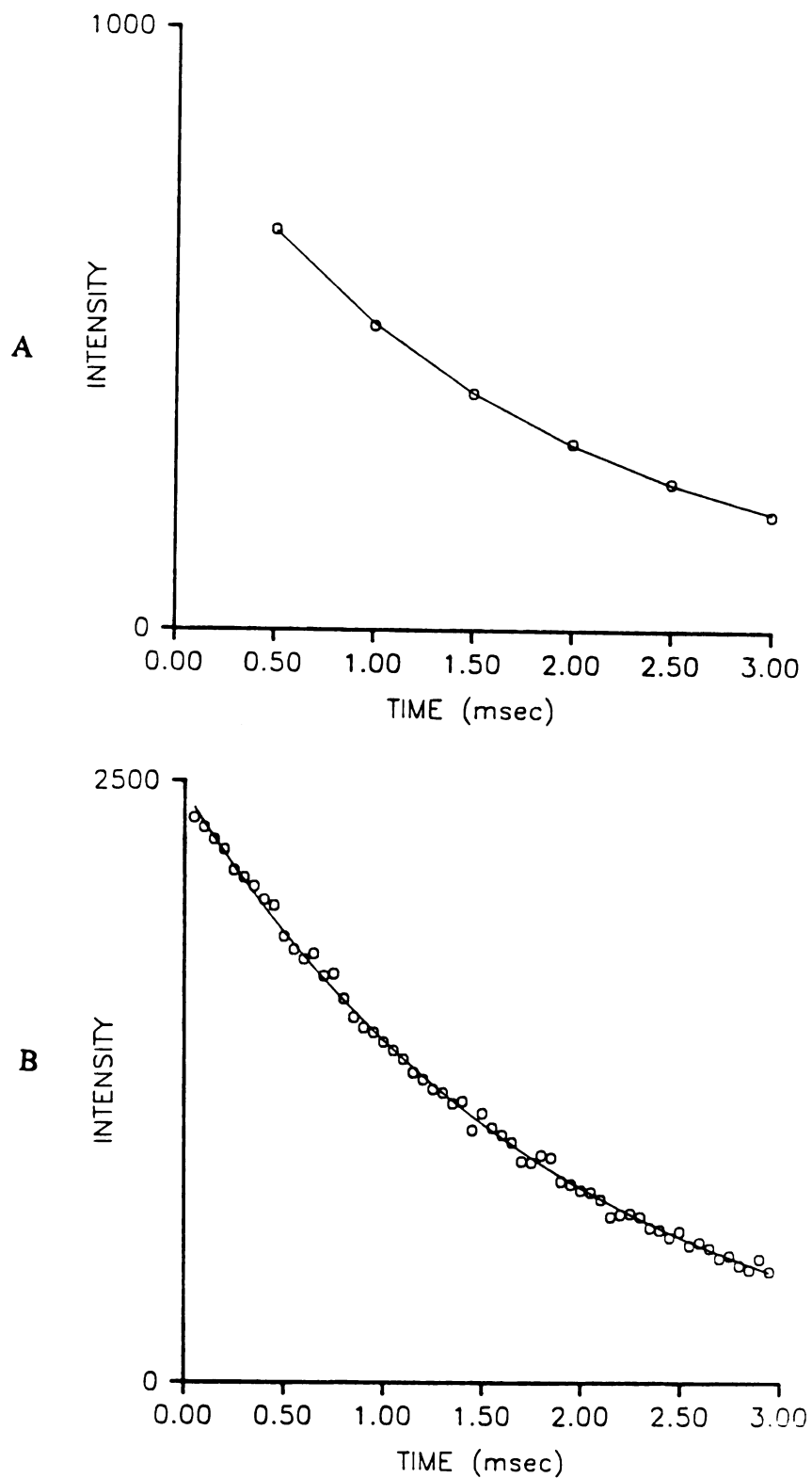
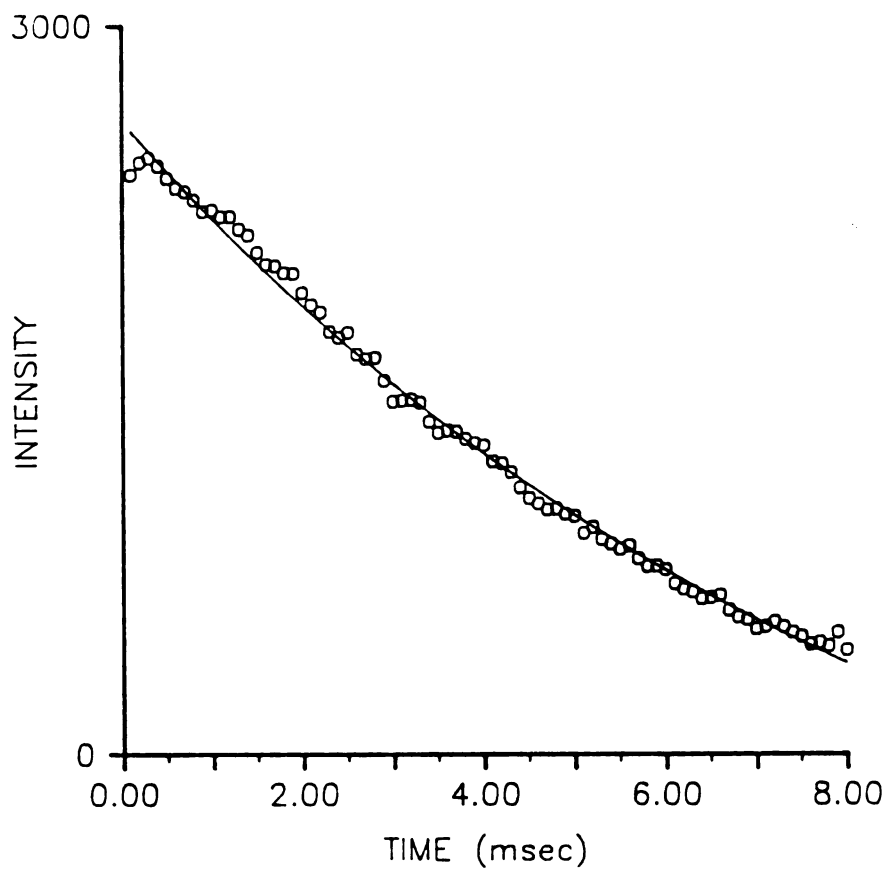


Figure 6.13

Phosphorescence decay of naphthalene. Data from, A) Perkin-Elmer LS-5, B) home-built instrument. Curve through data points represents the best fit to data as determined by the single exponential decay of equation 6-1.

the observed lifetime. Since both instruments determined the lifetime of naphthalene to be about 2 ms, instrumental errors are not believed to be the source of this error. Investigation of this phenomenon is reserved for future work.

The lifetime of pyrene was investigated using the home-built instrument. The decay of the phosphorescence (Figure 6.14) was fit to equation 6-1. The parameters of this fit are  $I_0 = 3741$ ,  $k = 1.139 \times 10^{-4}$ , and  $B = -130$ . The standard deviation is 0.0056. The lifetime of pyrene from this fit is 8.78 ms. Similar results were obtained by another researcher in our laboratory using a different experimental set-up [9]. The reported lifetime of pyrene is 0.93 ms [8]. The Stern-Volmer equation predicts that quenchers present in the sample solution will decrease the lifetime of the phosphore. The lifetime observed in these experiments are all longer than reported in the literature. This contradicts the effect predicted by the Stern-Volmer equation. The phosphorescence lifetime on naphthalene was determined to be approximately 2 ms on both instruments using different algorithms to calculate the lifetime. Therefore, systematic error is not suspected to be the source of discrepancy in the observed phosphorescence lifetimes. The explanation of this observation of increased phosphorescence lifetimes is reserved for future work.



**Figure 6.14** Phosphorescence decay of pyrene. Data from home-built instrument. Curve represents best fit of data to single exponential decay.

## CHAPTER VI REFERENCES

1. Cline Love, L.J.; Skrilec, M.; Habarta, J.G., *Anal. Chem.*, **1980**, *52*, 754
2. Kalyanasundaram, K.; Grieser, F.; Thomas, J.K., *Chem. Phys. Lett.*, **1977**, *51*, 501
3. Díaz García, M.E.; Sanz-Medel, A., *Anal. Chem.*, **1986**, *58*, 1436
4. Parker, C.A., *Photoluminescence of Solutions*, Elsevier: Amsterdam, 1968
5. Gratzel, M.; Thomas, J.K., In *Modern Fluorescence Spectroscopy*, Wehry, E.L., Ed.; Plenum: New York, 1976; Vol. 2, Chapter 4
6. Scypinski, S.; Cline Love, L.J., *Anal. Chem.*, **1984**, *56*, 322
7. Wentzell, P., XYFIT: a FORTRAN curve fitting program using the Simplex algorithm, Michigan State University, 1986
8. Skrilec, M.; Cline Love, L.J.; *Anal. Chem.*, **1980**, *52*, 1559
9. Kim, H.-D., Ph.D. research in progress, Department of Chemistry, and the Pesticide Research Center, Michigan State University, 1987

**CHAPTER VII**  
**ROOM TEMPERATURE PHOSPHORESCENCE**  
**with FLOW INJECTION ANALYSIS SAMPLE INTRODUCTION**

In this chapter, a system is introduced for making RTP measurements in a flowing stream. Flow injection analysis (FIA) is used as the means of sample introduction. The flow cell used in these studies is described first. Then, experiments to determine the optimum carrier are presented. Different carriers were used to pump the sample zone, and the effect of these on the peak luminescence profile was investigated. Based on the results of this study, the carrier yielding the best peak profile was selected. Three methods of deoxygenating flowing streams are examined. The results from these experiments determined the deoxygenation method that was used. Phosphorescence calibration curves obtained with the RTP/FIA configuration are then presented.

**Flow Injection System**

The components of a typical FIA system, a pump, polymeric tubing, sample injection valve, flow cell, and readout, were discussed in Chapter 5. In this work, a flow through micro fluorimeter cell (type 43, Starna Cells Inc., Atascadero, CA) with an internal volume of approximately 220  $\mu\text{l}$ , 5 mm pathlengths, and four polished windows is used. The cell is constructed from fused Spectrosil Quartz and is suitable for use between 170 nm and 2600 nm. The cell is reported to show no fluorescence, but does have a strong absorption band at 2700 nm [1]. The cell has external dimensions of 12.5 mm  $\times$  7.3 mm. Therefore, a template was constructed to hold the cell square in

sample chambers designed for 12.5 mm square cells. This template ensures that the cell is centered in the sample chamber. The "U-shaped" template was constructed so that all four windows of the cell are not blocked by the template.

The effect of the smaller solid angle of the flow cell on the luminescence intensity observed was investigated by observing the fluorescence of pyrene in 0.15 M SDS. Identical solutions were placed in the 1 cm<sup>2</sup> cuvette and the flow cell. Spectra of these solutions were then obtained on both the Perkin-Elmer LS-5 and the home-built instrument. The intensities of the major fluorescence peaks for both cells were then compared. Data from this experiment are shown in Table 7.1. These data show that there is an 11.1% decrease in luminescence intensity in the flow cell as compared to the static cell. Results of a similar experiment done on the home-built instrument are shown in Table 7.2. The luminescence intensity with the flow cell is 21.5% less than with the static cell in the home-built system. This larger difference in intensities on the home-built instrument is due to the optical components. Lenses were not used to focus the excitation radiation or the emitted luminescence from the cell in the home-built instrument. A carefully matched optical system, such as that used in the LS-5, would decrease this difference. To obtain maximum luminescence intensity, all subsequent work is performed on the LS-5 spectrofluorimeter.

Table 7.1

Comparison of Static and Flow Cell in Perkin-Elmer LS-5<sup>a</sup>

	Fluorescence Intensity <sup>b</sup>		
	374 nm	385 nm	395 nm
Static cell	79.70	75.60	80.85
Flow cell	72.10	66.45	71.70
% decrease:	9.8	12.1	11.3
average decrease:	11.1%		

<sup>a</sup> 3 nm bandpass  
<sup>b</sup> arbitrary units

Table 7.2  
Comparison of Static and Flow Cell in Home-Built Instrument<sup>a</sup>

Fluorescence Intensity <sup>b</sup> 395 nm	
Static cell	3189
Flow cell	2503
% decrease:	21.5

<sup>a</sup> 8 nm bandpass  
<sup>b</sup> arbitrary units

### Carrier Study

Due to mixing of the carrier and the sample zone within the FIA manifold, the carrier will affect the luminescence peak profile. This effect was first observed when data were being acquired for a fluorescence calibration curve of pyrene in 0.15 M SDS. The fluorescence intensity of pyrene was monitored at 395 nm with an excitation wavelength of 335 nm. Water was used as the carrier. A very non-symmetric peak profile was observed, as can be seen in Figure 7.1A. A solution of 0.15 M SDS was then used as the carrier, and, as can be seen in Figure 7.1B, there was a marked change in the peak profile. These latter peaks show an increase in the observed fluorescence intensity with a shorter time to return to the baseline. Two explanations of this difference can be postulated: ionic strength, and surface tension effects. The difference in the ionic strengths of the sample zone and the water carrier can result in poor mixing of the two solutions. As the interface of these two solutions passes through the flow cell, the convective mixing can be observed as fluctuations in the fluorescence intensity. Mixing of the sample zone and the carrier is also affected by the surface tension of the surfactant solution. The lower surface tension of the surfactant decreases the extent of

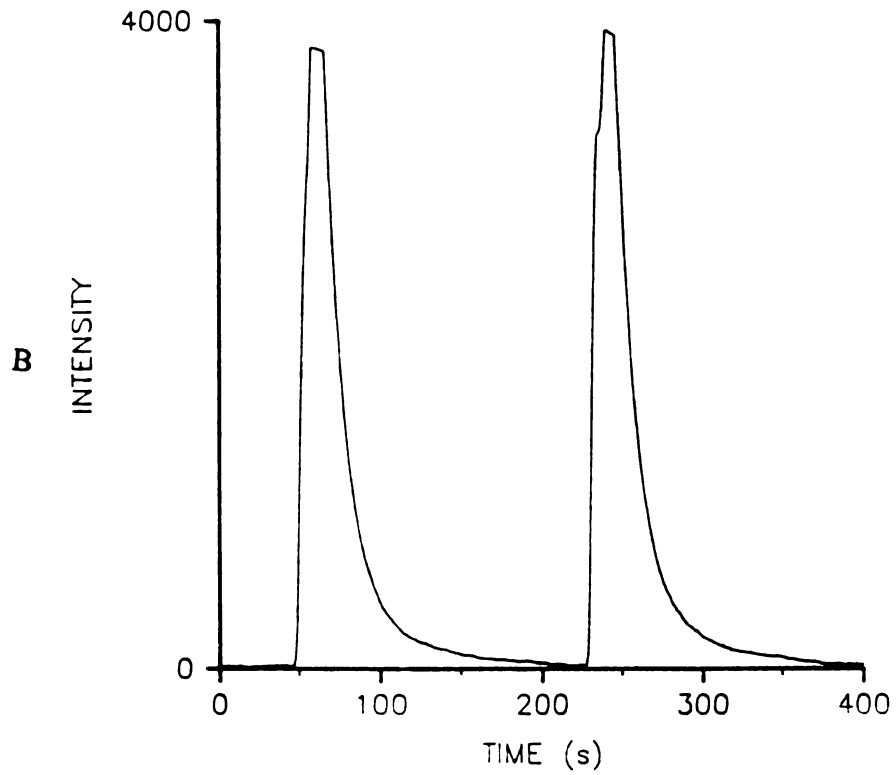
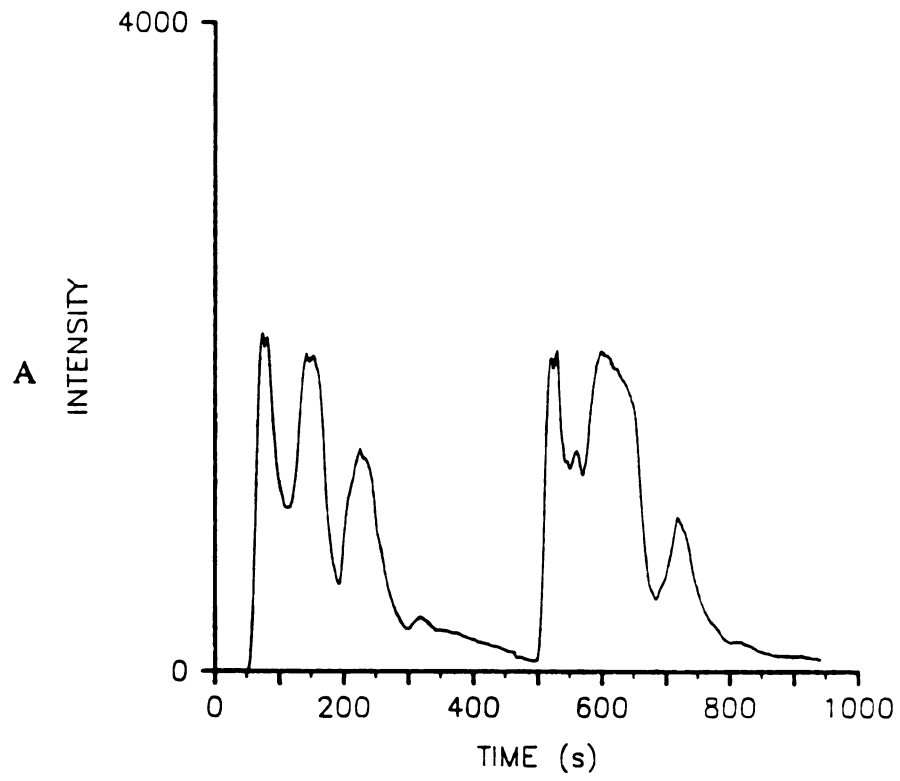


Figure 7.1 A) fluorescence peak profile of pyrene obtained with water as the carrier, and B) SDS carrier.

mixing of the sample zone and the water. The observed effect is then the same as for ionic strength differences.

An experiment was performed in which several solutions were used as carriers: water, and 0.15 M solutions of SDS, NaCl, NaBr,  $\text{NaC}_2\text{H}_3\text{O}_2$ , and LiCl. The characteristic peak profiles obtained are shown in Figure 7.2. Although the salt solutions do not show the anomalous peak characteristic of water, the intensities of these peaks are much less than for SDS. The baseline of these peaks is also quite noisy. Because the salt solutions all have the same ionic strength as the SDS, the difference in ionic strength in the solutions is not the cause of the decreased fluorescence intensities. However, at the carrier/sample zone interface, the mixing of the solutions can cause a change in the micelle concentration. This can be due to a change in the aggregate number of the micelle through counter-ion effects. Therefore, to obtain maximum signal intensity, SDS was used as the carrier for all subsequent experiments.

### **Deoxygenation of Flowing Streams**

To obtain RTP, the analyte solution must be thoroughly deoxygenated as discussed in Chapter III. For a flowing stream there is the additional problem that the solution must remain deoxygenated as it flows through the manifold. Three methods of deoxygenating flowing streams were investigated. Two of these methods (Cr(II)/Zn(Hg) reduction of  $\text{O}_2$ , and a vacuum method) are based on the diffusion of oxygen across a gas permeable membrane. The third method is the reduction of oxygen by reaction with sulfite. This is an "internal" method and requires no special equipment.

#### ***Chromium(II)/Zn(Hg) Oxygen Scavenging***

The Cr(II)/Zn(Hg) deoxygenation method is based on the production of a concentration gradient across a gas permeable membrane. Oxygen diffuses across the membrane into a scavenging solution containing acidic Cr(II). This solution

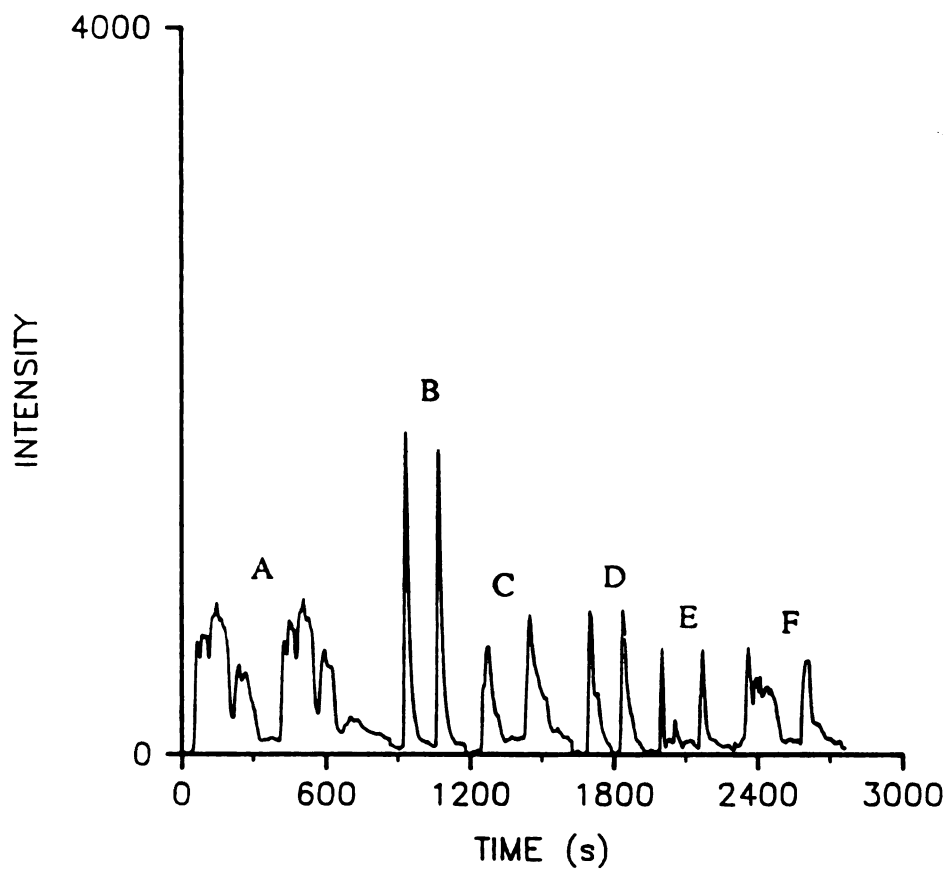
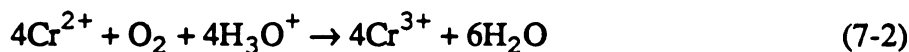
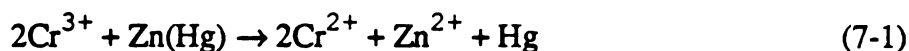


**Figure 7.2** Characteristic fluorescence peak profiles obtained with A) water, B) SDS, C) NaCl, D) NaBr, E) NaC<sub>2</sub>H<sub>3</sub>O<sub>2</sub>, and F) LiCl.

immediately reduces oxygen to water. The  $\text{Cr}^{2+}$  is generated by the reduction of  $\text{Cr}^{3+}$  in presence of amalgamated zinc:



This approach was originally reported by Rollie, Ho, and Warner [2] as a means to minimize the quenching effect of oxygen on fluorescence. It was then developed by Rollie, Patonay, and Warner [3] for the purpose of fluorescence enhancement in flowing streams. An oxygen concentration gradient is developed across a 0.2 mil very low density polyethylene membrane mounted in a 12 in. dialyzer assembly.

In the studies reported here, pyrene was used to evaluate the deoxygenation apparatus because of its long fluorescence lifetime (450 ns [4]) and sensitivity to oxygen quenching. Pyrene solutions were prepared in cyclohexane. The efficiency of deoxygenation was determined by calculating an enhancement factor, which is the ratio of the luminescence intensity of the deoxygenated solution to the intensity of solutions open to air. Enhancement factors as large as 16 have been reported for pyrene by Warner et al. [2,3]. In our studies, a 50 cm concentric tube dialyzer was constructed with Gore-Tex tubing (TA001, W.L. Gore and Associates, Inc., Elkton, MD) as the gas permeable membrane, as shown in Figure 7.3. This tubing has an internal diameter of 1.0 mm and a maximum pore size of 2.0  $\mu\text{m}$ . The large surface area of this dialyzer design increases the diffusion of  $\text{O}_2$  into the  $\text{Cr}^{2+}$  reducing solution. This is compared to a channel dialyzer where a flat membrane separates the two solutions. Pyrene standards were prepared in 0.15 M SDS with concentrations over the range of 1-20  $\mu\text{M}$ . All solutions were air-equilibrated prior to running the experiment. The manifold used is shown in Figure 7.4. Samples were injected in triplicate. The residence time of the sample zone in the dialyzer at the carrier flow rate used is approximately 25 s. The outer tube of the dialyzer was flushed with water to obtain the fluorescence intensities of pyrene in air-equilibrated solutions. A solution of Cr(II) was

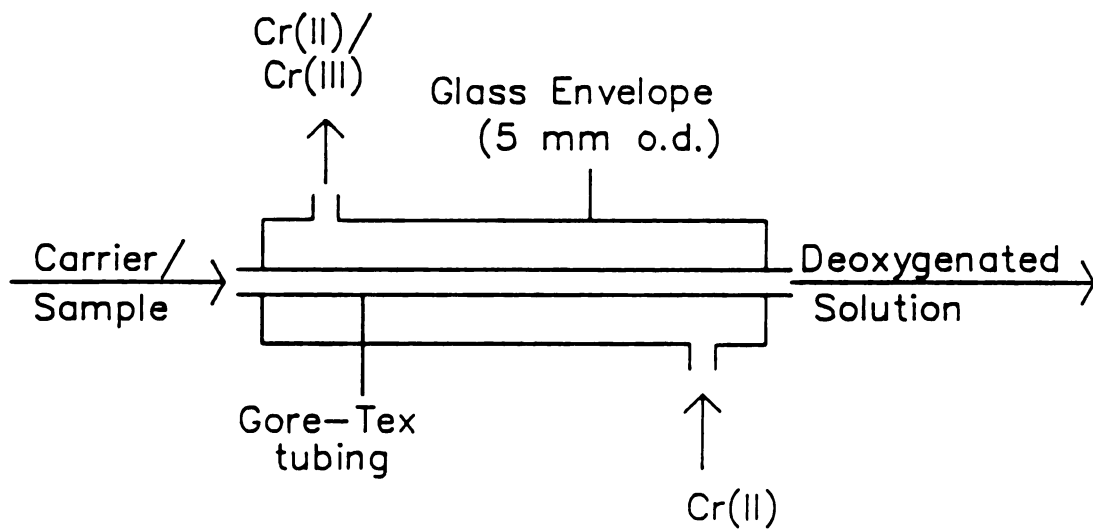


**Figure 7.3** Concentric tube dialyzer used for deoxygenation with Cr(II).

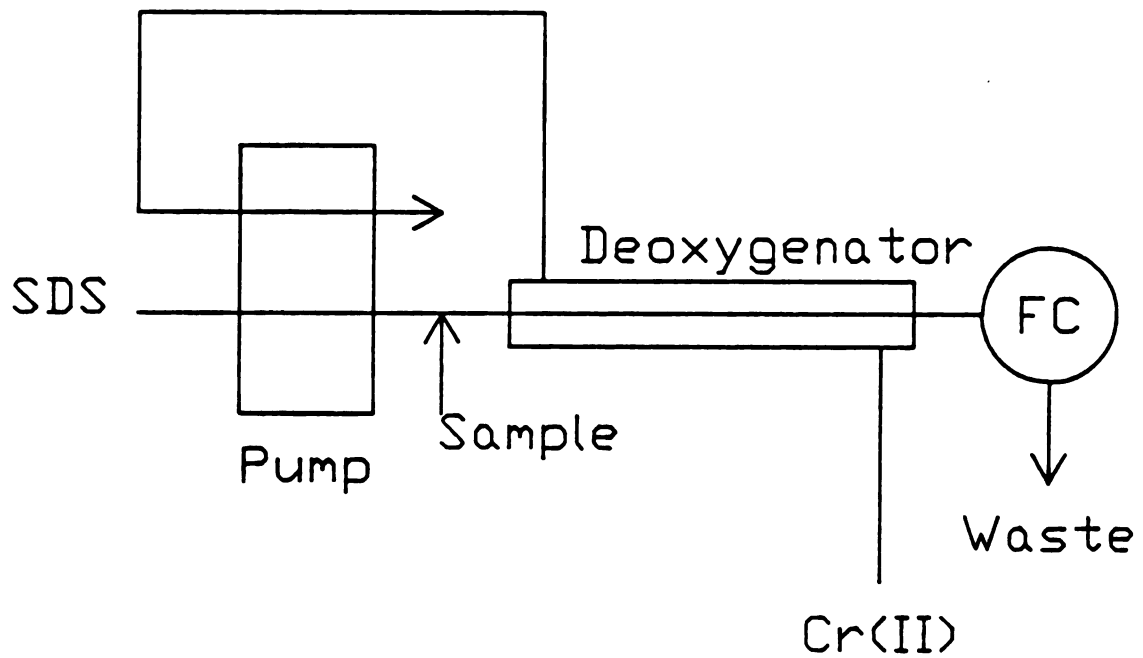


Figure 7.4 FIA manifold used for deoxygenation with concentric tube dialyzer

then pumped counter-current through the outer tube to deoxygenate the sample zone as it flowed through the dialyzer. The fluorescence intensities obtained at 395 nm ( $\lambda_{ex} = 335$  nm) are listed in Table 7.3. The peak profiles are shown in Figure 7.5A and the average peak intensities are plotted versus the pyrene concentration in Figure 7.5B.

Table 7.3

## Fluorescence Enhancement Factors

[Pyrene] ( $\mu\text{M}$ )	air- equilibrated <sup>a</sup>	deoxygenated <sup>a</sup>	Enhancement Factor
20	1663	2142	1.29
15	1405	1802	1.28
10	975	1335	1.37
5	528	758	1.44
1	119	164	1.38
average			1.35

<sup>a</sup> arbitrary units

Although the enhancement factors determined in our work are considerably less than reported in the literature [2,3], the basic principle of fluorescence enhancement by deoxygenation was observed. Immediate observation indicates that greater enhancement factors could be obtained with increased residence time in the dialyzer tube. However, during an experiment with a longer sample residence time in the dialyzer, the waste solution was observed to be tainted green. Absorption spectra of the pyrene sample, the chromium deoxygenating solution, and the waste solution were obtained. These spectra, Figure 7.6, confirmed the suspicion that some chromium had passed through the membrane and was contaminating the sample solution. The increase in absorbance observed at wavelengths lower than 300 nm for the contaminated solution (Figure 7.6C) is not present in the pyrene sample (Figure 7.6A), but is present in the chromium solution (Figure 7.6B). A similar effect was noted when a second concentric

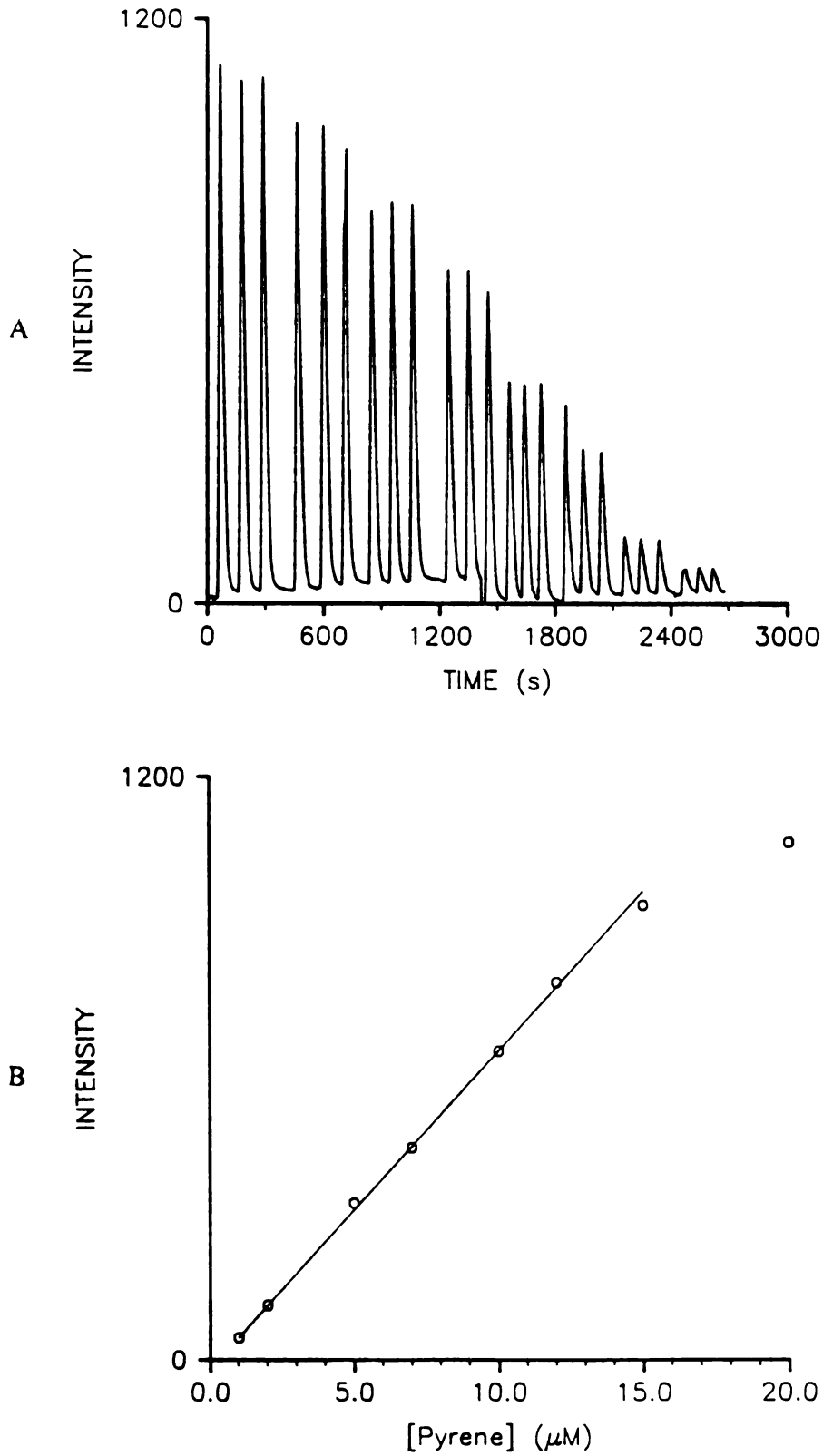


Figure 7.5

A) Fluorescence peak profiles obtained for pyrene by FIA. Sample concentrations from left to right are 20, 15, 12, 10, 7, 5, 2, and 1  $\mu\text{M}$ , respectively. B) Calibration curve using average maximum peak intensity obtained from A.

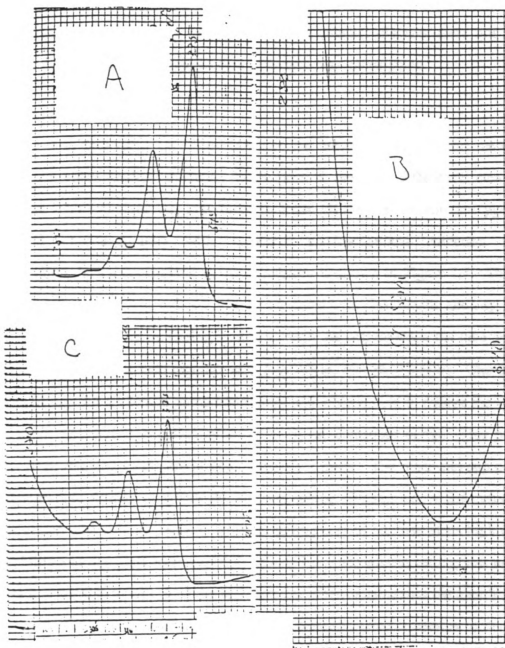


Figure 7.6 Absorbance spectra of A) pyrene in 0.15 M SDS, B) Chromium deoxygenating solution, and C) pyrene waste solution showing contamination of pyrene sample by chromium.

tube dialyzer was constructed. It was therefore assumed that the Gore-Tex microporous tubing is too fragile to withstand the construction of this dialyzer or that the pore size allows diffusion of chromium. Membranes for a channel dialyzer were not readily available; therefore, a new deoxygenation technique was investigated.

### ***Vacuum Deoxygenation***

Vacuum deoxygenation is also based on the use of a gas permeable membrane. The oxygen concentration gradient results from a pressure difference created by evacuation. This technique was introduced by Reim [5] for post column deoxygenation for liquid chromatography with reductive electrochemical detection. The deoxygenation device constructed in our laboratory is shown in Figure 7.7. The clear plastic shell (7.25 in.  $\times$  2 in. o.d.  $\times$  1.5 in. i.d.) is fitted with clear plastic end caps (3 in.  $\times$  3 in.  $\times$  0.5 in.). A 1 7/8 in. O-ring is used to form the seal between the tube and the end caps. The device is held together with four 3/8 in. assembly screws. One end cap contains fittings for a vacuum pump connection and a bleed hole to relieve the vacuum in the shell. Vacuum is supplied by a Cenco Hyvac 2 vacuum pump. This pump is capable of developing a pressure of approximately 1 mtorr. The other end cap contains chromatographic fittings to which the silicone tubing (0.8 mm i.d.  $\times$  2.4 mm o.d.  $\times$  3 m) is sealed with silicone sealant. Silicone tubing is used because of its high oxygen permeability and chemical inertness [6,7]. Gore-Tex microporous tubing was not used because it is not able to withstand the high pressure differential across the membrane.

Preliminary tests were performed on the deoxygenation apparatus to determine its ability to maintain vacuum without leaking. Water was pumped through the silicone tubing and the pump was turned on. The apparatus was able to hold a vacuum of less than 1 torr as determined by a mercury manometer. When a small air bubble was introduced into the tubing, the disappearance of this bubble in the silicone tube was monitored while in the vacuum apparatus. It was noted at this point that small air bubbles ( $\sim 16 \mu\text{l}$ ) took approximately 15 min. to diffuse through the membrane and

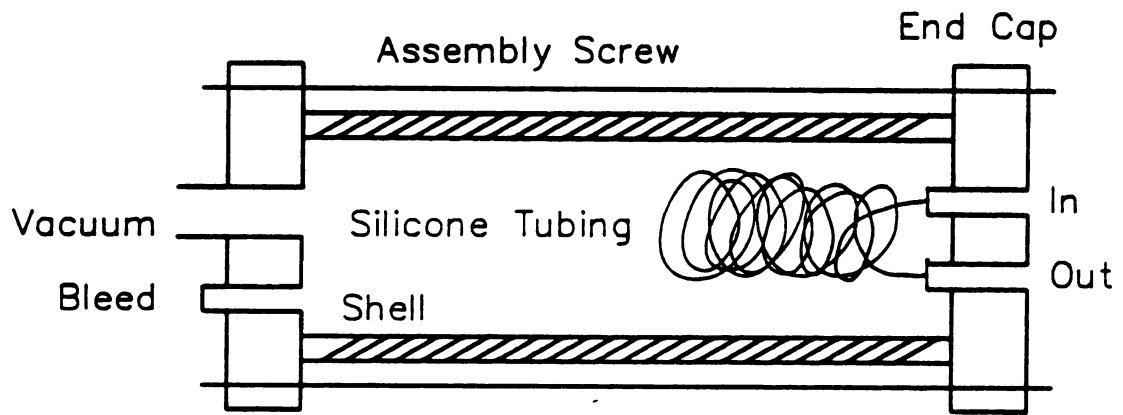


**Figure 7.7** Vacuum deoxygenation apparatus.

disappear. The gas flux across the membrane wall,  $J_p$ , due to a pressure difference is given by

$$J_p = -K (\Delta p/l) \quad (7-3)$$

where  $K$  is the permeability coefficient of the membrane,  $\Delta p$  is the difference in gas pressure at the inner and outer membrane wall, and  $l$  is the membrane thickness [10]. For a given membrane, this relationship shows that if the membrane thickness is decreased the gas flux across the membrane will increase. Unfortunately, thinner walled membranes were not conveniently available. Likewise, equation 7-3 predicts that as the pressure differential  $\Delta p$  increases the gas flux will increase. This pressure differential is limited by the vacuum pump and the ability of the deoxygenating apparatus to hold vacuum. The vacuum generated in our apparatus was measured to better than 1 torr, which is the maximum vacuum capable of being developed with the pump used. Therefore, an alternate deoxygenation technique was evaluated.

### ***Sodium Sulfite Deoxygenation***

Sodium sulfite was previously shown to be effective in the deoxygenation of RTP solutions prior to spectral scanning (see Chapter VI). For 0.10 M SDS solutions, sulfite was shown to require a minimum of 10 min. for RTP to be observed (Figure 6.8). Because of the gas permeability of the polymeric tubing used in FIA, the RTP of a deoxygenated sample can be quenched due to diffusion of oxygen through the membrane into the sample. Nylon tubing has been reported to show the least permeability towards oxygen [7]. Therefore, with the exception of the pump tubes and sample injection valve connections, nylon tubing (1 mm i.d.) was used throughout the FIA manifold. This manifold is shown in Figure 7.8. It was designed to keep sample dispersion to a minimum to avoid mixing of the deoxygenated sample zone with the carrier.

A probe solution of 10  $\mu$ M naphthalene in 0.10 M 30/70 Tl/Na DS with 10 mM  $\text{Na}_2\text{SO}_3$  was prepared and allowed to deoxygenate for 15 min. The home-built

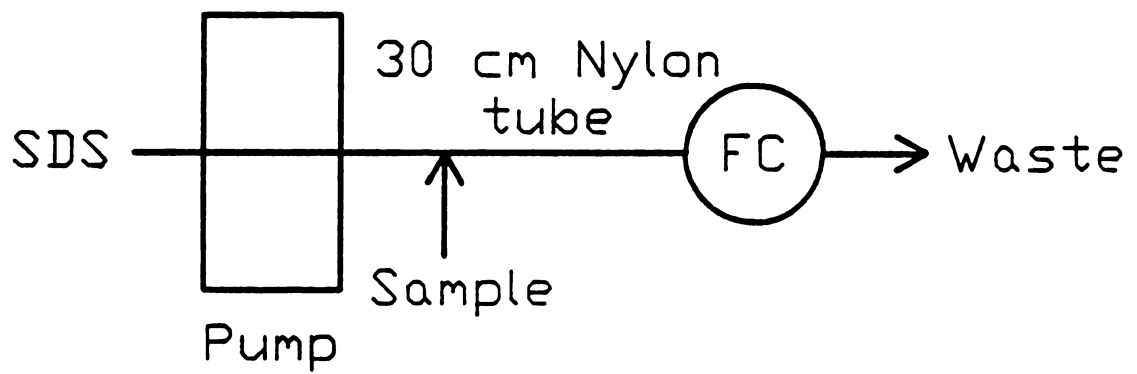


Figure 7.8

FIA manifold used for RTP determinations.

instrument was used as the detector with excitation and emission wavelengths of 280 nm and 485 nm, respectively. Several injections of the solution gave no discernible RTP signal. This indicates that oxygen diffusing through the tubing was quenching the RTP. Therefore, for one injection, the pump was stopped while the sample zone was in the flow cell. After approximately 6.5 min., the characteristic rise in RTP was observed, as shown in Figure 7.9. Oxygen that had diffused into the sample solution was reduced to water during this period enabling RTP to be observed. Further diffusion of oxygen into the sample solution was prevented by the quartz cell which is non-permeable to gases. This method limits the procedure to a batch-mode analysis since time must be allowed for the sulfite to deoxygenate the sample solution. Time must also be allowed for the oxygen diffusing into the sample through the conduit to be reduced before RTP can be observed. In spite of these time limitations, RTP can be observed in flowing streams.

### **RTP/FIA Calibration Curves**

The studies discussed above show that at present the sulfite reaction is the most successful deoxygenation method for RTP/FIA. With the sulfite deoxygenation technique, calibration curves were obtained for naphthalene, 2-bromonaphthalene, biphenyl, and pyrene in 0.10 M 30/70 TI/Na DS. Analyte solutions were prepared containing 10 mM  $\text{Na}_2\text{SO}_3$  were allowed to deoxygenate for a minimum of 10 minutes before use. The deoxygenated sample solution (500  $\mu\text{L}$ ) was then injected into the 0.10 M SDS carrier. Although the carrier was air-equilibrated, it could also be deoxygenated with sulfite. The pump was stopped when the sample zone was in the flow cell. The phosphorescence intensity was then monitored for 10 minutes. Each sample is injected in triplicate and averaged. For naphthalene, 2-bromonaphthalene, and biphenyl, the characteristic rise in RTP due to the reduction of oxygen by sulfite was observed (Figures 6.8, 7.9). However, since the oxygen in the flowing stream is

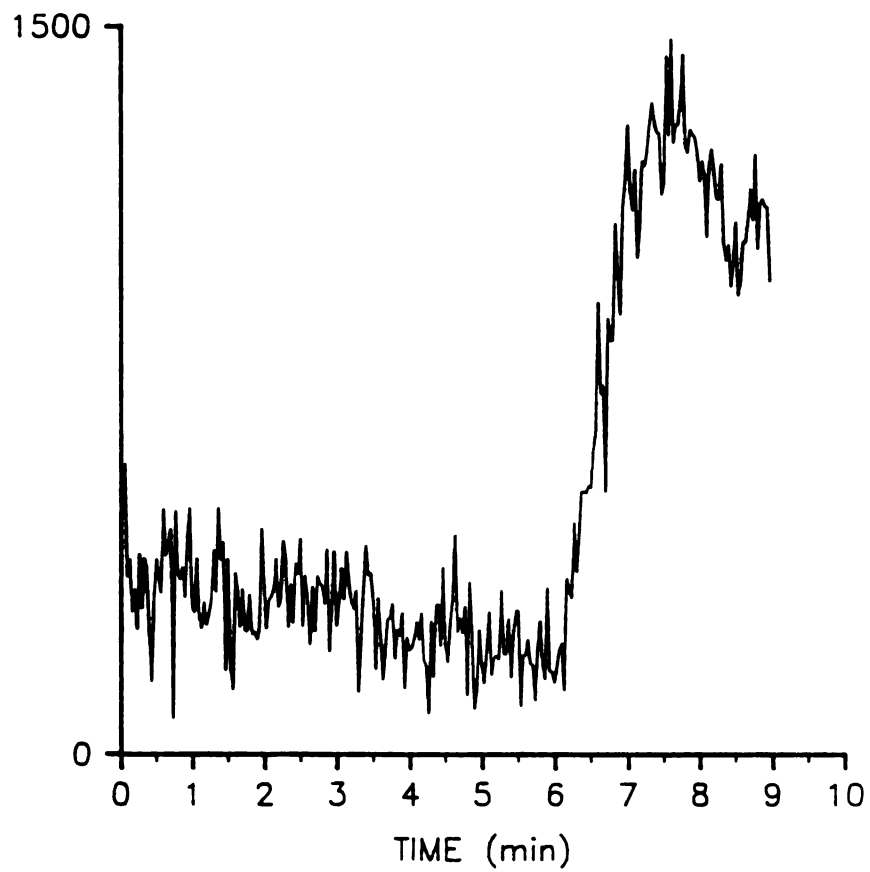


**Figure 7.9** Rise in RTP observed for RTP/FIA system.

due solely to diffusion of oxygen through the manifold tubing, the oxygen concentration in the sample will be less than in air-equilibrated solutions. Therefore, the lag time prior to the rise in RTP should be shorter using the RTP/FIA configuration than observed in Figure 6.8. Figure 7.10 shows the rise in RTP observed for naphthalene samples with concentrations of 1-140  $\mu\text{M}$ . The lag time until RTP is observed for all samples in Figure 7.10 is roughly 100 s. This shows that only a small amount of oxygen diffuses through the tubing into the sample solution. The RTP intensity rises quickly to a steady-state. The steady-state RTP intensities are plotted versus concentration in Figure 7.11. Results of a weighted linear regression are listed in Table 7.4. The plot exhibits a slight "S"-shaped curvature. This may be attributed to the technique used to prepare the solutions. Samples with concentrations 30  $\mu\text{M}$  and above were diluted from the stock solution with a 100-1000  $\mu\text{L}$  digital pipette; the 1-10  $\mu\text{M}$  solutions were diluted with a 10-100  $\mu\text{L}$  digital pipette. It is possible that one or both of the pipettes are slightly out of calibration. This may account for the small offset observed in the plot.

Table 7.4

## Results of Weighted Linear Regression for Naphthalene Calibration Curve

Number of Points:	6
Slope:	5.32
Intercept:	3.99
Chi-square:	70.5
Correlation Coefficient:	0.995
Standard Deviation of the Slope:	0.045

Similar results were obtained for 2-bromonaphthalene. The lag time is approximately 100 s. This is consistent with the lag time observed for naphthalene. Steady-state RTP intensities for 2-bromonaphthalene are plotted plotted versus

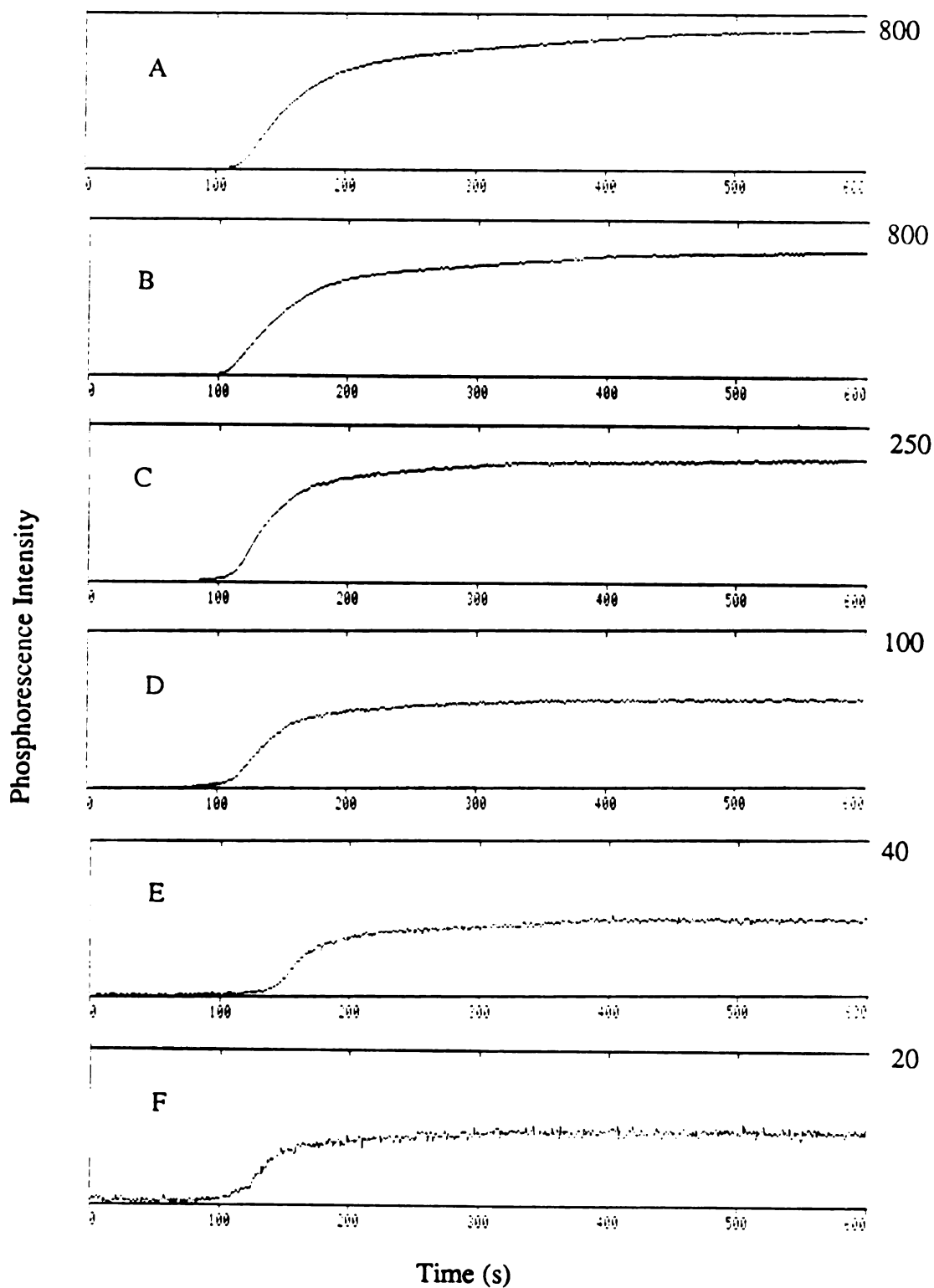


Figure 7.10 Rise in RTP for naphthalene observed with RTP/FIA system for A) 140  $\mu\text{M}$ , B) 100  $\mu\text{M}$ , C) 30  $\mu\text{M}$ , D) 10  $\mu\text{M}$ , E) 3  $\mu\text{M}$ , and F) 1  $\mu\text{M}$  solutions. Time is relative to injection of sample.

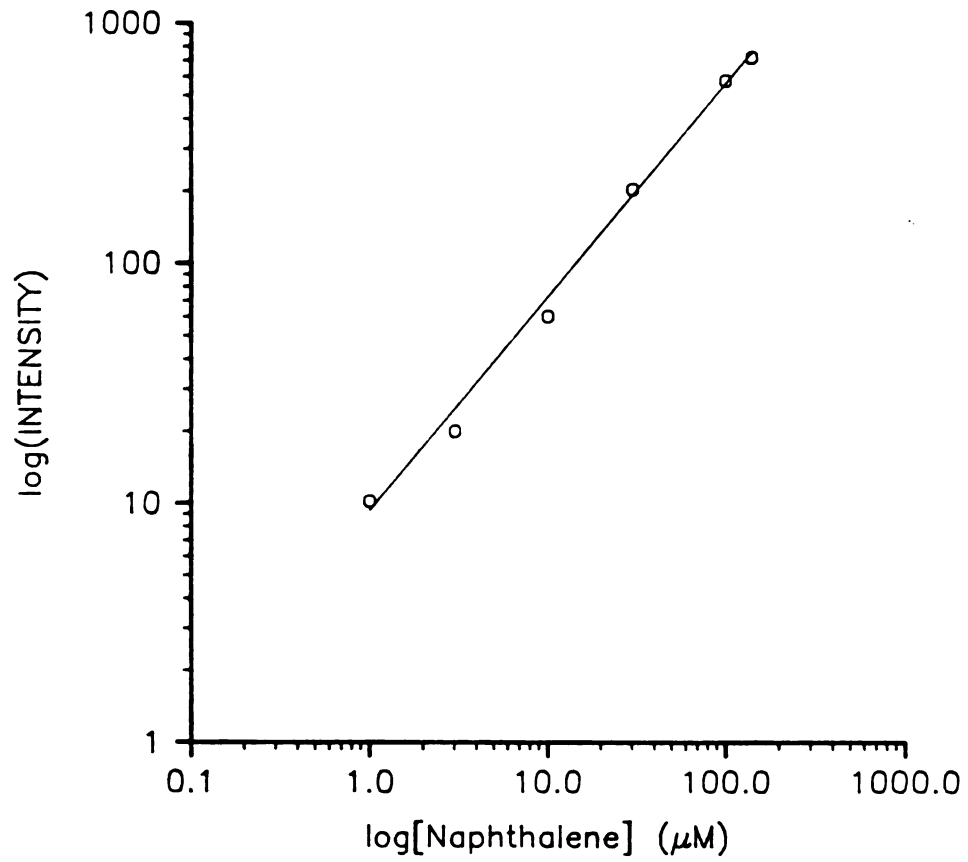


Figure 7.11

Calibration curve for naphthalene by RTP/FIA. RTP intensity is in arbitrary units.

concentration in Figure 7.12. Results of a weighted linear regression are listed in Table 7.5. The offset observed in Figure 7.11 is also present in Figure 7.12.

Table 7.5

Results of Weighted Linear Regression for 2-Bromonaphthalene Calibration Curve

Number of Points:	6
Slope:	7.16
Intercept:	6.61
Chi-square:	75.7
Correlation Coefficient:	0.997
Standard Deviation of the Slope:	0.048

The lag times for biphenyl samples with concentrations less than 100  $\mu\text{M}$  are the same as naphthalene and 2-bromonaphthalene. The 100  $\mu\text{M}$  biphenyl solution has a longer lag time and does not follow the rapid rise in RTP observed in Figures 6.8, 7.9, and 7.10. The rise appears to be exponential, as shown in Figure 7.13. If this rise in RTP follows an exponential equation, the steady-state intensity can be predicted from

$$I_p(t) = I_{ss} (1 - \exp^{-kt}) \quad (7-4)$$

where  $I_p(t)$  is the time-dependent phosphorescence intensity,  $I_{ss}$  is the steady-state RTP intensity,  $k$  is a rate constant for the rise in RTP intensity, and  $t$  is the time in seconds relative to the start of RTP,  $t_0$ . This time is approximated by taking an initial slope of the curve above 500 s. This was done to avoid the initial induction period observed at times earlier than 500 s. The value for  $t_0$  obtained in this manner is 406 s. Relative to this time,  $I_p(t)$  and  $t$  are determined from Figure 7.13 and fit to equation 7-4 using a Simplex fitting routine [8]. The results of this determination are;  $I_{ss} = 769$ ,  $k = 0.00150$ . The sum of the squares of the residuals for 40 data points is 6160, and the standard error of the estimate is 13. These data are shown in Figure 7.14.

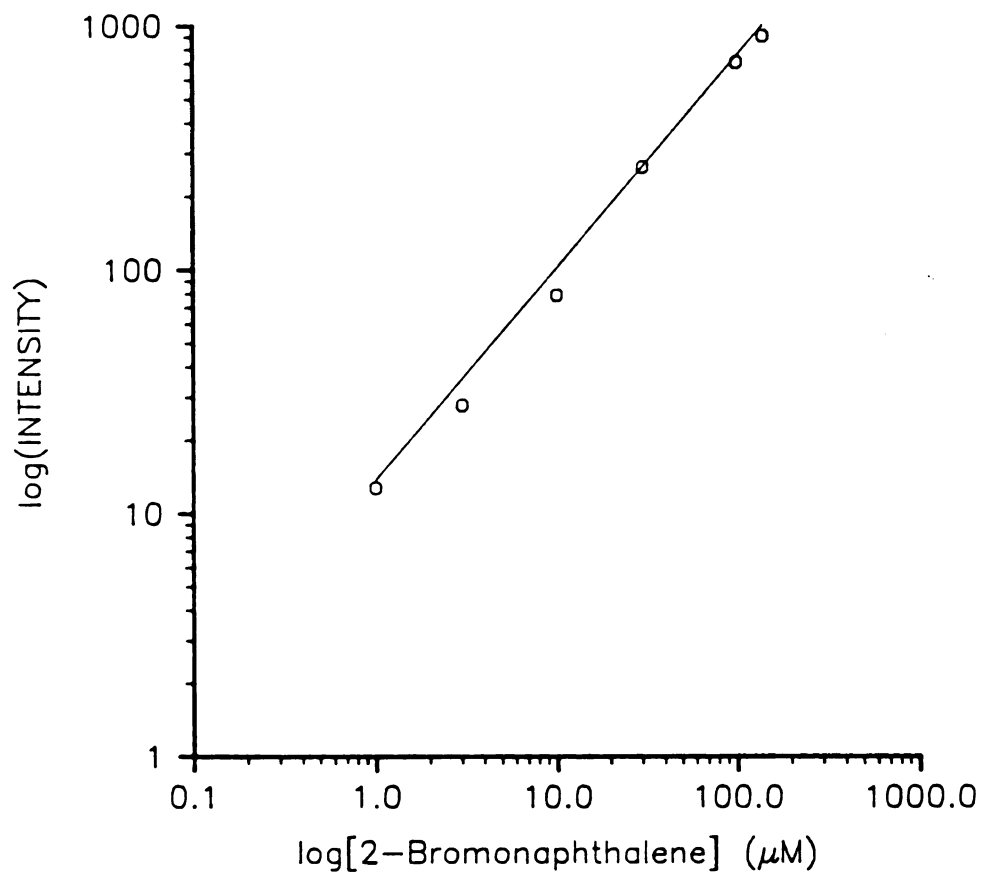


Figure 7.12 Calibration curve for 2-bromonaphthalene by RTP/FIA. RTP intensity is in arbitrary units.

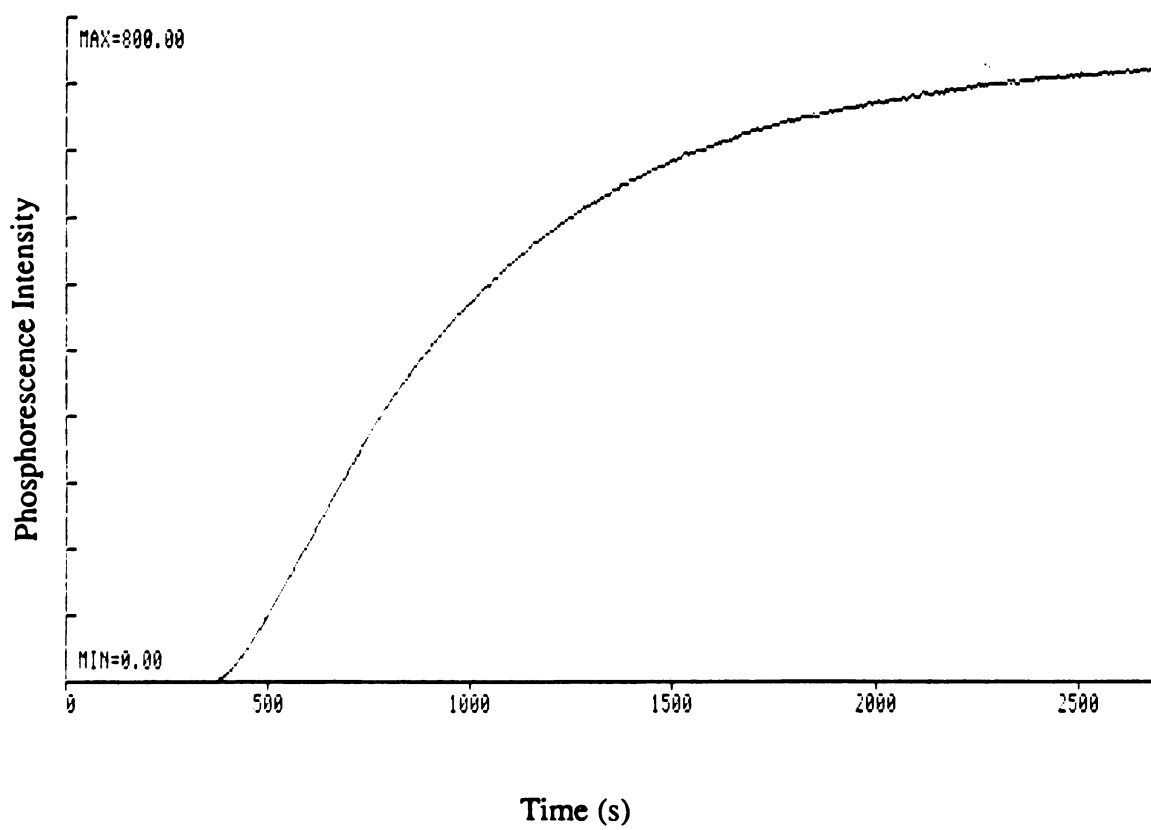


Figure 7.13 Rise in RTP observed for 100  $\mu$ M biphenyl.

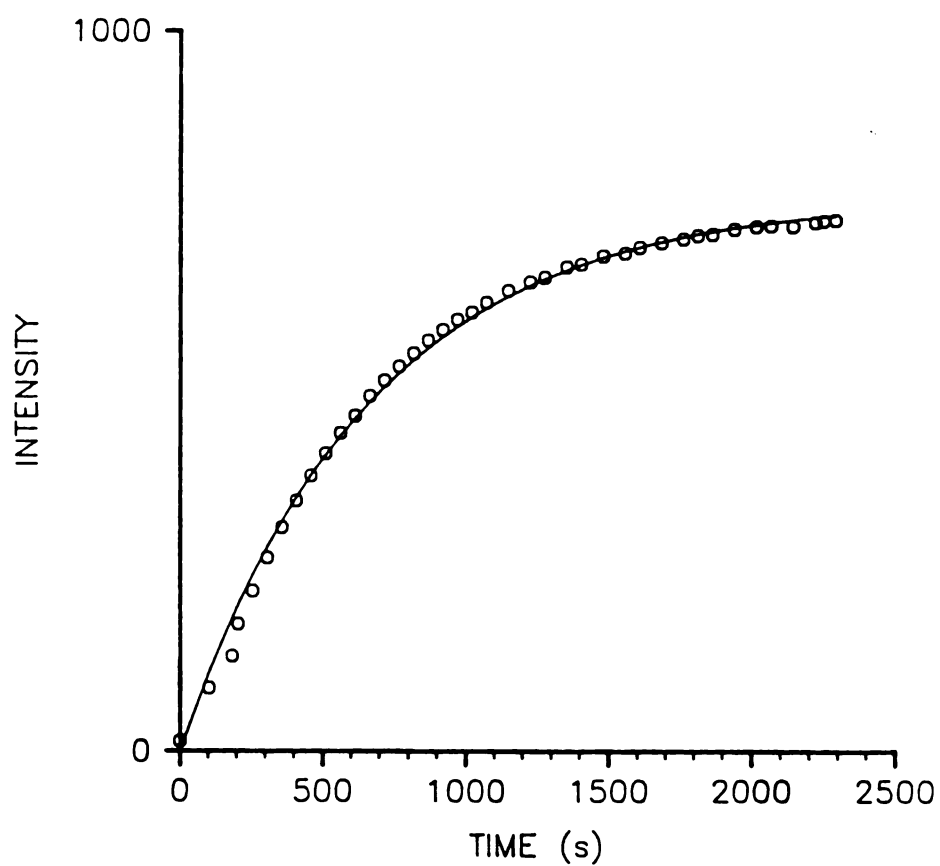


Figure 7.14 Fit of rise in RTP for 100  $\mu\text{M}$  biphenyl to an exponential equation.

The steady-state RTP intensities for biphenyl are plotted versus concentration in Figure 7.15. Results of a weighted linear regression are listed in Table 7.6.

Table 7.6

Results of Weighted Linear Regression for Biphenyl Calibration Curve<sup>a</sup>

Number of Points:	4
Slope:	21.67
Intercept:	-6.47
Chi-square:	24.36
Correlation Coefficient:	0.998
Standard Deviation of the Slope:	0.35

-----  
<sup>a</sup> 100  $\mu\text{M}$  sample not included in regression

The calculated intensity for the 100  $\mu\text{M}$  sample does not fall on the best fit line and was not included in the regression. However, the curvature observed could be due to the inner filter effect. The common test for the inner filter effect is to dilute the sample to observe what effect this has on the phosphorescence intensity. In this experiment, concentrations up to 30  $\mu\text{M}$  fall on a linear curve which are essentially dilutions of the 100  $\mu\text{M}$  sample. Therefore, the inner filter effect may be a cause of the observed curvature.

A second cause for the curvature could be due to an interaction of the biphenyl with some component(s) in the sample solution. The long lag time prior to the observance of RTP for the 100  $\mu\text{M}$  biphenyl sample indicates that the biphenyl may have some effect on the sulfite-oxygen reaction or that the sulfite is reacting with the biphenyl.

Pyrene also does not exhibit the expected sharp rise in RTP. The rise in RTP for samples with concentrations 1-200  $\mu\text{M}$  obtained with the RTP/FIA system are shown in Figure 7.16. For all pyrene samples,  $t_0$  was determined and the rise in RTP was fit to

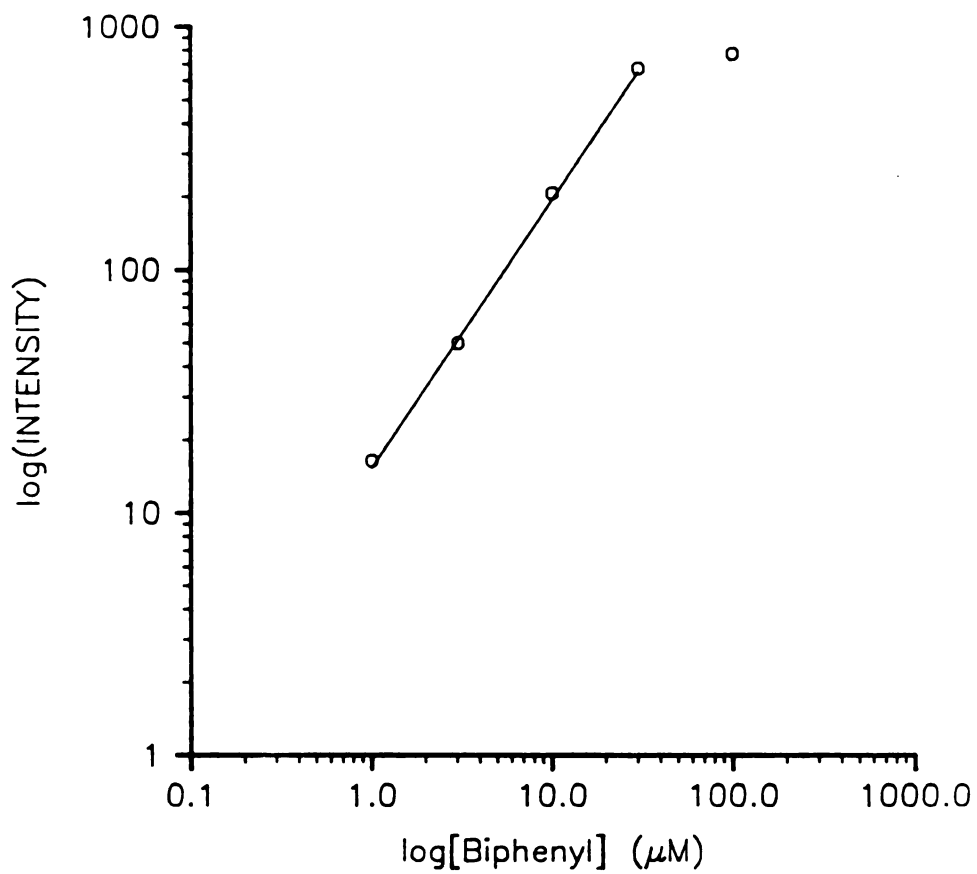


Figure 7.15

Calibration curve for biphenyl by RTP/FIA. Intensity of  $100 \mu\text{M}$  sample obtained from equation 7-4. RTP intensity is in arbitrary units.

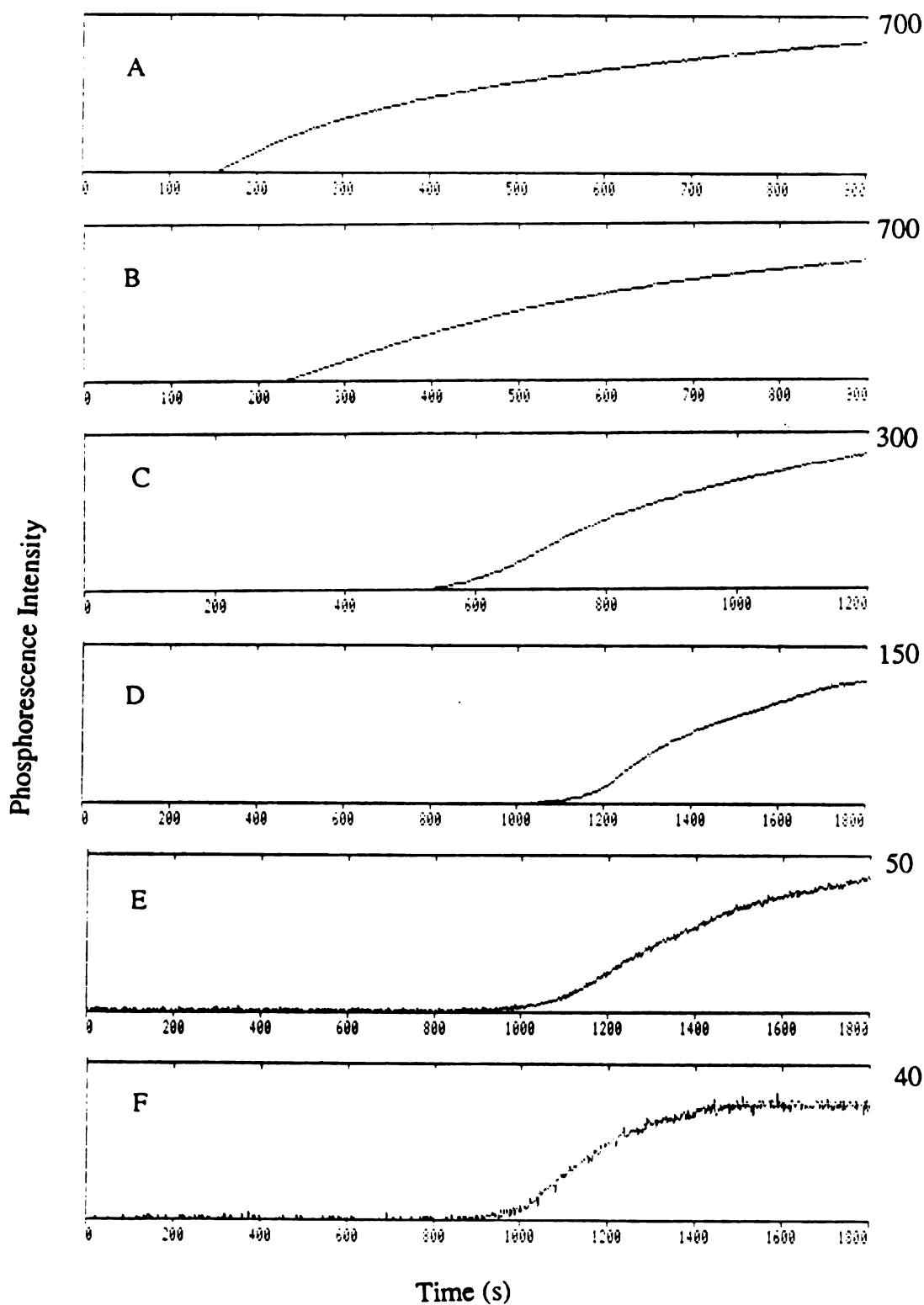


Figure 7.16

Rise in RTP for pyrene observed with RTP/FIA system for A) 200  $\mu\text{M}$ , B) 100  $\mu\text{M}$ , C) 30  $\mu\text{M}$ , D) 10  $\mu\text{M}$ , E) 3  $\mu\text{M}$ , and F) 1  $\mu\text{M}$  solutions. Time is relative to injection of sample.

equation 7-4. These plots are shown in Figure 7.17. Table 7.7 lists the results of the fit to equation 7-4.

Table 7.7

Parameters for Pyrene fit to Exponential Rise in RTP

[pyrene] ( $\mu\text{M}$ )	n	$I_{ss}$	k ( $\times 10^3$ )	SSR <sup>a</sup>	SEE <sup>b</sup>
1.0	31	30	3.33	37	1.
3.0	36	54.	1.83	18.6	0.7
10.0	34	141	2.34	122	2.
30.0	35	372	2.24	392	3.
100.	36	704	2.13	628	4.
200.	35	620	3.08	3773	11.

<sup>a</sup>Sum of the squares of the residuals

<sup>b</sup>Standard error of the estimate

The plot of  $I_{ss}$  vs. pyrene concentration is shown in Figure 7.18. In this plot, the 100 and 200  $\mu\text{M}$  samples show a negative deviation from linearity. This is believed to be due to the inner filter effect for reasons mentioned above. Results of the linear regression over the range of 1-100  $\mu\text{M}$  are listed in Table 7.8. Although the linear correlation coefficient for pyrene indicates the largest deviation from linearity for the four compounds tested, calibration curves are obtainable from data that exhibit a slow rise in RTP and do not reach a steady-state intensity. In Chapter IV reproducible timing was mentioned as one of the characteristics of FIA. Commonly in FIA, a steady-state peak intensity does not have to be attained because of this characteristic. The determination discussed above is an example of how reproducible timing can be used in kinetic determinations in FIA.

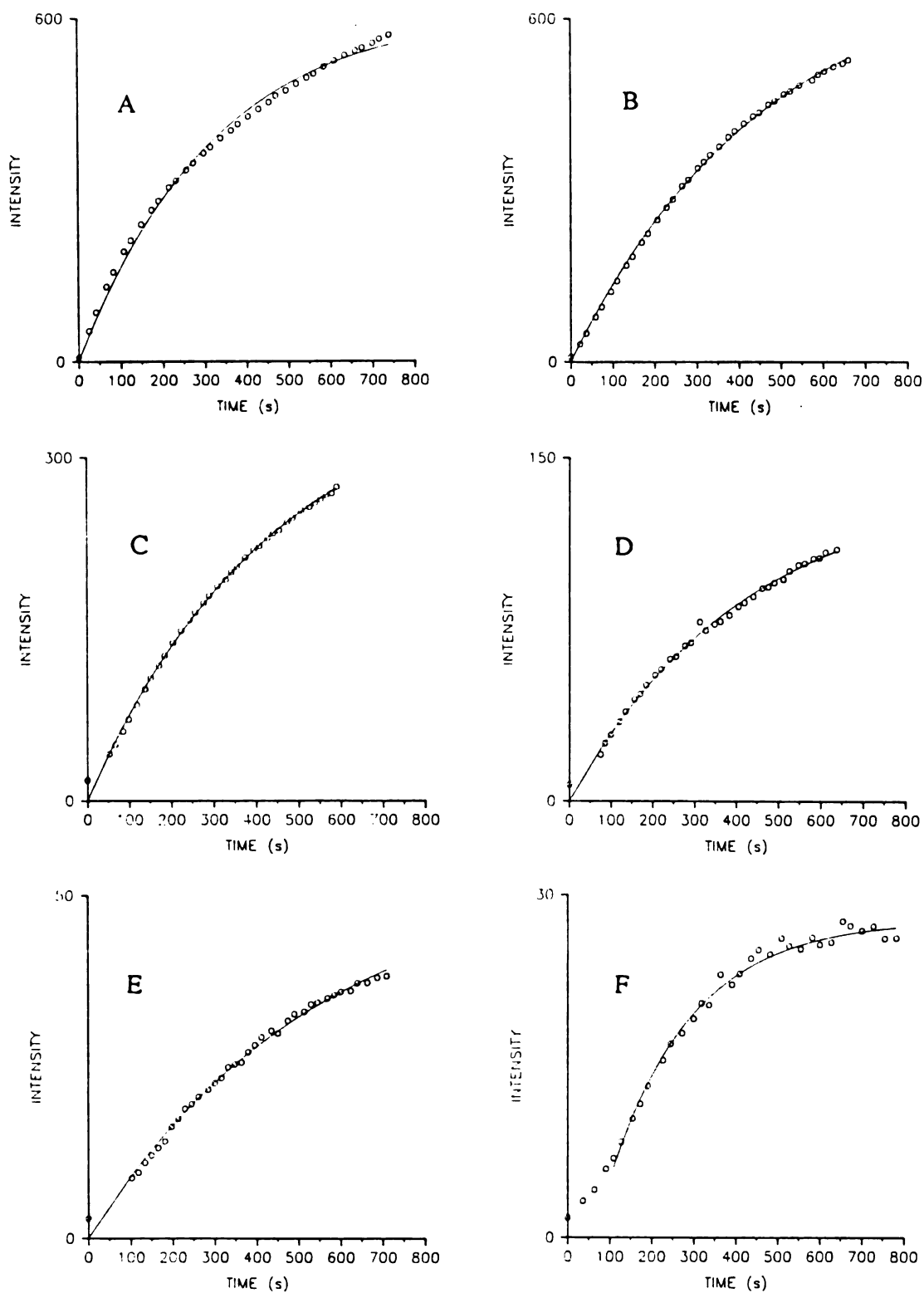


Figure 7.17

Fit of rise in RTP for pyrene samples to equation 7-4. See text for explanation. Curves correspond to A) 200  $\mu\text{M}$ , B) 100  $\mu\text{M}$ , C) 30  $\mu\text{M}$ , D) 10  $\mu\text{M}$ , E) 3  $\mu\text{M}$ , and F) 1  $\mu\text{M}$  pyrene sample concentrations.

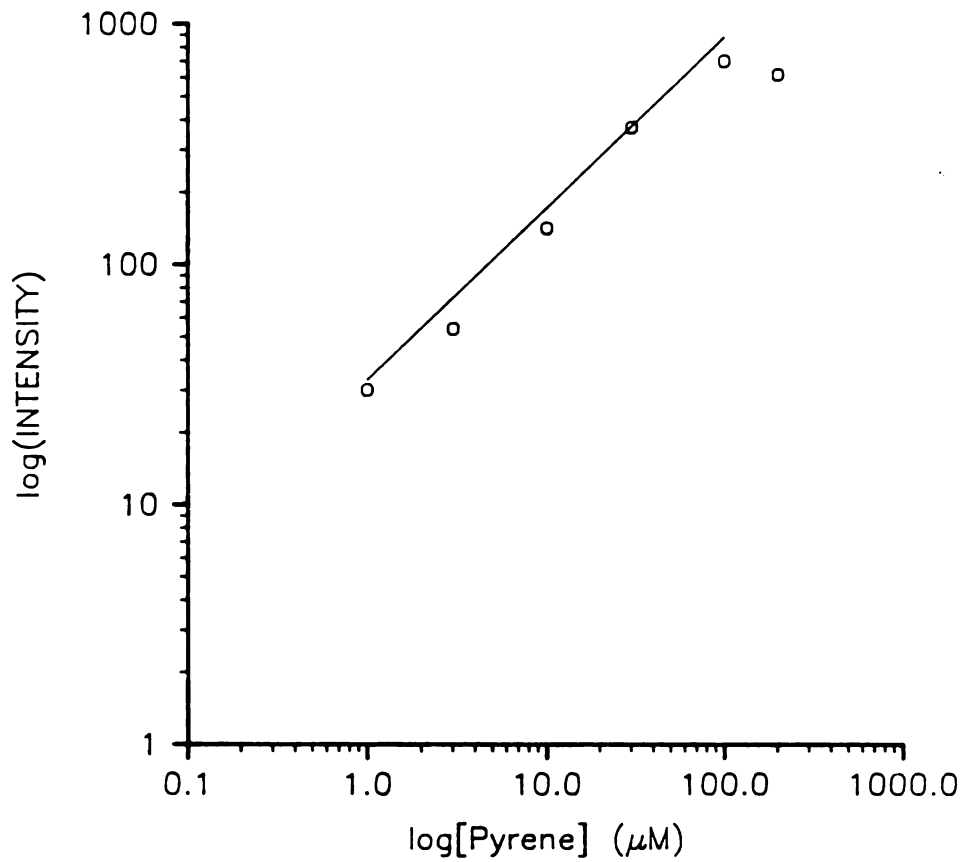


Figure 7.18

Calibration curve for pyrene by RTP/FIA. RTP intensities are obtained from fit of data in Figure 7.17 to equation 7-4.

Table 7.8

Results of Weighted Linear Regression for Pyrene Calibration Curve<sup>a</sup>

Number of Points:	5
Slope:	8.57
Intercept:	24.51
Chi-square:	44.0
Correlation Coefficient:	0.960
Standard Deviation of the Slope:	0.054

---

<sup>a</sup> 200  $\mu$ M sample not included in regression

This chapter demonstrates the first known use of FIA in connection with micelle-stabilized RTP. Results obtained for naphthalene, 2-bromonaphthalene, and biphenyl indicate that each sample requires about 5 minutes from injection into the FIA manifold until a steady-state RTP intensity is reached. This translates to a sampling frequency of approximately 12 samples per hour. An instrument developed by Vo-Dinh, Walden, and Winefordner [10] for solid-surface RTP with a continuous filter paper device requires approximately 3 minutes per sample. This corresponds to 20 samples per hour. Although the solid-surface RTP approach exhibits a higher sampling frequency, the technique requires much more sophisticated equipment than the FIA approach. This increases the cost of the apparatus required and increases the likelihood of instrument down time. The studies reported here indicate that MS-RTP can be automated with FIA as long as efficient deoxygenation is used. The sulfite deoxygenation used in this research has the advantage that it is "internal" and is therefore able to eliminate any oxygen that diffuses into the FIA system; however, sulfite may not be compatible with all compounds used for phosphorescence measurements. This compatibility would have to be investigated for each individual analyte used.

## CHAPTER VII REFERENCES

1. Starna Spectrophotometer Cell Catalog, Starna Cells Inc., Atascadero, CA
2. Rollie, M.E.; Ho, C.-N.; Warner, I.M., *Anal. Chem.*, **1983**, *55*, 2445
3. Rollie, M.E.; Patonay, G.; Warner, I.M., *Anal. Chem.*, **1987**, *59*, 180
4. Birks, J.B., *Photophysics of Aromatic Molecules*; Wiley-Interscience: New York, 1970
5. Reim, R.E., *Anal. Chem.*, **1983**, *55*, 1188
6. Yasuda, H.; Peterlin, A., *J. Appl. Polym. Sci.*, **1973**, *17*, 433
7. Gerritse, R.G., *J. Chromatogr.*, **1973**, *77*, 406
8. Wentzell, P., XYFIT: a FORTRAN curve fitting program using the Simplex algorithm, Michigan State University, 1986
9. Vo-Dinh, T.; Walden, G.; Winefordner, J.D., *Anal. Chem.*, **1977**, *49*, 1126
10. Vo-Dinh, T.; Walden, G.L.; Winefordner, J.D., *Anal. Chem.*, **1977**, *49*, 1126

## CHAPTER VIII

### WHAT'S NEXT?

Throughout the course of this research, experiments performed have provided ideas for additional research. These projects can be divided into two categories, phosphorescence lifetimes, and sample deoxygenation. This chapter discusses these projects and proposes possible methods of approaching them.

In Chapter VI, the phosphorescence lifetime of naphthalene was determined using two different algorithms. The lifetimes calculated by these methods are significantly longer than reported in the literature. Three factors can influence the phosphorescence lifetime: temperature, purity of the analyte, and the nature and concentration of concomitants in the sample matrix. The temperature dependence of RTP will depend on the rate of micelle formation and dissociation. Therefore, a decrease in the sample temperature should increase the phosphorescence lifetime due to a decrease in the association/dissociation rates of the micelles. Therefore, temperature control will be necessary for accurate lifetime determinations

Studies performed by Cline Love et al. [1] have shown that the dynamics of micelle-analyte interaction will also influence the phosphorescence lifetime. The dynamics of this interaction is a complicated process. The Stern-Volmer equation predicts that the impurities in the reagents should decrease the lifetime. Therefore, studies should be performed to determine accurately the RTP lifetime in micellar solutions. All reagents should be purified meticulously prior to use. In the studies reported in this dissertation, many reagents were used as supplied. Purification removes

impurities that decrease the phosphorescence yield and lifetime. Accurate lifetimes can then be determined in these solutions.

Deoxygenation of flowing streams attempted by diffusion of oxygen across a gas permeable membrane was not successful in this research. The two methods investigated, vacuum deoxygenation and chemical scavenging, both failed due to problems with the gas permeable membrane. The vacuum deoxygenation apparatus is believed to have failed due to the thickness of the membrane wall. Use of a thinner-walled membrane will increase the gas flux across the membrane. This should decrease significantly the time required for deoxygenation of the flowing stream.

The concentric tube dialyzer failed as a deoxygenation technique because reagents (e.g. chromium) crossed the membrane into the analyte stream. Chromium present in the analyte solution can act as a counter-ion for the micelle and be held in close proximity to the analyte. However, the low atomic number of chromium relative to thallium and silver indicates that it will not be as efficient at spin-orbital-coupling as thallium and silver. Therefore, RTP was not observed in the chromium contaminated solutions. If the dialyzer is constructed with a membrane that will not allow chromium to cross, then this technique could be useful for deoxygenating flowing streams. The Cr(II)/Zn(Hg) method has been reported in the literature [2,3] using a channel dialyzer. The concentric tube dialyzer was attempted in this research so that the higher surface area of the permeable membrane would increase the flux of oxygen across the membrane. This will decrease the deoxygenation time.

The rise in RTP observed for pyrene and higher concentrations of biphenyl shows a slow rise in RTP. The observed concentration-dependent rise in RTP for these compounds should be investigated to determine the cause of this observed slow rise in RTP. It is possible that there is an interaction between the analyte and the sulfite ion. The source of this interaction was not investigated through the course of this research. Studies should be performed using substituted pyrene derivatives or biphenyl

compounds to observe the effect substitution on the parent molecule has on the rise in RTP.

The suggested improvements to the gas permeable membrane deoxygenators would enable RTP/FIA to be performed on-line. On-line deoxygenation would enable RTP/FIA to be used as a detection system for HPLC effluents. This arrangement could use the HPLC column for sample separation and clean-up with the RTP/FIA system for post column derivatization and detection.

**CHAPTER VIII REFERENCES**

1. Cline Love, L.J.; Habarta, J.G.; Skrilec, M., *Anal. Chem.*, **1981**, *53*, 437
2. Rollie, M.E.; Ho, C.-N.; Warner, I.M., *Anal. Chem.*, **1983**, *55*, 2445
3. Rollie, M.E.; Patonay, G.; Warner, I.M., *Anal. Chem.*, **1987**, *59*, 180

**CHAPTER IX**  
**PORTABLE DUAL BEAM FIBER OPTIC-BASED**  
**PHOTOMETRIC COMPARATOR\***

This chapter presents work that was performed under a grant provided by Neogen Corporation. Neogen desired an instrument to be used as a portable and easy-to-operate detector for an immunoassay for aflatoxins. To meet these demands, an inexpensive and portable dual-beam photometric comparator was developed. It has an advantage over existing single beam systems in that direct comparisons about a critical decision point can be made with minimal error from stray radiation. A light emitting diode (LED) was used as the light source because of its fixed wavelength, narrow emission profile, low current requirements, and low cost. The comparator was designed for photometric determinations where it is desirable to know if the analyte concentration is within a certain range. The sample introduction system can accommodate microtiter wells (as cuvettes), such as those often used in routine immunoassay procedures. The unit has been designed to be operated by non-technically oriented persons. It can be battery powered for field use or operated from ac power.

**Introduction**

The development and use of chemicals in agriculture, animal husbandry, and human health and nutrition have increased the awareness of the importance of the chemical environment and the effects of synthetic compounds in the flora and fauna of

---

\*Submitted for publication in *Analytical Chemistry*.  
Co-authors: Adrian P. Wade, S.R. Crouch, J.F. Holland, and Brinton M. Miller

the earth. While modern research and service-oriented laboratories of industrialized nations are utilizing increasingly sophisticated instrumentation, there is a growing need for compact, rugged, inexpensive, and portable instruments which can perform determinations in regions isolated from the conveniences of modern laboratories. This is a consequence of the demand for instant analyses in areas remote from established facilities. In most situations a complete quantitative determination is not required. What is required is an indication of whether the analyte concentration in a sample is within or outside of an acceptable range; for example, are the active ingredients of a chemical treatment potent enough?; is the concentration of a trace contaminant below established levels?; is it safe to eat?; is it safe to discard? In these instances the analyte concentration in a sample need only to be compared to a standard. For example, since toxin and threshold limit values are defined in the Food and Drug Administration's Code of Federal Regulations [1] and the Federal Register [2], compliance to these rulings often reduces the determination of these species to a binary decision based upon a threshold level. In this work we report the development of a dual-beam fiber optic-based photometric instrument which directly compares two solutions. The unit compares the transmittance of a sample to that of a reference and indicates whether the sample contains a higher, lower, or a range of approximately equivalent analyte concentration relative to the reference. Using the reference solution as the decision point calibration standard reduces the determination to a single measurement. The unit is light-weight and powered by either an automobile battery (through a 12 V cigarette lighter adapter) or by ac line voltage with an external transformer unit.

Although this instrument was designed for binary decision analyses, the comparator basis enables it to be operated in two additional modes: i), multi-reference bracket and ii), semiquantitative mode. These modes can be more quantitative in their analysis than the binary comparison mode. The design of the instrument allows non-

technically oriented persons to perform determinations precisely with a minimum knowledge of how the instrument operates.

The methods described here are similar in principle to isomation or null-point methods [3-6]. True null comparison methods require, however, that the reference concentration (or unknown) be adjusted until a null point is reached. In the techniques described here the comparison system is utilized to give an off-null or null indication. No attempt is made to feed this information back to adjust one of the concentrations so that a true null point is obtained. This system thus acts as an open loop comparator [7].

## **Experimental**

### ***Optical Arrangement.***

A light emitting diode (LED) is used as the light source. The LED was used as a light source because of its relatively narrow emission profile ( $\lambda_{\text{max}} = 660 \text{ nm}$ ), its low power requirements and its ruggedness. The bandwidth (ca. 15 nm) is narrow compared to the absorption bandwidths of most solution absorbers; therefore no filters are required. This significantly reduces the cost of the apparatus. Determinations requiring a visible wavelength other than 660 nm may be accomplished by choosing a LED that emits at the desired wavelength.

A bifurcated fiber optic is used for light transport and significantly simplifies the optical layout. It also minimizes the effects of stray light and drift in the source LED intensity. Lenses to focus the light onto the photodiode were not necessary using this design. Silicon photocells were chosen for the detectors because of their high radiant sensitivity in the visible spectrum where the intended analyses are to be run.

### ***Analytical Manifold.***

The manifold was constructed from aluminum and is shown in Figure 9.1. The microtiter wells used as cuvettes for the determinations (Neogen Corp. 620 Leshner

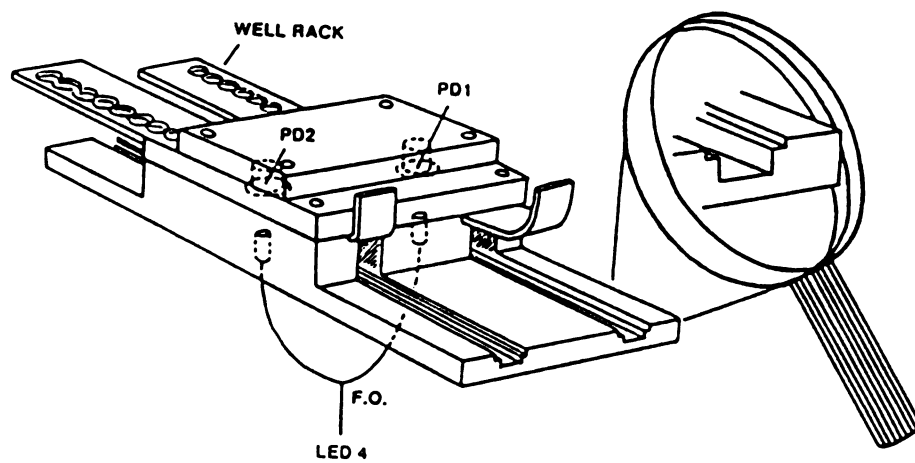


**Figure 9.1.** Manifold of the optical comparator showing configuration of the source, fiber optic, and photodiodes. The grooved tracks minimize scratches in the bottom of the analysis cups.

Place, Lansing, MI 48912) were found to be quite susceptible to scratching. This was found to scatter light and have deleterious effects on the results. Therefore, the instrument was designed with recessed tracks so that the centers of the bottoms of the wells were not in direct contact with any part of the apparatus.

The strip of wells is placed in a rack which allows indexing of individual wells. With this mechanism, entire strips are not required for an analysis. Individual well placement was controlled by a double ball-bearing gripping mechanism designed in our machine shop. This provides a high degree of precision in the placement of the wells, a feature which was found to be quite critical if repeatable comparisons were to be made.

#### ***Circuit description.***

The circuit design, Figure 9.2, is based on a light balance detection circuit suggested by Hamamatsu Corporation [8]. The components of the comparator circuit are listed in Table 9.1. This enables the photocurrents of the sample and reference diodes (PD1 and PD2 respectively) to be nulled easily with just one offset adjustment and reduces the number of electronic components required. With this circuit, the output voltage ( $V_o$ ) of operational amplifier OA1 is given by

$$V_o = R_f \times (I_{sh2} - I_{sh1}) \quad (9-1)$$

where  $R_f$  is the feedback resistor and  $I_{sh1}$  and  $I_{sh2}$  are the short circuit currents of the two photodiodes. When light of equal intensity strikes both photodiodes,  $V_o$  is zero. In the unbalanced state  $V_o$  is determined by the difference in the short circuit currents of the photodiodes and the value of  $R_f$ . Capacitor C1 was included to slow the response of the circuit via a low pass RC filter with a time constant of 0.3 s.

A window comparator circuit was selected since it enables the voltage levels for the upper and lower boundaries to be set asymmetrically when the photodiode photocurrents are balanced. Three conditions for the sample and reference photocurrents are then possible: sample < reference, sample  $\approx$  reference, and sample > reference. These boundaries are set with the trimming potentiometers which

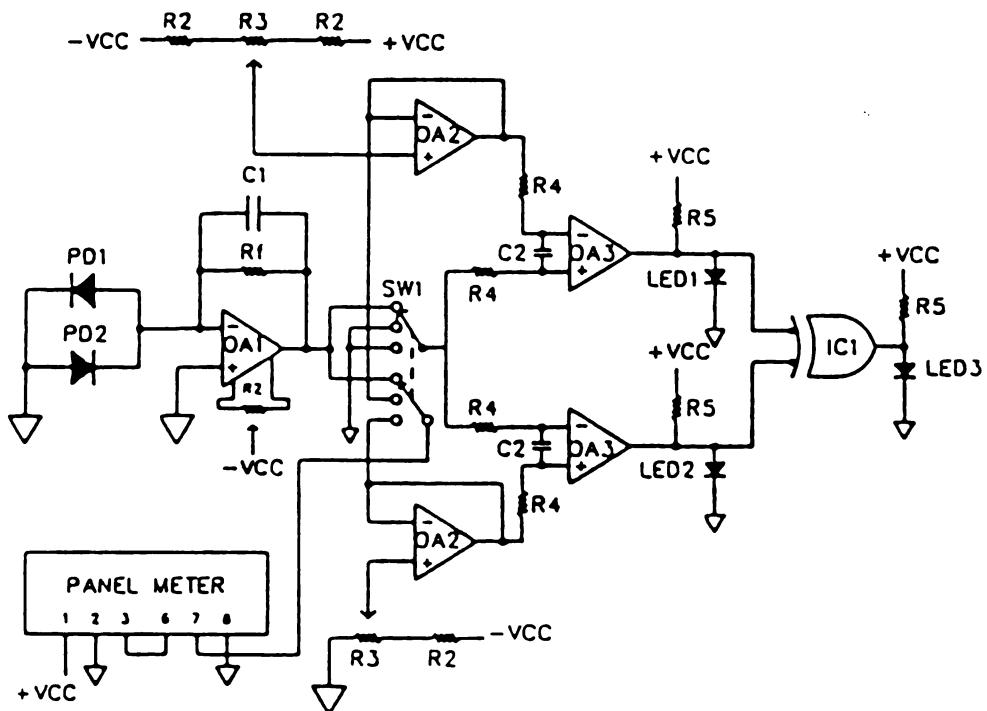


Figure 9.2. Circuit schematic for optical comparator circuit. Light from LED4 illuminates photodiodes PD1 and PD2 through the bifurcated fiber optic.

Table 9.1

## Components of Comparator Circuit

Component	Value or type
PD1, PD2	Silicon Photocell (Hamamatsu #S1336-5BK)
OA1	TL081 operational amplifier
OA2	TL082 operational amplifier
OA3	LM311 comparator
IC1	exclusive NOR gate
Rf	3.3 M $\Omega$
R1	10 k $\Omega$ 10 turn potentiometer
R2	470 k $\Omega$
R3	10 k $\Omega$ trimming potentiometer
R4	10 k $\Omega$
R5	390 $\Omega$
C1	0.1 $\mu$ F
C2	20 pF
LED1	Green light emitting diode
LED2	Red light emitting diode
LED3	Yellow light emitting diode
LED4	ER-300 High brightness (660 nm, Radio Shack #276-066)
SW1	2 pole 3 position rotary switch
meter	Acculex #DP-352
FO	Bifurcated Fiber Optic (#EK1512: Static Controls Corp., 8240 Goldie St., Walled Lake, MI 48088,

vary the reference voltage on the LM311 comparators (OA3). The window boundaries can also be selected to account for any uncertainty in the determination. The sensitivities of the comparators are limited partially by their hysteresis. The accuracy of the binary decision can be better than 0.01 absorbance units, depending on the window boundaries and the value of  $R_f$  this enables extremely precise decisions to be performed.

A panel meter was included primarily for diagnostic purposes. The window boundaries may be adjusted accurately via a 3-way selector switch connected to the reference voltages. This grounds the input of the comparator and allows the selected reference voltage to be monitored. When both boundaries are set, the switch is then positioned so that the output of the voltage follower is monitored. Thus,  $V_o$  is not related directly to the absorbance of the solutions and serves only as a reference for the magnitude of the concentration difference between the reference and sample solutions.

### **Results and Discussion**

The instrument was characterized with a dye of known absorbance characteristics. Methylene blue was chosen since it has an absorption maximum at 660 nm which is at the maximum of the source spectral distribution. Before inserting the sample and reference wells, the output of OA1 was nulled with the photodiodes using air as the reference. This was performed to minimize errors emanating from inconsistencies in the transmittances of the wells. This error may be minimized through judicious selection of the window boundaries.

In the null-point comparison mode a reference solution is used to determine if the concentration of the sample solution is greater than, less than, or approximately equivalent in concentration to the reference. Dye samples with absorbances of 0.20, 0.21, and 0.25 were compared against a reference with an absorbance of 0.21. Results were obtained which showed equality of the two solutions with the 0.21 absorbance. The samples with absorbances of 0.20 and 0.25 were indicated as being respectively

'low' and 'high' on the LED output. Thus the unit has a precision of better than 0.01 absorbance unit. This may be further improved if necessary by increasing the resistance of  $R_f$ .

Although the instrument was designed to be used as a decision point comparator we found two other modes of operation to be available: multi-reference bracket, and semiquantitative where the panel meter is read to determine the transmittance equality of two solutions (or two wells).

The multi-reference bracket mode is used to approximate the concentration of the analyte when a series of reference solutions are available. Reference solutions are selected sequentially until consecutive reference solutions are found which have lower and higher concentrations than the sample. The concentration of the sample solution is then known to be within the range of the two reference solutions.

The multi-reference mode can also be used to determine if the analyte concentration is within an acceptable range. The window boundaries may be set with reference solutions with concentrations that define the minimum and maximum acceptable analyte concentrations. With the instrument calibrated in this manner, results will be obtained that indicate if the analyte concentration in the sample is within or outside of the defined window.

When a higher correlation between reference and sample concentrations is required or if equality of two reference solutions of apparently the same concentration needs to be checked, the instrument can be operated in a single beam mode where the sample channel is referenced against air. The magnitude of the panel meter reading is monitored for both of the solutions. Although the meter reading does not directly indicate the difference in concentration of the two solutions, the concentrations will be comparable when the meter reading difference is minimal. Instruments such as this and that reported elsewhere [9] will play an increasingly important role in analytical chemistry, particularly where resources are limited and low cost is important.

One application for which this instrument has been used is in the determination of aflatoxins. Aflatoxins are potential carcinogens produced by certain types of molds which may be found in corn, peanuts, and other food items. They are soluble in water and in organic solvents such as methanol and ethanol but are insoluble in oils. These fungal toxins are stable to heat, cold, and light and do not degrade naturally unless metabolized by enzymes such as those produced in the liver or by microorganisms. Aflatoxins are colorless, odorless, and tasteless. The toxic nature of aflatoxins was first reported following a large "turkey kill" in 1960 in England [10,11]. The causative agent was aflatoxins in moldy feed. Their detection is of considerable analytical interest and has been possible by a competitive binding immunoassay procedure (Neogen Corp.).

In this analysis, an aflatoxin derivative is conjugated with an enzyme. This conjugate is used as the 'known antigen'. Antibodies specific to the aflatoxin are coated to the base of a plastic microtiter well. The aflatoxin in a food item is extracted with a 55% (v/v) methanol-water solvent. The extract is then mixed with the enzyme-conjugate and the resulting mixture is placed in the antibody coated well. The aflatoxin in the sample competes with the enzyme-conjugate for active sites on the attached antibody. Unbound aflatoxin or enzyme-conjugate is then rinsed away. An enzyme is then added to each well which catalyzes the color change of the substrate from colorless to blue. As the amount of aflatoxin in the sample increases the blue color intensity decreases. The absorbance maximum of the substrate is at 650 nm. The substrate has approximately 90% of its absorbance at 660 nm, the principal wavelength of the LED used in this instrument.

Results have been obtained which have demonstrated that the instrument is capable of discerning absorbance differences of 0.01 or less. The comparator nature of this instrument enables semi-quantitation of sample concentrations to be performed.

## CHAPTER IX REFERENCES

1. Code of Federal Regulations, Food and Drug Administration, vol. 21
2. Federal Register, July 30, 1982, vol. 47
3. Ramaley, L.; Enke, C.G., *Anal. Chem.*, **1965**, *37*, 1073
4. Malmstadt, H.V.; Winefordner, J.D., *Anal. Chim. Acta*, **1960**, *20*, 283
5. Malmstadt, H.V.; Chambers, W.E., *Anal. Chem.*, **1960**, *32*, 225
6. Malmstadt, H.V.; Enke, C.G., *Electronics for Scientist*, W.A. Benjamin, Inc., Menlo Park, CA, 1962, Chapter 6
7. Malmstadt, H.V.; Enke, C.G.; Crouch, S.R., *Electronics and Instrumentation for Scientists*, Benjamin/Cummings, Menlo Park, CA, 1981
8. Hamamatsu Photocell Catalog, P.O. Box 6916, Bridgewater, N.J. 08807
9. Bauer, W.E.; Wade, A.P.; Crouch, S.R., accepted for publication in *Analytical Chemistry*
10. Sargeant, K.; Sheridan, A.; O'Kelly, J., *Nature*, **1961**, *192*, 1096
11. Nesbitt, B.F.; O'Kelly, J.; Sargeant, K.; Sheridan, A., *Nature* 1962, *195*, 1062

**APPENDIX**  
**FORTH SOURCE CODE LISTING**

## Block Number: 9

```

0 ( USER DISK DIRECTORY)
1 10 23 THRU : A/D 1 SAMPLE A/D 0 SAMPLE ;
2 EXIT
3
4
5
6 CHECK THE SIGNAL TO NOISE RATIO.....40-41
7 GET SOME XY DATA WITH AVERAGING.....50-51
8 MANUALLY GET A SPECTRUM.....55-66
9 DECAY OF RTP PEAK.....70-73
10 RISE OF RTP .....76-78 CHOPPER MOTOR
CONTROL.....160-165
11
12
13
14
15

```

## Block Number: 10

```

0 ( DAC WORDS AND CHIP-SELECT TESTING)
1 DECIMAL
2
3 CODE 0DAC ( n->) 0 POP 0.0DAC MOV B NEXT 0 0DAC
4 CODE 1DAC ( n->) 0 POP 0.1DAC MOV B NEXT 0 1DAC
5 CODE 2DAC ( n->) 0 POP 0.2DAC MOV NEXT 0 2DAC
6
7 FORTH
8
9
10
11
12
13
14
15

```

## Block Number: 11

```

0 ( PIO INITIALIZATION BLOCK)
1 : SCUM-HEAD ;
2
3 8 CONSTANT .AIN 0 CONSTANT .AOUT
4 2 CONSTANT .BIN 0 CONSTANT .BOUT
5 4 CONSTANT .CUPPERIN 0 CONSTANT .CUPPEROUT
6 1 CONSTANT .CLOWERIN 0 CONSTANT .CLOWEROUT
7 : A-IN .AIN OR ; : A-OUT .AOUT OR ;
8 : B-IN .BIN OR ; : B-OUT .BOUT OR ;
9 : C-UPPERIN .CUPPERIN OR ; : C-UPPEROUT .CUPPEROUT OR ;
10 : C-LOWERIN .CLOWERIN OR ; : C-LOWEROUT .CLOWEROUT OR ;
11 : SET-PIO 128 ; : PIO-INIT .PIO-INIT C! ;
12
13 SET-PIO A-OUT B-OUT C-LOWERIN C-UPPEROUT PIO-INIT
14
15 FORGET SCUM-HEAD

```



## Block Number: 12

```

0 (MULTIPLEXER)
1
2 CODE MUX (n->) 0 POP 0 MUXADR MOV B NEXT 0 MUX
3 CODE SAMPLE (n->) 0 POP 0 HOLDER MOV B NEXT 0 SAMPLE
4
5 FORTH EXIT
6
7
8 USE OF THE MULTIPLEXER:
9   The channel to be multiplexed to the ADC input is selected
10  by n MUX where n=0->3 as indicated on the S/H chips on the
11  multiplexer card.
12  The status of the four inputs to the S/H's are latched by
13  executing n SAMPLE. 0 SAMPLE clears all S/H's, 1 latches Q0,
14  2 latches Q1, and 3 latches Q0 and Q1. "0 SAMPLE" MUST be
15  executed in order to update a S/H.

```

## Block Number: 13

```

0 (ADC ROUTINES) HEX
1 CODE A/D STCONV STA B ( start 12-bit conversion)
2   HLT ( F4 C, halt processor during convert)
3   STCONV LDA 0 0 HI XCHG B 0 ROR 0 ROR
4   0 ROR 0 ROR 0 PUSH NEXT DECIMAL
5
6 : CHECK 25OFF BEGIN CR A/D DUP 1 4094 WITHIN NOT IF BELL THEN
7   9 U.R ?TERMINAL END ;
8
9 : DCHK 25OFF BEGIN A/D 0 511 0 DO A/D 0 D+ LOOP 512 M/ CR
10  DUP 1 4094 WITHIN NOT IF BELL THEN 9 U.R ?TERMINAL END ;
11 EXIT
12 CODE ACQUIRE STCONV STA B BEGIN ADSTAT LDA B
13  80 #B 0 AND 0= NOT END STCONV # W MOV
14  W ) 0 HI MOV B W INC W ) 0 MOV B
15  0 SHR 0 SHR 0 SHR 0 SHR 0 PUSH NEXT DECIMAL

```

## Block Number: 14

```

0 (GOOD WORDS FOR THE 9513 COUNTER/TIMER)
1
2 CODE CMD COMAND # W MOV 0 POP STOS B NEXT
3 ( sends data to command register)
4
5 CODE @DRG DATAREG # W MOV 1 1 SUB 0 0 SUB W ) 1 MOV B
6  W ) 0 MOV B 256 # 2 MOV 2 MUL 10 ADD 0 PUSH NEXT
7 ( fetch the lo and hi bytes from the data-register and
8  pushes the 16-bit number onto the stack)
9
10 CODE >DRG 0 POP 0 DATAREG MOV B 0 HI DATAREG MOV B NEXT
11 ( puts a 16-bit number into the data-register as lo byte
12  then hi byte)
13
14 CODE HALT HLT NEXT FORTH ( halts the processor till interrupt)
15

```

**Block Number: 15**

```

0 ( 9513 COUNTER/TIMER)
1
2 BINARY
3
4 : CLK-INITIALIZE
5 11111111 CMD ( Master reset for 9513)
6 01011111 CMD ( load all counters; recommended for start-up)
7 11100111 CMD ( select 8-bit bus)
8 11101000 CMD ( disable data pointer sequencing)
9 00010111 CMD ( go to Master Mode)
10 1101000010110000 >DRG
11 ( BCD div, disable pointer, 8-bit, FOUT off, /1
12 SOURCE=F1, compares disabled, TOD disabled) ;
13 : CLK-INIT CLK-INITIALIZE CR ." 9513 INITIALIZED! " BELL ;
14
15 CLK-INITIALIZER DECIMAL

```

**Block Number: 16**

```

0 ( DATA ACQUISITION ROUTINE - DATA BUFFER, CONSTANTS, MISC)
1 3072 CONSTANT DATA-BUFFER
2 VARIABLE DATA DATA-BUFFER ALLOT VARIABLE #PTS VARIABLE DARK
3 ( A place to put all the data; the number of data points)
4
5 : FRESH DATA DATA-BUFFER ERASE 0 #PTS ! ; FRESH
6 ( Make sure the buffer is all clear and there are 0 #pts)
7
8 : SPY 25OFF DATA #PTS @ BDMP ;
9 ( Sneak a peak at what's stored in the data buffer)
10
11 CODE !DATUM DATA # W MOV #PTS 0 MOV 0 SHL 0 W ADD 0 POP
12 STOS #PTS # W MOV 1 # 0 MOV 0 W ) ADD NEXT ( 49 usec)
13 ( Stores the datum and increments the #PTS pointer)
14
15 CODE -DARK 0 POP DARK 0 SUB 0 PUSH NEXT FORTH ( 32 usec)

```

**Block Number: 17**

```

0 ( SAVE THE DATA INTO A BLOCK!)
1
2 : "DDISK" ." DATA.FTH " ;
3 ( The name of the FORTH disk on the 11/23)
4
5 : DDISK 11SPEC 25 BLANK ['] "DDISK" 3 + 11SPEC 25 MOVE ;
6 ( Put the disk name in 11SPEC)
7
8 : "DATA" ." DATA DISK" ;
9 ( Title of FORTH floppy data disk)
10
11 : ?RITE EMPTY-BUFFERS 0 BLOCK 9 0 DO DUP ['] "DATA" 3 + I +
12 C@ SWAP I + C@ = NOT IF ." Wrong disk you clod! ok"
13 CR DROP BELL QUIT THEN LOOP DROP ;
14 ( Are you trying to write on the correct disk?)
15

```

Block Number: 18

```

0 ( DATA STORAGE)
1   ( get the date and time from the 11/23)
2
3 VARIABLE D:T 16 ALLOT
4
5 : GTSTR BEGIN WCHARREC U1DATA C@ DUP 62 = END DROP ;
6
7 : TM 0 .11" TIME" UPCR GTSTR ;
8
9 : ?TIME TM D:T DUP 17 + DO DUP 30 < IF DROP
10   R> 1+ >R ELSE I C! THEN -1 +LOOP BEGIN 0= END
11   D:T C@ 45 = ABORT" LOG-IN BONE-HEAD! " ;
12
13 VARIABLE GAIN : ?GAIN CR ." Gain factor? " >NUMBER GAIN ! ;
14 VARIABLE PMT : ?PMT CR ." PMT voltage? " >NUMBER PMT ! ;
15

```

Block Number: 19

```

0 ( STORE THE DATA IN A BLOCK AND FLUSH IT)
1   VARIABLE IDENT 34 ALLOT
2 : ?IDENT IDENT 36 BLANK CR ." Please enter identifier: "
3   CNT @ >R IDENT 36 EXPECT R> CNT ! ;
4
5 : ?#BLKS #PTS @ 32 + 512 /MOD SWAP IF 1+ THEN ;
6   ( finds how many FORTH blocks it takes to store the data)
7
8 : ?FBLOCK ?#BLKS 0 BLOCK 10 + DUP @ >R +! R> UPDATE FLUSH ;
9   ( leaves start block number for storage on stack & updates)
10
11 : IDENTIFY-DATA-BLOCK ( start block # ->) ?#BLKS 0 DO
12   I 2* DUP PREV 2! DUP I + IDENTIFY UPDATE LOOP DROP ;
13   ( identifies block number with block buffer and UPDATES)
14
15 : ZAP-BUFR FIRST @ DUP 5120 + SWAP DO 0 I! 2 +LOOP ;

```

Block Number: 20

```

0 ( STORE THE DATA IN A BLOCK AND FLUSH IT cont.)
1
2 : INSRT ( blk# ->) EMPTY-BUFFERS ZAP-BUFR FIRST @ DUP 64 BLANK
3   DUP D:T SWAP 18 MOVE ( date and time)
4   DUP 18 + IDENT SWAP 38 MOVE ( identifier string)
5   DUP 54 + #PTS @ SWAP ! ( the number of points)
6   DUP 56 + ?#BLKS SWAP ! ( the number of FORTH blocks)
7   DUP 58 + GAIN @ SWAP ! ( the keithley gain)
8   DUP 60 + PMT @ SWAP ! ( the PMT voltage)
9   DUP 62 + DUP >R ROT SWAP ! ( the FORTH data disk block)
10   64 + DATA SWAP #PTS @ 2* MOVE ( get the data there)
11   CR ." Data stored in block" R> @ 4 U.R SPACE ;
12
13 : STORE ?RITE ?TIME ?IDENT ?GAIN ?PMT ?FBLOCK DUP INSRT
14   IDENTIFY-DATA-BLOCK FLUSH ;
15

```

Block Number: 21

```

0 ( READ LINE 0 OF DATA BLOCK)
1
2 : WHAT ( n->) BLOCK >R
3 I      18 TYPE CR   ( get date and time)
4 I 18 +   36 TYPE CR   ( get the identifier)
5 I 54 + @ ." #PTS =" 5 U.R CR
6 I 56 + @ ." #BLKS:" 5 U.R CR
7 I 58 + @ ." GAIN =" 5 U.R CR   ( get the gain)
8 R> 60 + @ ." PMT =" 5 U.R CR   ( the PMT voltage) ;
9
10 : DDMP ( n->) EMPTY-BUFFERS DUP DUP WHAT
11 BLOCK 54 + DUP @ >R ( #pts) 2+ @ ( #blocks) 0 DO
12 DUP I + BLOCK DROP LOOP BLOCK 64 + R> BDMP ;
13 ( dumps the data along with the header)
14
15

```

Block Number: 22

```

0 ( ELAPSED TIMING using counter group #5 of 9513)
1
2 OCTAL : SET 5 CMD 5450 >DRG 15 CMD 0 >DRG ;
3 : DISARM 401 CMD ; DECIMAL
4
5 : ELAPSE -' NOT IF DISARM
6 SET 80 CMD 48 CMD ( get ready)
7 EXECUTE ( start task)
8 176 CMD 21 CMD ( read time)
9 @DRG 166 - ( subtract overhead)
10 CR ." Elapsed time: " 5 U.R ." micro-seconds "
11 ELSE DROP ." There ain't no such word chump! " THEN ;
12
13 ( Overhead determined as time taken between starting the
14 timer and reading the register. This was done by removing
15 the EXECUTE statement.)

```

Block Number: 23

```

0 ( SEND DATA BLOCKs TO THE 11/23 AS RSX FILE)
1
2 : #blks ( block # ->) BLOCK 56 + @ ;
3
4 : 4-PIP .11" FPI C TI:/L B";
5
6 : /R .11" .RSX/R " DONE ;
7
8 : DEB CR DUP 5 U.R ;
9
10 : UPDAT ( block # ->) 4-PIP DUP (.) UPCHAR /R DUP
11 #blks 0 DO DUP I + DEB BLOCK SENDDAT ! UPCHUCK LOOP DROP
12 SDONE ;
13
14
15

```

Block Number: 24

```

0 ( AUTOMATED PUMP)
1 ( Updated for new totally automated pump)
2
3 ( Speed control)
4 : PMP 2585 1000 */;      : PUMP ( n->) PMP 1DAC ;
5 : RACE 255 1DAC;        : IDLE 2 1DAC;      0 PUMP
6
7 ( Direction control)
8 VARIABLE <BPIO>
9
10 CODE FWRD 1 # <BPIO> OR <BPIO> 0 MOV 0 .BPIO MOV B NEXT
11
12 CODE RVRS 255 #0 MOV 1 #0 SUB 0 <BPIO> AND <BPIO> 0 MOV
13   0 .BPIO MOV B NEXT
14
15

```

Block Number: 40

```

0 ( VARY SLITS TO OBSERVE S/N - WHAT NOISE DO WE HAVE?)
1
2 OCTAL
3 : 2LOAD ( N->) 02 CMD 6445 >DRG 12 CMD >DRG 102 CMD ;
4 ( Use counter 2 since it has the interrupt line;
5   source is F3 @ 10kHz; N = 10,000 for 1 second)
6
7 : 2ARM 42 CMD ; ( arms counter #1)
8 : 2DISARM 202 CMD ; ( disarms counter #2)
9 DECIMAL
10
11 : #COUNTS CR ." Acquisition rate? (ms) " >NUMBER 10 * 2LOAD ;
12
13   VARIABLE NPNTS
14 : HOW_MANY CR ." How many points? " >NUMBER NPNTS ! ;
15 : ?OK #PTS @ ABORT" Empty data buffer first clay-head ok" ;

```

Block Number: 41

```

0 ( VARY SLITS TO OBSERVE S/N - WHAT NOISE DO WE HAVE? cont.)
1
2 160 LOAD ( load the chopper control)
3
4 : GET_DARK -LIGHT CR ." Hit key when ready to get dark current"
5   1KEY DROP
6   2ARM HALT A/D 0 NPNTS @ 1- 0 DO HALT A/D 0 D+ LOOP
7   2DISARM NPNTS @ M/ DARK ! ;
8
9
10 : LET'S_GO CR ." Hit key when ready chump " BELL 1KEY DROP ;
11
12 : S/N ?OK #COUNTS HOW_MANY GET_DARK LET'S_GO +LIGHT 2ARM
13   NPNTS @ 0 DO HALT A/D -DARK !DATUM LOOP 2DISARM -LIGHT ;
14
15

```

Block Number: 55

```

0 ( LOAD BLOCK FOR SPECTRUM TAKING)
1
2 0 0DAC
3
4 : ?TYPE 160 LOAD 56 57 THRU
5   CR ." Use the chopper for delays? [Y/N] "
6   KEY 89 ( Y) =
7   IF ( chopped) 59 61 THRU
8   ELSE ( normal) 58 LOAD
9   THEN 62 65 THRU ;
10
11   ?TYPE
12
13
14
15

```

Block Number: 56

```

0 ( BETTER SPECTRUM TAKING set-up)
1
2 VARIABLE WAVE      ( the emission wavelength)
3 VARIABLE STEP      ( the step)
4 VARIABLE SET       ( the number of ADC counts to average)
5 VARIABLE CURRENT   ( the current ave of ADC counts)
6 VARIABLE RAW       ( the raw ave of ADC counts)
7 VARIABLE VDAC      ( the 0DAC value used for chopper)
8 VARIABLE #TGR      ( the delay time in usec)
9
10 : SAVE_EM WAVE @ !DATUM CURRENT @ !DATUM ;
11   ( stores data as wavelength:intensity pairs)
12 : ?READY CR ." Hit any key when ready [Q=quit] " 1KEY 81 ( Q)
13   = IF ." QUIT ok" CR QUIT THEN ;
14
15

```

Block Number: 57

```

0 ( BETTER SPECTRUM TAKING the questions)
1
2 : ?SET CR ." How many ADC counts to average? " >NUMBER SET ! ;
3
4 : ?L1 CR ." Initial emission wavelength:  " >NUMBER ;
5
6 : ?L2 CR ." Final emission wavelength:  " >NUMBER 1+ ;
7
8 : ?STEP CR ." Enter the step you want to use: " >NUMBER
9   STEP ! ;
10
11 : PAIRS CR 2DUP - ABS STEP @ / 1+ DUP ." Pairs =" 3 U.R
12   ." #PTS =" 2* 3 U.R ;
13
14 : ?PREPS ?SET ?L1 ?L2 ?STEP PAIRS ;
15

```

## Block Number: 58

```

0 ( BETTER SPECTRUM TAKING more words)
1
2 0 #TGR! 0 0DAC -LIGHT
3
4 :GET_EM 0 0 SET @ 0 DO A/D 0 D+ LOOP
5   SET @ M/ DUP RAW! -DARK CURRENT! ;
6   ( reads and sums the A/D counts)
7
8
9 : DRK CR ." Time to take the background. " -LIGHT ?READY
10  GET_EM RAW @ DARK! +LIGHT ;
11   ( gets the dark value and stores it in DARK)
12
13 : TST +LIGHT CHECK -LIGHT ;
14
15

```

## Block Number: 59

```

0 ( SET-UP THE 9513 FOR DELAY AFTER H->L CHOPPER TRANSITION)
1 OCTAL
2
3 : TGR
4   2 CMD ( mode #2) 175445 >DRG
5   12 CMD ( load #2) #TGR @ >DRG
6   102 CMD ( load register) 42 CMD ( arm) ;
7 ( act lo edge gate 2, count falling edge, F1, reload from
8  load, count repetitively/binary/down, act lo TC pulse.
9  Delays N us after HI->LO chopper signal and sends pulse to
10  interrupt line- used to start micro again)
11 : TRIG ( n->) #TGR ! TGR ; ( start trigger in one word)
12 : -TGR 302 CMD ; ( stops counter #2)
13   DECIMAL
14 : MSK IMSK C@ 1 OR IMSK C! ; ( mask interrupt line)
15 : -MSK IMSK C@ 254 AND IMSK C! ; ( reset interrupt line)

```

## Block Number: 60

```

0 ( MORE NEET STUFF FOR DELAYED DATA TAKING IN SPECTRUM)
1 :GET_EM 0 0 SET @ 0 DO HALT A/D 0 D+ LOOP
2   SET @ M/ DUP RAW! -DARK CURRENT! ;
3   ( read and sum and average the ADC counts)
4
5 : dly 10000 0 DO LOOP ;
6
7 : DRK CR ." Take the background!" 0 0DAC dly -LIGHT ?READY
8   0 0 SET @ 0 DO A/D 0 D+ LOOP SET @ M/ DARK !
9   VDAC @ 0DAC TGR ;
10
11 : ?TGR CR ." What trigger delay? [usec] " >NUMBER #TGR ! ;
12
13 : ?DAC CR ." What 0DAC value? " 15 SPACES >NUMBER VDAC ! ;
14
15 : ?PREPS ?TGR ?DAC ?PREPS ;

```

## Block Number: 61

```

0 ( USE THE DELAYED A/D CONVERSION TO SET RANGES)
1
2
3
4 : DLCHK 25OFF TGR VDAC @ 0DAC BEGIN CR HALT A/D DUP 10 U.R
5   1 4094 WITHIN NOT IF BELL THEN
6   ?TERMINAL END 0 0DAC dly -LIGHT ;
7
8 : DLSET ?TGR ?DAC DLCHK ;
9
10
11
12
13
14
15

```

## Block Number: 62

```

0 ( BETTER SPECTRUM TAKING presentation - box format)
1
2 : -> ( n->) 0 DO ZCRIGHT LOOP ; ( moves right n spaces)
3
4 : BX CLR-SCR
5   20 3 CURSOR ." WAVELENGTH AVE. ADC AVE. ADC - DARK"
6   20 4 CURSOR ." (nm) (counts) (counts)"
7
8   16 1 47 03 BOX EZG
9
10  32 2 CURSOR 115 EMIT ZCDOWN ZCLEFT 2 ZSIDES 117 EMIT
11
12  45 2 CURSOR 115 EMIT ZCDOWN ZCLEFT 2 ZSIDES 117 EMIT XZG ;
13
14
15

```

## Block Number: 63

```

0 ( BETTER SPECTRUM TAKING presentation - continued)
1 : L25 SZCUR 25ON 11 25 CURSOR ERALIN REVERSE ." #PTS=      #
2 SETS/PT=      TGR=      DARK=      " RZCUR NORMAL ;
3   ( sets up the 25th line)
4
5 : UD25      REVERSE 16 25 CURSOR #PTS @ 4 U.R
6           35 25 CURSOR SET @ 5 U.R
7           50 25 CURSOR #TGR @ 5 U.R
8           64 25 CURSOR DARK @ 5 U.R NORMAL      ;
9   ( updates 25th line information)
10 : NEXTWAVE WAVE @ REVERSE . NORMAL 10 -> ." " 10 ->
11   ." " RZCUR ;
12   ( reports the next wavelength in table in reverse video)
13
14 : REPORT RZCUR WAVE @ . 10 -> RAW @ 4 U.R 10 ->
15   CURRENT @ 4 U.R BELL ; ( reports the current values)

```

## Block Number: 64

```

0 ( BETTER SPECTRUM TAKING almost there)
1
2 : SCREEN BX L25 UD25 23 6 CURSOR SZCUR ;
3
4 : ?SURE #PTS @ ABORT" You've already got data dope! ok" ;
5
6 : GRSU GET_EM REPORT SAVE_EM UD25 ;
7
8 : CIRCLE #PTS 20 > IF 1 5 CURSUR DELLIN 23 20 CURSOR THEN ;
9
10
11
12
13
14
15

```

## Block Number: 65

```

0 ( BETTER SPECTRUM TAKING the final frontier)
1
2 : SET-UP 1 8 CURSOR ?PREPS ;
3 : 23del 1 22 CURSOR DELLIN DELLIN DELLIN ;
4
5 : SPECTRUM ?SURE CLR-SCR 0 DARK !
6   SET-UP          ( get initial information)
7   CR CR DRK      ( get background)
8   SCREEN          ( set-up the video screen)
9   SWAP DO 23del RZCUR INSLIN RZCUR
10  I WAVE ! NEXTWAVE
11  1 23 CURSOR ?READY RZCUR GRSU STEP @ +LOOP
12  1 23 CURSOR ERALIN ." DONE!!! " 23del
13  0 0DAC ;
14
15

```

## Block Number: 70

```

0 ( WATCH DECAY OF RTP PEAKS)
1
2 160 LOAD          ( the chopper stuff)
3 56 57 THRU       ( variables and core words)
4 59 61 THRU       ( set-up 9513 and more neet words)
5
6 VARIABLE T1      ( initial delay time)
7 VARIABLE T2      ( final delay time)
8
9 : ?T1 CR ." Enter initial delay time [usec] " >NUMBER T1 ! ;
10 : ?T2 CR ." Enter final delay time [usec] " >NUMBER 1+ T2 ! ;
11
12 : TOTPTS CR T2 @ T1 @ - STEP @ / 1+ 2* ." #PTS =" DUP 4 U.R
13  2* DATA-BUFFER > IF CR ." TOO MUCH DATA FOR BUFFER! ok" BELL
14  CR QUIT THEN ;
15 : QUESTIONS ?T1 ?T2 ?STEP TOTPTS ?DAC ?SET ;

```

Block Number: 71

```

0 ( WATCH DECAY OF RTP PEAKS cont.)
1
2
3 : ?SURE #PTS @ ABORT" You've already got data clay-head! ok" ;
4
5
6 : L25 25OFF 25ON SZCUR 11 25 CURSOR REVERSE ." #PTS =
7 #SET/PT=      TGR=      DARK=      " NORMAL RZCUR ;
8
9
10 : UD25 SZCUR REVERSE 16 25 CURSOR #PTS @ 4 U.R
11           35 25 CURSOR SET @ 5 U.R
12           50 25 CURSOR #TGR @ 5 U.R
13           64 25 CURSOR DARK @ 5 U.R NORMAL RZCUR ;
14
15

```

Block Number: 72

```

0 ( WATCH DECAY OF RTP PEAKS cont.)
1
2 : REPORT ( time->) CR ." delay time:" 5 U.R ." intensity:"
3   CURRENT @ 5 U.R (." STD = " STD @ 5 U.R) UD25 ;
4
5 : PREPARE ?SURE CLR-SCR 0 DARK ! 0 0DAC 1 10 CURSOR
6   QUESTIONS DRK VDAC @ 0DAC T1 @ #TGR ! TGR L25 UD25
7   CR CR ." Time to decay!" ?READY ;
8
9 : DECAY PREPARE CR
10  T2 @ T1 @ DO I#TGR ! TGR UD25 GET_EM I WAVE !
11  SAVE_EM I REPORT STEP @ +LOOP CR ." frequency testing: "
12  FRK 0 0DAC 25OFF dly -LIGHT ;
13
14
15

```

Block Number: 76

```

0 ( WATCH RISE OF RTP AFTER ADDITION OF SULFITE- initialization)
1 160 LOAD ( chopper stuff)
2   VARIABLE TIME      ( how many seconds to take data)
3   VARIABLE INTRVL    ( how often to take data: sec)
4   VARIABLE LAG       ( ignore time for mixing: sec)
5   VARIABLE SETS      ( how many datum to average)
6   VARIABLE DELAY     ( delay time after H->L: usec)
7   VARIABLE DAC       ( DAC value for chopper)
8 : ?TIME CR ." Minutes to take data: " >NUMBER 60 * TIME ! ;
9 : ?INTRVL CR ." Enter interval [sec]: " >NUMBER 100 * INTRVL ! ;
10 : ?LAG CR ." Enter lag time [sec]: " >NUMBER 1- LAG ! ;
11 : ?SETS CR ." # sets to average: " >NUMBER SETS ! ;
12 : ?DELAY CR ." Delay time [usec]: " >NUMBER DELAY ! ;
13 : ?DAC CR ." Enter dac value: " >NUMBER DAC ! ;
14 : >#PTS TIME @ LAG @ 1+ - INTRVL @ 100 // 1+ 2* ." #PTS= " . ;
15 : PREPARE ?TIME ?INTRVL ?LAG CR >#PTS ?SETS ?DELAY ?DAC ;

```

**Block Number: 77**

```

0 ( WATCH RISE OF RTP AFTER ADDITION OF SULFITE- CLOCK SET-UP)
1
2 OCTAL
3 : 1TMR 1 CMD 007442 >DRG 11 CMD INTRVL @ >DRG 101 CMD ;
4 : 1ARM 41 CMD ; ( uses F5 and counter #1 to count sec)
5 : 2TMR 2 CMD 175445 >DRG 12 CMD DELAY @ >DRG 102 CMD ;
6 : 2ARM 42 CMD ; ( wait for H->L on chopper then delay)
7 DECIMAL
8
9 CODE TURNOVER BEGIN COMAND # W MOV 161 # 0 MOV 0 W ) MOV B
10 17 # 0 MOV 0 W ) MOV B
11 1 1 SUB 0 0 SUB DATAREG # W MOV W ) 1 MOV B
12 W ) 0 MOV B 256 # 2 MOV 2 MUL 1 0 ADD 0 DEC
13 0= END NEXT FORTH
14 ( read hold reg. of cntr 1 and wait for TC)
15

```

**Block Number: 78**

```

0 ( WATCH RISE OF RTP AFTER ADDITION OF SULFITE- )
1 : CLOCKS 1TMR 1ARM 2TMR 2ARM ;
2 : GDAT 0 0 SETS @ 0 DO HALT A/D 0 D+ LOOP SETS @ M/ -DARK ;
3
4 CODE INT/100 INTVRL 0 MOV 100 # W MOV CWD W IDIV 0 PUSH NEXT
5
6 : CHT CLOCKS TIME @ 1+ INT/100 DO TURNOVER CR I DUP 5 U.R
7 ." seconds" LAG @ > IF BELL I !DATUM
8 ." ave." GDAT DUP !DATUM 6 U.R THEN INTRVL @ 100 / +LOOP ;
9
10 : GDRK -LIGHT CR ." Hit key for dark." 1KEY DROP
11 0 0 SETS @ 0 DO A/D 0 D+ LOOP SETS @ M/ DUP 5 U.R DARK ! ;
12 : ?RDY CR ." Hit any key when ready [Q to quit]" 1KEY 81
13 = IF ." ok" CR QUIT THEN ;
14 : RTP-RISE #PTS @ ABORT" Do FRESH" PREPARE GDRK DAC @ 0DAC
15 ?RDY CHT 0 0DAC 1000 0 DO 100 0 DO LOOP LOOP -LIGHT ;

```

**Block Number: 160**

```

0 ( NUDGE THE CHOPPER WHEEL A LITTLE)
1 : NUDGE 150 0DAC 150 0 DO LOOP 0 0DAC ;
2 ( moves the chopper wheel a little bit)
3
4 : SPD ( n->) ['] NUDGE 2 + ! ; : ?SPD ( ->) ['] NUDGE 2 + @ ;
5 ( changes speed) ( fetches speed)
6 : DLY ( n->) ['] NUDGE 8 + ! ; : ?DLY ( ->) ['] NUDGE 8 + @ ;
7 ( changes delay) ( fetches delay)
8
9 : ?STAT .CPIO C@ 1 AND ; : WHEEL NUDGE 1000 0 DO LOOP ;
10 ( checks status of C0) ( moves wheel and waits)
11
12 : -LIGHT ?STAT IF BEGIN WHEEL ?STAT NOT END THEN ;
13 ( makes sure light path is blocked)
14 : +LIGHT ?STAT NOT IF BEGIN WHEEL ?STAT END THEN ;
15 ( makes sure light path is not blocked)

```

Block Number: 161

```

0 ( CHOPPER STUFF USING GATE #1 AS COUNTER AND #2 PERIOD TIMER)
1
2             BINARY
3 : CHOP-SET 11000011 CMD ( disarm 1&2)
4 (#1: count pulses) 00000001 CMD 0000011100101000 >DRG
5             00001001 CMD 0 >DRG ( load w/zero)
6 (#2: time 1 sec) 00000010 CMD 1100111000000101 >DRG
7             00001010 CMD 1111101000 >DRG ( 1000!);
8             DECIMAL
9
10 : 1CHOP CHOP-SET 99 CMD ( load&arm) HALT ( halt while counting)
11   ( output #2 is active low TC pulse which starts the micro)
12   161 CMD ( save counts) 17 CMD ( hold reg. #1) @DRG ;
13
14 : ?FREQ 1CHOP CR ." Frequency =" 5 U.R SPACE ." Hz " CR ;
15

```

Block Number: 162

```

0 ( CHOPPER STUFF cont.)
1
2 VARIABLE FREQ-CNT 2 ALLOT ( hold the frequency counts)
3
4 : 1SEC ( 1 second period) 1000 ['] CHOP-SET 44 + ! ;
5 : 10SEC ( 10 second period) 10000 ['] CHOP-SET 44 + ! ;
6
7 : INTT-FRK CHOP-SET 0. FREQ-CNT 2! ;
8
9 : ?FORMAT ['] CHOP-SET 44 + @ 10000 = IF <# # # 46 HOLD #S #>
10   ELSE <# # 46 HOLD #S #> THEN ;
11
12 : FRK INTT-FRK SZCUR
13   10 0 DO RZCUR I 1+ 4 U.R 1CHOP 0 FREQ-CNT D+! LOOP
14   FREQ-CNT 2@ RZCUR ?FORMAT 2 SPACES TYPE ." Hz" SPACE ;
15

```

Block Number: 164

```

0 ( LET MICRO SET THE CHOPPING FREQUENCY)
1
2 VARIABLE TOLERANCE 1 TOLERANCE ! ( default to +/- 1%)
3 : %TOLERANCE TOLERANCE ! ;
4
5 : +LMT ( n ->) 100 TOLERANCE @ + 100 * / ;
6 : -LMT ( n ->) 100 TOLERANCE @ - 100 * / ;
7
8 : FRK-?OK ( actual, desired->F) DUP -LMT SWAP +LMT WITHIN ;
9
10
11
12
13
14
15

```

Block Number: 165

```
0 ( LET MICRO SET THE CHOPPING FREQUENCY cont.)
1 VARIABLE FREQUENCY VARIABLE SUPPLY 75 SUPPLY !
2
3 : STATUS-REPORT ( freq->) 5 U.R SUPPLY @ 5 U.R 13 EMIT ;
4
5 : ADJUST 2DUP = IF 2DROP 1 ELSE > IF -1 SUPPLY +!
6   ELSE 1 SUPPLY +! THEN SUPPLY @ 0DAC 0 THEN ;
7
8 : ALRIGHT ( ." WITHIN" TOLERANCE @ 3 U.R ." % TOLERANCE!");
9
10 : WHAT_TODO ( s1,s2,F->) IF ADJUST ELSE ALRIGHT 2DROP 1 THEN ;
11
12 : SPEED-CONTROL 1CHOP ( DUP STATUS-REPORT)
13   FREQUENCY @ 2DUP FRK-?OK NOT WHAT_TODO ;
14
15 : HZ FREQUENCY ! SUPPLY @ 0DAC BEGIN SPEED-CONTROL END ;
```